Analysis and Manipulation of Cell-Mediated Immune Responses in Shiga Toxin-Induced Kidney Injury

Inaugural-Dissertation
zur
Erlangung des Doktorgrades

Dr. rer. nat.

der Fakultät für
Biologie

an der

Universität Duisburg-Essen

vorgelegt von

Judith-Mira Pohl
aus Castrop-Rauxel

Mai 2017

DOI: 10.17185/duepublico/44541
URN: urn:nbn:de:hbz:464-20201214-113900-4

Die der vorliegenden Arbeit zugrunde liegenden Experimente wurden am Institut für Experimentelle Immunologie am Universitätsklinikum Bonn begonnen und am Institut für Experimentelle Immunologie und Bildgebung in der Arbeitsgruppe Immundynamik der Universität Duisburg-Essen weitergeführt und beendet.

1. Gutachter: Prof. Dr. Daniel Robert Engel
2. Gutachter: Prof. Dr. Joachim Fandray
3. Gutachter: Prof. Dr. Linda Diehl
Vorsitzender des Prüfungsausschusses: Prof. Dr. Gero Hilken

Tag der mündlichen Prüfung: 26.09.2017

Table of Contents

1 Abstract/Zusammenfassung

1.1 Abstract

Shiga toxin (Stx)-producing enterohemorrhagic *Escherichia coli* (STEC) are the primary cause of hemolytic uremic syndrome (HUS), a life-threatening disease characterized by hemolytic anemia, thrombocytopenia and acute kidney failure. Endothelial cells were shown to be the main target for the cytotoxic effects of Stx leading to endothelial damage, recruitment of leukocytes, and thrombus formation. However, the precise contribution of monocytes, macrophages and neutrophils in the pathogenesis of HUS remains unclear and a therapy for STEC-HUS is still elusive.

In this study, we have investigated the contribution of specific monocyte/macrophage subsets and the role of neutrophil recruitment to the pathology of HUS. To this end, a murine HUS model was employed in which mice were intravenously injected with a combination of Stx and lipopolysaccharide (LPS) to mimic a STEC infection.

We observed impaired renal function as well as elevated levels of monocyte/macrophage- and neutrophil-recruiting chemokines in the kidney of Stx/LPS-injected mice. Accordingly, flow cytometric analysis revealed increased numbers of CCR2-dependent $Gr1^{high}$ monocytes and neutrophils within the kidney, demonstrating myeloid cell infiltration during HUS. Positron emission tomography-magnetic resonance (PET-MR) imaging revealed renal injury mainly in the kidney cortex coinciding with the detection of $Gr1^{high}$ monocytes and neutrophils in this renal compartment. Indeed, reduced recruitment of $Gr1^{high}$ monocytes in *Ccr2*-deficient (*Ccr2*$^{-/-}$) mice significantly ameliorated kidney injury and improved survival of these mice. Moreover, *Ccr2*$^{-/-}$ *x Cx*$_3$*cr1*$^{gfp/gfp}$ mice, which showed reduced abundance of $Gr1^{high}$ monocytes and $Gr1^{low}$ macrophages in the kidney, were completely protected from renal damage, indicating an essential role of both cell subsets.

Furthermore, targeting CXCR2-dependent recruitment of neutrophils in either *Cxcr2*-deficient mice or by pharmacological inhibition (SB 225002) significantly ameliorated HUS and reduced mortality.

Conclusively, this study identifies PET-MR imaging as a potential non-invasive approach to evaluate kidney damage in STEC-HUS. Moreover, these data demonstrate the crucial role of $Gr1^{high}$ monocytes, $Gr1^{low}$ macrophages and CXCR2-mediated neutrophil recruitment in renal injury in the murine model of HUS. Targeting the recruitment of these myeloid cells may serve as a first therapy against this devastating and severe disease.

1.2 Zusammenfassung

Das hämolytisch urämische Syndrom (HUS) ist eine lebensbedrohliche Krankheit, welche klinisch durch das Auftreten einer mikroangiopathischen Anämie, einer Thromozytopenie und akutem Nierenversagen gekennzeichnet ist. Die primäre Ursache für HUS ist eine Infektion mit Shiga Toxin (Stx)-produzierenden *Escherichia Coli*, so genannten STEC. Die Pathogenität dieser Bakterien wird hauptsächlich über das Stx vermittelt, welches an Endothelzellen der Niere bindet und Endothelschäden, die Einwanderung von Immunzellen und die Bildung eines Thrombus induziert. Obwohl mehrere deskriptive Studien auf eine Rolle von Monozyten, Makrophagen und neutrophilen Granulozyten im HUS hinweisen, ist der Beitrag dieser myeloiden Zellen zum Nierenschaden bisher noch nicht vollständig aufgeklärt und effektive Interventionsstrategien gegen HUS fehlen.

Aus diesem Grund werden in dieser Studie die Rolle verschiedener Monozyten/Makrophagen-Subtypen und der Beitrag der Neutrophilen-Rekrutierung zur Nierenschädigung im Kontext des HUS untersucht. Hierzu wurden Mäuse mit einer Kombination aus Stx und Lipopolysacchariden (LPS) injiziert um eine STEC-Infektion zu simulieren.

In Nierenhomogenaten von Stx/LPS-behandelten Mäusen wurden erhöhte Mengen von Chemokinen nachgewiesen, welche Monozyten/Makrophagen und Neutrophile Granulozyten rekrutieren. Weiterhin konnte durch durchflusszytometrische und histologische Analysen gezeigt werden, dass die Zellzahlen von inflammatorischen CCR2-abhängigen $Gr1^{high}$ Monozyten und neutrophilen Granulozyten hauptsächlich in den kortikalen Bereichen der Niere nach Stx/LPS-Injektion erhöht waren. Untersuchungen mittels Positronen-Emissions-Tomographie und

Magnetresonanztomographie (PET-MR) deuteten darauf hin, dass die Infiltration des Nieren-Kortex durch myeloide Zellen mit einem erhöhten Endothelschaden in diesem Bereich koinzidierte. Tatsächlich führte eine verminderte Rekrutierung von $Gr1^{high}$ Monozyten in *Ccr2*-defizienten (*Ccr2*$^{-/-}$) Mäusen zu verringertem Nierenschaden und verminderter Mortalität. *Ccr2*$^{-/-}$ *x Cx*$_3$*cr1*$^{gpf/gfp}$ Mäuse, welche reduzierte Zellzahlen von sowohl $Gr1^{high}$ Monozyten als auch $Gr1^{low}$ Makrophagen zeigten, waren vollständig vor der Entstehung von Nierenschäden geschützt. Diese Daten weisen auf eine Beteiligung von $Gr1^{high}$ Monozyten und $Gr1^{low}$ Makrophagen an Stx-vermittelten Endothelschäden in der Niere hin.

Des Weiteren wurde in Stx/LPS-injizierten Mäusen, in denen die CXCR2-vermittelte Neutrophilen-Rekrutierung genetisch (*Cxcr2*$^{d/d}$) oder pharmakologisch (SB 225002) inhibiert wurde, reduzierter Nierenschaden und verringerte Letalität nachgewiesen. Dies deutet auf eine essentielle Rolle der Neutrophilen-Rekrutierung im HUS hin.

Zusammenfassend konnte in dieser Studie die PET-MR Bildgebung als eine neue nicht-invasive Methode zur Evaluierung von Endothelschäden in HUS identifiziert werden. Des Weiteren wurde eine Beteiligung von $Gr1^{high}$ Monozyten und $Gr1^{low}$ Makrophagen sowie ein Beitrag CXCR2-vermitteltet Neutrophilen-Rekrutierung am Nierenschaden während des HUS gezeigt. Therapeutika, welche die Rekrutierung myeloider Zellen inhibieren, könnten daher vielversprechende Therapieansätze im HUS darstellen.

2 Introduction

2.1 The Immune System

Throughout our live we are exposed to numerous diverse infectious agents including bacteria, viruses and fungi[1]. The immune system, comprising immune cells and effector molecules, protects the body from such infectious agents. Depending on the immune cell function, the immune system of vertebrates is divided into two parts, the innate and the adaptive immune response[2, 3].

2.1.1 Innate immunity

Evolutionarily, innate immunity is the oldest protective response that is essential for an immediate immune reaction against invading pathogens[4].To this end, it is termed the "first line of defense"[2]. The innate immune system is formed by immune cells, such as monocytes, macrophages, dendritic cells and neutrophils, and by a humoral response, called the complement system (Fig. 2.1)[5]. Although the innate immune system responds to a broad spectrum of pathogens, the immune responses are rather non-specific. This immediate reaction depends on a variety of receptors expressed on innate immune cells, the commonly called pattern recognition receptors (PRR), which recognize pathogen-associated molecular patterns (PAMPs)[6, 7]. In most cases the innate immune response is sufficient to either delay the infection or fully combats invading pathogens. However, given that microbes have developed strategies to evade innate immunity, the initiation of the adaptive immune response is required to protect the host from infections[2].

2.1.2 Adaptive immunity

In contrast to innate immunity, the adaptive immune system launches a highly specific immune response against pathogens. This specificity is achieved by selection and expansion of lymphocyte clones, which express antigen-specific receptors[4]. Hence, the adaptive immune response is delayed and effector responses take several days to eliminate pathogens[2]. Importantly, the adaptive immune system harbors a memory

function protecting the host from recurrent infections. Similar to the innate immune system, adaptive immunity comprises cellular components like B- and T-lymphocytes as well as humoral components such as antibodies (Fig. 2.1)[5].

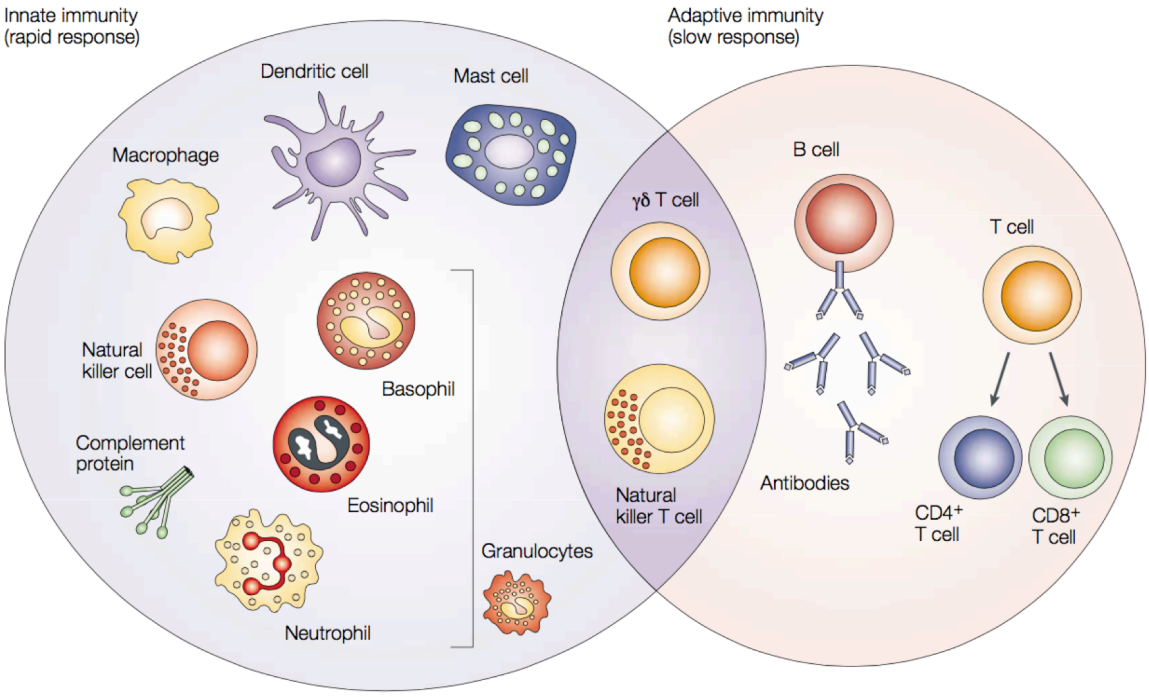

Figure 2.1: The innate and adaptive immune system.
The figure gives an overview of components that form the innate and adaptive immune system. Innate immunity is provided by mast cells, dendritic cells (DC), macrophages, natural killer cells, various granulocytes and the complement system. Adaptive immunity consists of $CD4^+$ T-cells, $CD8^+$ T-cells, B cells and antibodies. Natural killer T-cells and γδ T-cells harbor features of both arms of immunity. The figure was adopted from Dranoff, G., Nature Reviews Cancer, 2004[5].

2.2 Monocytes and Macrophages

Monocytes and macrophages together with dendritic cells (DC) constitute the mononuclear phagocyte system. These cells are of hematopoietic origin and derive from a common precursor cell referred to as monocyte, macrophage and DC precursor cell (MDP) (Fig. 2.2)[8, 9]. Additionally, some macrophages in tissues, such as the brain, skin as well as kidney partially derive from yolk sac progenitors and develop independently of MDPs[10]. Monocytes are described as blood-circulating leukocytes that do not proliferate under steady state conditions[8]. In total, they represent 4% of all leukocytes in murine blood[11].

Monocytes play an important role during both homeostasis and immunity and harbor various effector functions, which involve phagocytosis of apoptotic cells, digestion of microorganisms as well as scavenging of toxic products[11, 12, 13]. Moreover, these cells produce several effector molecules, such as cytokines and chemokines, to recruit other immune cells and interact with them[14]. Typical morphological features of monocytes are an irregular cell shape with oval- or kidney-shaped nucleus, cytoplasmic vesicles and a high cytoplasm-nucleus ratio[11]. Moreover, murine blood monocytes are defined by a typical forward scatter- (FSC-) side scatter- (SSC-) profile in flow cytometric analysis and the expression of CD115, CD11b and F4/80[11, 15]. When blood monocytes enter the tissue CD115 expression is downregulated and they differentiate into macrophages and DCs[16].

Blood monocytes are classified into two subtypes dependent on their differential expression of the Ly6C antigen. Ly6C is recognized by different antibody-clones, the AL-21 clone is specific for Ly6C, whereas the anti-Gr1 antibody binds to Ly6C and to Ly6G. The latter is exclusively expressed by neutrophils. In this work, the anti-Gr1 antibody in combination with antibodies against monocyte/macrophage-specific antigens (CD115, F4/80) was used to discriminate between Ly6C^{high} monocytes and neutrophils. To this end, the above-mentioned blood monocyte subtypes are referred to as Gr1^{high} and Gr1^{low} monocytes throughout the thesis.

Gr1^{high} (Ly6C^{high}) monocytes express high levels of CCR2 and low levels of CX_3CR1 and are termed inflammatory monocytes, whereas Gr1^{low} (Ly6C^{low}) monocytes lack CCR2, but express high levels of CX_3CR1. The latter are often referred to as resident or patrolling monocytes. Moreover, Gr1^{high} monocytes are larger (10-14 µm) and contain more granules than Gr1^{low} monocytes which are 8-12 µm in size[17]. These two monocyte subtypes are not only phenotypically distinct, but also exhibit functional differences (Fig. 2.2).

Gr1^{high} monocytes are considered as classical monocytes, that under inflammatory conditions, are rapidly recruited towards the site of infection and injury, where they enter the tissue and differentiate into macrophages and TNF- and inducible nitric oxide synthase (iNOS)- producing DCs, known as TipDCs[18, 19, 20]. Gr1^{high} monocytes have high phagocytic capability and play a major role in pathogen defense in diverse infectious

models by initiating inflammatory M1-type responses[17, 21]. Moreover, it was shown that Gr1^{high} monocytes are essential for the initiation of naïve T cell responses *in vivo*[22, 23].

In contrast, resident Gr1^{low} monocytes have longer half-lives in blood and survey vascular endothelial cells under homeostatic conditions[11]. To this end, they are crawling on endothelial cells of blood vessels and scavenge cell debris, pathogens and oxidized lipids[24, 25]. Notably, Gr1^{low} monocytes also exhibit important function under inflammatory conditions by initiating early inflammatory responses. For example upon *Listeria monocytogenes* infection, Gr1^{low} monocytes have been shown to migrate into the inflamed peritoneum, where they secrete chemokines to recruit other inflammatory phagocytes, such as neutrophils[24]. However, within the inflamed tissue patrolling Gr1^{low} monocytes differentiate into alternatively activated macrophages, also called M2-like macrophages, which promote wound healing, angiogenesis and tissue repair[11, 26].

Macrophages (F4/80$^+$, CD11b$^+$, Gr1$^-$) are resident phagocytes, which are present in lymphoid and non-lymphoid tissues [8]. In this thesis, resident F4/80-expressing Gr1^{low} cells in the kidney were defined as Gr1^{low} macrophages. Under steady state conditions, they play an important role in tissue homeostasis through the production of growth factors and removal of apoptotic cells[14]. Comparable to monocytes, macrophages engulf and digest pathogens and toxins. Further, they modulate immune responses by producing inflammatory mediators such as cytokines, chemokines and reactive oxygen species (ROS), which are involved in pathogen-defense[2, 27].

2.2.1 Terminology of monocytes and macrophages

As described above Gr1^{high} monocytes are rapidly recruited from the blood to the tissue under inflammatory conditions[11]. Accordingly, Gr1^{high} cells in both, blood (CD115$^+$) and tissue (F4/80$^+$), are termed Gr1^{high} monocytes throughout this thesis. In contrast, Gr1^{low} F4/80$^+$ cells, which are present in the organ during steady-state condition resemble resident tissue macrophages. For this reason, Gr1^{low} F4/80$^+$ cells in the kidney are referred to as Gr1^{low} macrophages, whereas Gr1^{low} CD115$^+$ cells in the blood are termed Gr1^{low} monocytes.

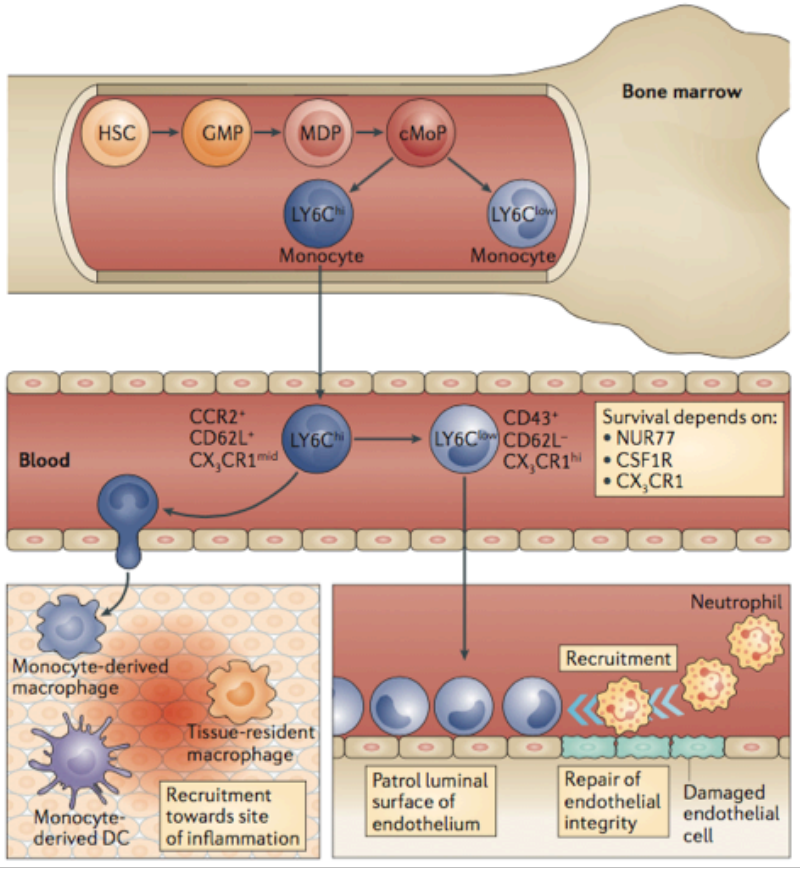

Figure 2.2: The mouse monocyte compartment.
Monocytes are generated from hematopoietic stem cells (HSCs) via precursor cells, namely macrophage and dendritic cell precursor (MDP) and common monocyte progenitor (cMoP). In the blood, two types of monocytes, $Gr1^{high}$ ($Ly6C^{high}CCR2^{+}/CD62L^{+}/CX_3CR1^{mid}$) and $Gr1^{low}$ ($Ly6C^{low}CCR2^{-}/CD62L^{-}/CX_3CR1^{high}$) monocytes, exist. The latter can develop from $Gr1^{high}$ monocytes in the blood. Both subtypes have distinct function. The classical $Gr1^{high}$ monocytes are recruited to the site of inflammation, where they give rise to tissue macrophages and DCs. In contrast $Gr1^{low}$ monocytes survey the endothelial surface, promote wound healing and recruit neutrophils to maintain endothelial integrity. Figure was adopted from Ginhoux, F. and S. Jung, Nature Reviews Immunology, 2014[9].

2.2.2 Role of CCR2 for bone marrow emigration of $Gr1^{high}$ monocytes into circulation

The chemokine receptor 2 (CCR2) is expressed on $Gr1^{high}$ monocytes and binds to the monocyte chemoattractant protein-1 (CCL2), which mediates chemotaxis of these cells. Serbina *et al.* showed that CCR2 mediates the egress of $Gr1^{high}$ monocytes from bone marrow into circulation, but is dispensable for the recruitment from the blood stream into the spleen in a murine *listeria monocytogenes* infection model[28]. Consistent with these findings, it was shown in a mouse model for urinary tract infection that CCR2 is required for the release of $Gr1^{high}$ monocytes from the bone marrow into the blood, but not required for its migration into the infected bladder[29]. Moreover, CCR2-deficient

(*Ccr2*$^{-/-}$) mice have reduced numbers of inflammatory Gr1^{high} monocytes in the blood under steady state and infectious conditions. However, upon microbial infection the number of monocytes is elevated within the bone marrow indicating that the Gr1^{high} monocytes accumulate there[28]. Consistently, targeting CCR2-ligands (e.g CCL2) also leads to decreased numbers of Gr1^{high} monocytes in murine blood[30].

In contrast, the number of Gr1^{low} monocytes in the blood of *Ccr2*$^{-/-}$ mice is unchanged, indicating that the bone marrow emigration of Gr1^{low} monocytes is CCR2-independent[29].

2.2.3 Role of CX_3CR1 in Gr1^{low} monocyte/macrophage function

CX_3CR1 has been shown to play an important role in the patrolling function of Gr1^{low} blood monocytes[31]. Intravital microscopy revealed reduced patrolling behavior in blood vessels of mice deficient in CX_3CR1 (*Cx$_3$cr1*$^{gfp/gfp}$)[24]. In a bacterial infection model it was shown, that CX_3CR1 is required for early recruitment of Gr1^{low} blood monocytes and partially also for recruitment of Gr1^{high} blood monocytes to the spleen[32]. Moreover, CX_3CR1-signaling provides survival signals for Gr1^{low} blood monocytes and resident Gr1^{low} macrophages in the tissue[33, 34, 35]. Thus, in the absence of this receptor, the numbers of Gr1^{low} blood monocytes and Gr1^{low} tissue macrophages are significantly reduced under homeostatic and inflammatory conditions[33, 35].

2.3 Neutrophil Granulocytes

General features

Neutrophil granulocytes are the most abundant cell type in the category of granulocytes, which also includes eosinophils, basophils and mast cells. Latter cell types are essential for immune responses against parasites and in allergy reactions. The term “Granuloycte” is attributed to the high number of granules and secretory vesicles in the cytoplasm of these cells[36]. Moreover, neutrophil granulocytes are also termed as polymorph nuclear cells (PMN) due to its segmented nucleus. They are the most abundant leukocytes within human blood (50-70%) and have a rather small size with 7-10 µm in diameter[37]. In mice, neutrophils constitute about 10-25% of white blood cells. They are short-lived cells with a half-life of about 1 h and 8 h in the circulation in mice

and humans respectively. However, upon inflammatory stimulation the life-span of neutrophils has been shown to increase up to several days[38].

Origin and maturation

Neutrophils are generated within the bone marrow from the hematopoietic stem cell precursor (HSC) via myeloid intermediates, including myeloblast, promyelocyte, myelocyte, metamyelocyte and band cell[39]. The generation of neutrophil granulocytes, called granulopoiesis, is driven by the granulocyte-colony stimulating factor (G-CSF)[40]. The retention and release of mature neutrophils from the bone marrow is regulated by the chemokine receptors CXCR2 and CXCR4[39].

Effector function

Neutrophils are efficient effector cells and the first leukocyte to be recruited during infections. Humans with reduced neutrophil counts in blood suffer from severe infections, underlining the major importance of these cells in pathogen defense[41]. Neutrophils use diverse intra- and extracellular strategies to eliminate pathogens (Fig. 2.3). Upon pathogen encounter, neutrophils phagocytose infectious particles and subsequently kill them by either reactive oxygen species (ROS) or by antimicrobial proteins stored within granules. Furthermore, the content of the granules can also be secreted to destroy extracellular pathogens[42]. Three different types of secretory vesicles are distinguished: the azurophilic/primary vesicles containing myeloperoxidases (MPO), specific/secondary granules, which contain lactoferin and cytochrome b558, and gelatinase/tertiary granules containing metalloproteinase-9 (MMP-9). Another important mechanism to eliminate pathogens is a process termed as NETosis, in which neutrophils release commonly called neutrophil extracellular traps (NETs) consisting of DNA, histones and antimicrobial proteins. These NETs immobilize microorganisms and facilitate subsequent phagocytosis as well as direct killing of pathogens[43].

Besides pathogen clearance, neutrophils are important for initiating and regulating innate and adaptive immune responses by releasing cytokines and other inflammatory mediators[14].

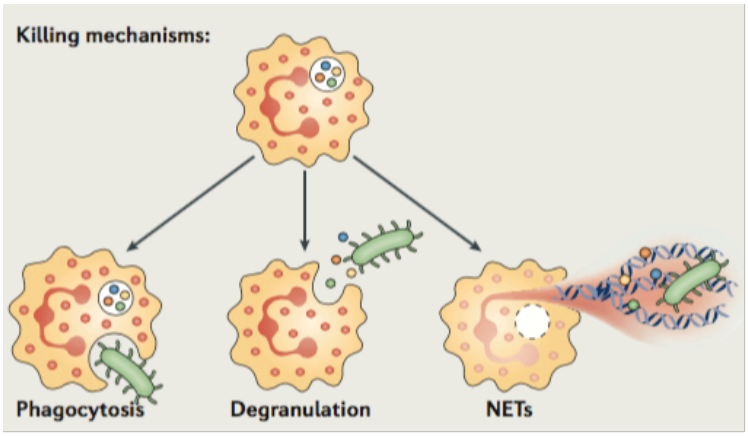

Figure 2.3: Pathogen-elimination strategies of neutrophils.
The three major killing mechanisms of neutrophils are phagocytosis of pathogens, degranulation of secretory vesicles and NET formation. Figure was adopted from Kolaczkowska, E. and P. Kubes, Nature Reviews Immunology, 2013[37].

Extravasation

During inflammation, neutrophils are recruited from circulation into the organ to execute their effector functions. This process, commonly known as extravasation, is a multiple-step cascade involving neutrophil rolling, adhesion, crawling, and transmigration (Fig. 2.4). The extravasation is regulated by chemokines and adhesion proteins (e.g. selectins, integrins), which are expressed on the granulocytic and endothelial cell surface. The cascade is initiated by resident macrophages, which produce inflammatory mediators (e.g. CXCL1/2, TNF-a, IL1b) upon pathogen encounter. These mediators stimulate endothelial cells to express selectins (e.g. P-selectin, E-selectin), which facilitate a loose contact between the endothelial cell and the neutrophil, a process also known as "tethering". Moreover, neutrophils bind to chemokines (e.g. CXCL1) on the endothelial surface via chemokine receptors (e.g. CXCR2), leading to conformational changes of granulocytic integrins from an inactive to an active state. This enables binding of integrins on neutrophils, such as the Lymphocyte Function-associated Antigen (LFA-1, CD18/CD11a) or the Very Late Antigen-4 (VLA-4, CD49d/CD29), to the corresponding endothelial ligands, e.g. Intracellular Adhesion Molecule-1 (ICAM-1) and Vascular Cell Adhesion Molecule-1 (VCAM-1). The binding of activated integrins to the adhesion molecules on the endothelial surface is named "adhesion". In order to reach the appropriate site for transmigration, neutrophils crawl along the endothelial lining ("crawling"). Finally,

neutrophils transmigrate either between or through endothelial cells to leave the vasculature and enter the inflamed tissue[37].

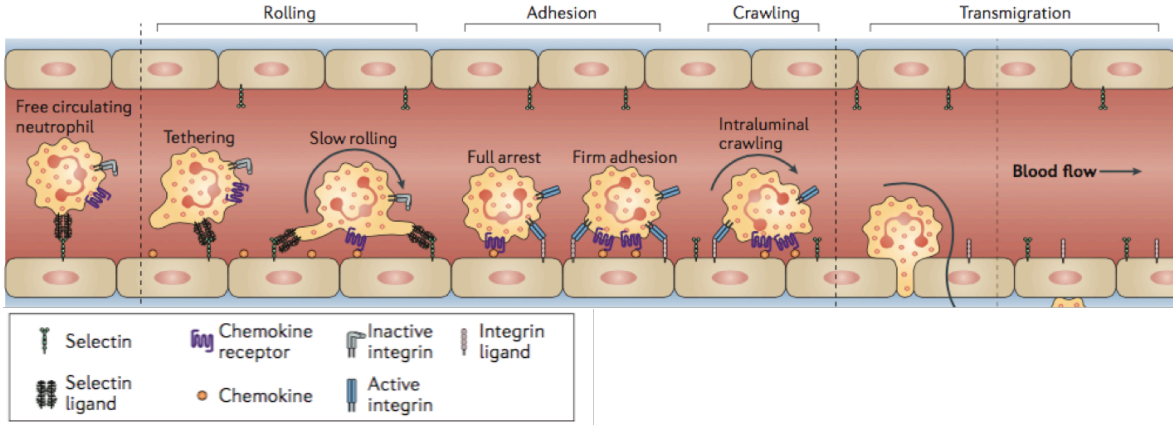

Figure 2.4: The extravasation cascade of neutrophils.
The figure shows an overview about the sequential steps of the neutrophil recruitment cascade including rolling, adhesion, crawling and transmigration. The rolling is selectin-dependent and the subsequent steps are mainly mediated by integrins. Chemokines (e.g. CXCL1) on the endothelial surface activate granulocytic integrins, which facilitates adhesion. A chemokine gradient guides neutrophils to the site of transmigration. Figure was adopted from Kolaczkowska, E. and P. Kubes, Nature Reviews Immunology, 2013[37].

Antigen expression

Phenotypically, neutrophils can be clearly distinguished from other myeloid cells by their unique expression of the Ly6G antigen[44]. In addition, they are described to express Ly6C, CD11b, and CXCR2 on their surfaces[45]. In flow cytometry, blood neutrophils can also be distinguished by their unique FSC-and SSC-profile due to their small size and high content of granules in the cytoplasm[46, 47].

2.4 The Kidney: Anatomy and Physiology

Kidneys are paired, bean-shaped excretory organs, which are located in the retroperitoneal space within the abdomen[48]. Their main function is to regulate the acid-base homeostasis and the water-electrolyte balance. To this end, blood is filtered and substances needed are retained within the body while the rest is excreted with the urine. Additionally, the kidney also regulates blood-pressure and fulfills important endocrine functions, such as the production of hormones (e.g. rennin and calciterol)[49].

Macroscopically, the kidney parenchyma can be divided into two main compartments: outer renal cortex and inner renal medulla (Fig. 2.5 cross section). The functional unit of the kidney is the nephron, that can be structured into a single glomerulus surrounded by a Bowman`s capsule, the proximal tubules, loop of Henle, and the distal tubule which ends in the collecting tube[50] (Fig. 2.5). The nephron spans the cortical and medullar parts of the kidney. The glomerulus, the proximal, and the distal tubule system are located within the cortex. While the descending arm of the loop of Henle leaves the cortex and enters the medulla, the ascending limb passes back to the cortex, where the distal tubule ends within the collecting tube[51].

The glomerulus is a network of capillaries and considered the major filtration unit of the kidney in which the blood is filtered to form primary urine[49]. This filter is composed of capillary endothelial cells, basal membrane and podocytes (Fig. 2.5). All large molecules such as proteins are retained, whereas smaller substances (≤ 45 kDa) such as water and ions are secreted into the primary urine. Interestingly, the filtration is not only dependent on size but also on the electrical charge of the substances[52, 53]. A recent study revealed approximately 14000 glomeruli per murine kidney by using novel imaging techniques involving fully automated evaluation[54]. Moreover, the glomerulus has an important function in assessing kidney health, because the filtration capability can be diminished in renal diseases (e.g glomerulonephritis)[55]. Under pathological conditions, urinary excreted substances, such as urea and creatinine, are improperly filtered leading to accumulation of these products resulting in elevated blood-urea-nitrogen (BUN) and creatinine (Crea) levels in the serum. An additional indicator for renal diseases is the presence of large molecules (> 45 kDa), e.g. proteins, in the urine[56, 57].

Many kidney diseases are classified as immune-mediated, in which pathogenic immune responses are initiated. This underlines the need for investigating and understanding the immune mechanisms in the kidney[50].

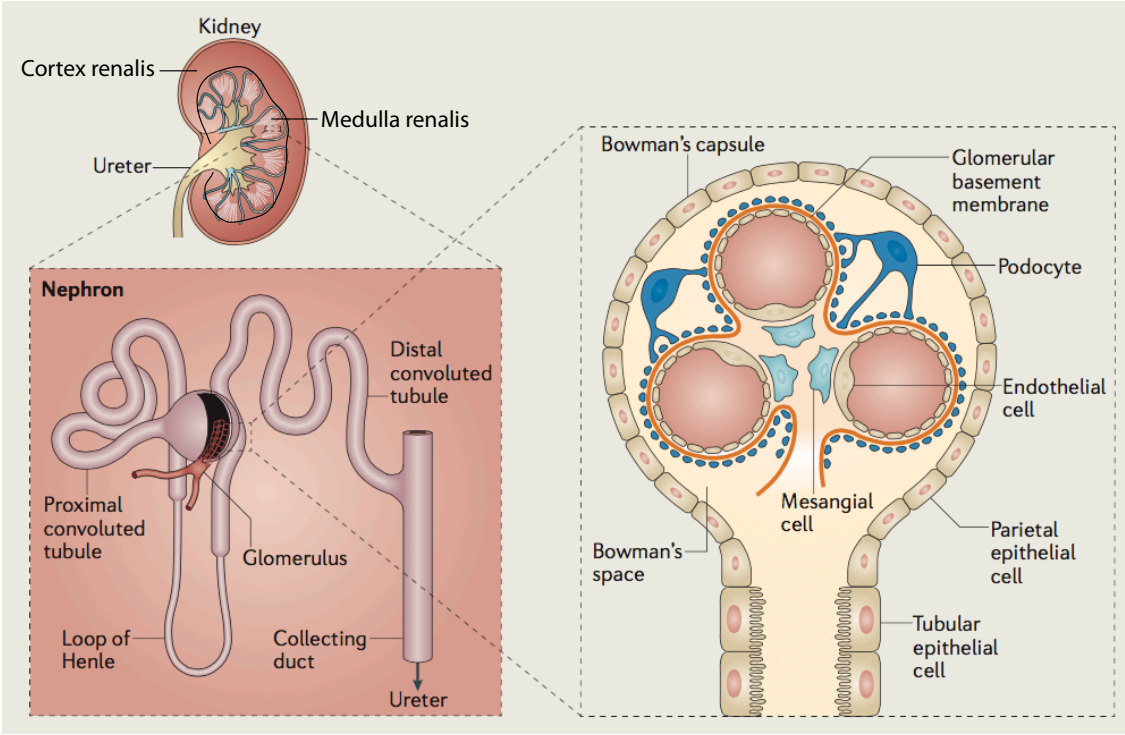

Figure 2.5: Basic anatomy of the kidney.
The upper figure shows a cross section of a kidney and its two compartments, the cortex renalis (outer area) and the medulla renalis (inner area). The kidney consists of several nephrons, which represent its structural and functional unit. A nephron consists of a glomerulus and a tubulus system. The glomeruli are located in the renal cortex and are responsible for blood filtration. The glomerular filtration barrier is built up of endothelial cells of the capillary, the glomerular basement membrane, and specialized epithelial cells, called podocytes. Modified from Kurts, C., et al., Nature Reviews Immunology, 2013[50].

2.5 The Hemolytic Uremic Syndrome (HUS)

2.5.1 Definition and epidemiology

The hemolytic uremic syndrome (HUS) is clinically defined as microangiopathic hemolytic anemia (loss of erythrocytes through destruction), thrombocytopenia (reduced platelet counts) and acute kidney injury (AKI)[58]. The main cause of this disease is an infection with Shiga toxin (Stx)-producing enterohaemorrhagic *Escherichia coli*, abbreviated as STEC[59]. The incidence of STEC-HUS is about 2 in 100.000. However, young children under the age of 5 years are affected more often by STEC-HUS (incidence of 6 in 100.000) making it the major cause of renal failure within childhood[59, 60]. STEC-HUS is a life-threatening disease with a mortality rate of 5-10% and even after survival many patients suffer from residual complications, such as renal injury and life-

long requirement for dialysis[61]. STEC-HUS is classified as a water- and food-borne disease in which patients get infected through the uptake of contaminated food or liquid[58, 62, 63]. The natural reservoir for STEC is cattle, but STEC were also detected in domestic animals[64]. Around 5-15% of patients which have been infected by STEC develop HUS, although the virulence differs between bacterial serotypes[65]. The most common serotype that causes STEC-HUS is O157:H7[58]. However, the recent outbreak in June 2011 in Europe, predominantly within Northern Germany, was caused by the serotype O104:H4. This serotype carried a 22% risk of developing HUS. In total, out of the 3.816 cases that were infected with this serotype 845 patients developed HUS among which 34 cases of death were reported[13, 66]. The pathogenicity of STEC is mediated by the ability to produce Shiga toxins (Stx). There are two types of Stx, Stx1 and Stx2, which have 56% homology at the amino acid level[67].

2.5.2 Shiga toxin in the pathogenesis of HUS

Pathogenesis of HUS

Upon intake of STEC-contaminated food or water, Stx is released within the gastrointestinal tract. Then, Stx passes the gastrointestinal epithelial cell barrier via a transcellular route and reaches the circulation[59]. However, it is unknown how Stx reaches its main target organs, because free Stx could not be detected in the serum of HUS patients so far[68]. It is discussed that blood cells, in particular neutrophils, might serve as shuttles, which transfer Stx to the target organs[69, 70, 71, 72] by binding Stx with a low affinity receptor[61]. Within the target organ Stx binds to its high affinity receptor globotriaosylceramide 3 (Gb3), a ceramide that is expressed on the endothelial surface. Gb3 is strongly expressed on endothelial cell within the kidney and the central nervous system (CNS)[73, 74, 75]. To this end, kidney and brain are referred to as main target organs for STEC-HUS[59].

Toxic effects of Stx

Due to their molecular configuration, Stx are classified as AB_5 proteins consisting of a single enzymatically active A-subunit and a pentameric B-subunit, which mediates binding to Gb3[75, 76]. After binding the receptor, Stx is internalized by endocytosis and subsequently transferred via the endosomes and the Golgi apparatus to the

endoplasmic reticulum, where the A-subunit is released from the B-subunit[59, 77]. Then, the enzymatically active A-subunit is translocated to the cytoplasm and exerts its toxic effects as an RNA N-glycosidase by cleaving an adenosine base of the 28S RNA of eukaryotic ribosomes[78, 79]. This results in a ribotoxic stress-response and inhibition of the protein synthesis causing cell death[59]. This endothelial cell death leads to exposure of subendothelial collagen to which platelets can bind via glycoprotein VI (GpVI). Subsequently, adhesive platelets aggregate and form a thrombus. As a consequence of thrombus formation, erythrocytes are destroyed within the narrow blood vessels leading to microangiopathic hemolytic anemia[61, 80].

Importantly, Stx also induces a systemic inflammatory response through increased production of inflammatory mediators by endothelial cells and leukocytes and an enhanced activation of the alternative complement pathway[59, 75, 81, 82, 83].

Treatment options

Antibiotic treatment for HUS patients is still controversially discussed, due to emerging evidence that the Stx-release is increased upon antibiotic treatment, which worsens the clinical outcome in patients[61, 64]. Currently, the therapy for STEC-HUS ranges from fluid- and electrolyte management, nutrition supply, control of hypertension to plasma exchange, dialysis and renal replacement[61, 75]. However, current management represents a rather supportive care as a promising STEC-HUS specific therapy is still missing[61] underlining the importance of this study.

2.6 Innate Immunity in HUS

There is emerging evidence that host immunity and myeloid cells in particular, such as monocytes/macrophages and neutrophils, play a pivotal role within the pathogenesis of HUS.

2.6.1 Role of monocytes/macrophages in HUS

Although monocytes have been shown to express the Stx-receptor Gb3 on their surface, these cells are resistant towards Stx-mediated cytotoxicity[84]. Instead, Stx-binding induces synthesis and secretion of pro-inflammatory cytokines in monocytes. It has been shown, that the monocytic cell line THP-1 and circulating blood monocytes

produce pro-inflammatory cytokines including IL-1β, IL-6 and TNF-α upon Stx-stimulation[82, 85, 86, 87, 88]. These findings were corroborated by studies in HUS patients, demonstrating elevated TNF-α level in urine and serum[89, 90]. These monocyte-produced inflammatory mediators can in turn sensitize endothelial cells towards Stx by inducing Gb3 expression on the target cells[91, 92, 93].

Moreover, endothelial cells have also been shown to secrete chemokines, which recruit and activate monocytes and macrophages. For instance, the monocyte chemoattractant CCL2 was produced by endothelial cells upon Stx-treatment *in vitro*[83]. Also in HUS patients, CCL2 levels were increased concomitant with elevated monocyte counts in human kidney biopsies[94]. Keepers *et al.* showed that inhibition of monocyte-recruiting chemokines (CCL2, CCL3, CCL4 and CCL5) reduces the infiltration of monocytes into the kidney and leads to decreased fibrin deposits in a mouse model of HUS[95]. These findings suggest an essential role for monocytes/macrophages in HUS. However, the contribution of the corresponding chemokine receptor (CCR2) and the specific role of monocyte/macrophage subtypes to Stx-mediated renal damage during HUS are still elusive.

2.6.2 Role of granulocytic neutrophils in HUS

In addition to macrophages, neutrophils have also been shown to intensify Stx-mediated toxic effects. As mentioned before, a potential role for neutrophils as Stx-carriers from circulation to the target organ has been suggested[69, 72]. Moreover, neutrophils exhibit an activated state with increased expression and release of reactive oxygen species, neutrophil elastase and NETs during HUS[96, 97, 98, 99]. Furthermore, Stx-stimulated endothelial cells express IL-8 (functionally homologous to CXCL1/2 in mice), which is a potent chemoattractant for neutrophils[83]. In accord with this *in vitro* data, HUS patients show elevated IL-8 levels in the serum and increased neutrophil counts, which correlates with poor clinical prognosis and increased mortality[100]. Moreover, reduced abundance of neutrophils limited the kidney damage and mortality in a Stx-mouse model[101, 102]. However, the contribution of chemokine-dependent recruitment and subsequent integrin-dependent adhesion of neutrophils to the renal microvasculature needs to be investigated.

2.7 HUS Mouse Model

In this study, a murine HUS model was utilized to investigate the role of monocytes, macrophages and neutrophils in this disease. Diverse HUS-mouse models, which differ in administration route of the toxin, inflammatory stimuli, Stx-type and Stx-concentrations are established[81, 95, 101, 103]. In this study Stx type 2, instead of type 1, was chosen as Stx2 is related to more severe diseases and has the higher chance to induce HUS[75]. The purified Stx2 was injected in combination with lipopolysaccharide (LPS), a compound of the outer membrane of Gram-negative bacteria, to mimic an infection with STEC. Previous studies have also shown, that LPS enhances the cytotoxic effects of Stx[103]. It is well described that Stx enters into circulation directly after passing gastrointestinal epithelial cells and mediates its toxic effects on endothelial cells[59]. Thus, Stx/LPS was administered intravenously to ensure localization within the blood vessels.

3 Aims of the Thesis

An involvement of monocytes, macrophages and neutrophils in HUS has been shown previously, but the contribution of specific monocyte/macrophage subsets and chemokine receptor-dependent recruitment in HUS remain elusive. Moreover, effective intervention strategies are still missing. This thesis aimed at investigating chemokine receptor-mediated recruitment of the aforementioned myeloid cells to the kidney and at identifying myeloid-specific key-mediators in HUS pathogenesis.

To this end a murine Stx-induced HUS model, which results in reduced kidney functionality had to be established. The composition of the monocyte/macrophage compartment and of neutrophils in blood and kidney of Stx-treated C57BL/6 mice was analyzed by flow cytometry. Next, the chemokine profile in kidney homogenates of Stx/LPS-injected mice was examined to identify potential stimuli for myeloid cell recruitment. Furthermore, myeloid cells and endothelial damage were localized by novel imaging techniques in order to evaluate the contribution of myeloid cells to kidney damage. To further investigate the role of distinct monocyte/macrophage subtypes in Stx-induced kidney injury, transgenic *Ccr2*-deficient mice, which lack inflammatory $Gr1^{high}$ monocytes and $Ccr2^{-/-}$ x $Cx_3cr1^{gfp/gfp}$ mice, which showed reduced numbers of $Gr1^{high}$ monocytes and $Gr1^{low}$ macrophages in the kidney, were employed.

The second aim of this study was to analyze the role of neutrophil recruitment to endothelial damage in HUS. As integrins and chemokine receptors are crucial for neutrophil-recruitment, these molecules were conditionally blocked either by the administration of antibodies and inhibitors or by employing constitutive knock out mice.

A thorough understanding of the role of distinct monocyte/macrophage subtypes and neutrophil recruitment in Stx-induced kidney damage enhances the understanding of this disease and facilitates the development of therapeutic agents to specifically target myeloid cells, potentially improving the clinical outcome in HUS.

4 Material and Methods

4.1 Material

4.1.1 Mice

Mice were used between 7-14 weeks of age and had been backcrossed for more than 10 generations to C57BL/6 mice. For intravital imaging juvenile mice in the age of 3-4 weeks were used, due to elevated numbers of superficial glomeruli in these mice. Mice were bred and maintained under pathogen-free conditions at the animal facilities of the University Clinic Essen and Bonn (House of Experimental therapy, HET). All mouse experiments were approved by governmental review boards (Bezirksregierung Köln, Landesamt für Natur, Umwelt und Verbraucherschutz NRW in Recklinghausen, Germany).

Cx$_3$cr1$^{gfp/+}$, *Ccr2$^{-/-}$*, *Ccr2$^{-/-}$ x Cx$_3$cr1$^{gfp/+}$* and *Ccr2$^{-/-}$ x Cx$_3$cr1$^{gfp/gfp}$* mice were used to investigate the role of monocytes and macrophages for disease development. To generate *Ccr2$^{-/-}$ x Cx$_3$cr1$^{gfp/+}$* and *Ccr2$^{-/-}$ x Cx$_3$cr1$^{gfp/gfp}$* mice, *Ccr2$^{-/-}$* mice[104] were crossed to *Cx$_3$cr1$^{gfp/gfp}$* mice[105] and subsequently the F1 population was backcrossed. *Cxcr2$^{d/d}$* mice[106] and heterozygous littermate controls were kindly provided by Ulf Panzer, III. Medical Clinic, Medical Center Hamburg-Eppendorf, Hamburg, Germany.

Table 4.1: Mouse strains

Mouse strain	Description
C57BL/6	Inbred wildtype mouse strain
Cx$_3$cr1$^{+/gfp}$	C57BL/6 background, reporter mouse line for CX_3CR1 expressing cells. One *Cx$_3$cr1* allele is transgenic with expression of EGFP under the endogenous *Cx3cr1* locus[105]
Cx$_3$cr1$^{gfp/gfp}$	C57BL/6 background, deficient in CX_3CR1, cells express EGFP under the endogenous *Cx$_3$cr1* locus[105]
Ccr2$^{-/-}$	C57BL/6 background, deficient in CCR2, which leads to an impaired bone marrow (BM) emigration of $Gr1^{high}$ monocytes into the periphery[104]
Ccr2$^{-/-}$ Cx$_3$cr1$^{+/gfp}$	C57BL/6 background, reporter mouse line for CX_3CR1 expressing cells, impaired BM emigration of $Gr1^{high}$ monocytes into the periphery due to CCR2-deficiency
Ccr2$^{-/-}$ Cx$_3$cr1$^{gfp/gfp}$	C57BL/6 background, deficient in CCR2 and CX_3CR1. Cells

	express EGFP under the endogenous *Cx3cr1* locus, impaired BM emigration of Gr1^{high} monocytes into the periphery due to CCR2-deficiency
Cxcr2$^{d/d}$	C57BL/6 background, deficient in CXCR2, reduced neutrophil recruitment[106]

4.1.2 Chemicals/Reagents

Table 4.2: Chemicals/Reagents

Chemical/Reagent	Company
Ammonium chloride (NH_4CL)	Carl Roth, Karlsruhe
Bovine Serum Albumin (BSA) Fraction V	PAA Laboratories GmbH, Pasching, Austria
Calibrite APC beads	BD Biosciences, Heidelberg
Collagenase D	Sigma-Aldrich, München
[^{64}Cu]NOTA-GPVI-Fc tracer	Werner Siemens Imaging Center, Tübingen
CXCR2 Antagonist (SB 225002)	Sigma-Aldrich, München
Complete Protease Inhibitor Mix	Roche, Karlsruhe
DNase	Sigma-Aldrich, München
Dimethyl sulfoxide (DMSO)	PanReac, AppliChem, Darmstadt
Disodium phosphate (Na_2HPO_4)	Carl Roth, Karlsruhe
Ethanol, ≥ 99,5%	Carl Roth, Karlsruhe
Ethanol, 70%	Carl Roth, Karlsruhe
Ethylenediaminetetraacetic acid (EDTA) Di-sodium salt	Carl Roth, Karlsruhe
Fetal calf serum (FCS)	Biochrome, Berlin
Fluorescein isothiocyanate (FITC)-dextrane	Sigma-Aldrich, München
Forene 100% (Isofluorane)	Abbott GmbH & CoKG, Wiesbaden
Heparin-Natrium 25.000	Ratiopharm, Ulm
High vacuum silicone grease	Sigma-Aldrich, München
Hoechst 33342 trihydrochloride, trihydrate	Invitrogen, Karlsruhe
Immu Mount	Sakura Finetek, Torrance, CA, USA
10% Ketamine	Bela-pharm, Vechta Medstar, Holz-Wickede
L-Lysine monohydrochloride	Sigma-Aldrich, München
Lipopolysaccharide (LPS)	Invivogen, San Diego, USA
Monosodium phosphate (NaH_2PO_4)	Sigma-Aldrich, München
OneComp eBeads	Ebioscience, Frankfurt

95% Paraformaldehyde (PFA)	Sigma-Aldrich, München
PBS tablet	*life*Technologies, Darmstadt
Penicillin/Streptomycin	PAA Laboratories GmbH, Pasching, Austria
Privigen hIgG 100mg/ml (10%)	CSL Behring, Marburg
Protease Inhibitor Mix	Roche, Mannheim
Sodium azide (NaAzid)	Carl Roth, Karlsruhe
Sodium hydrogen carbonate ($NaHCO_3$)	Carl Roth, Karlsruhe
Sodium hydroxide (NaOH)	Carl Roth, Karlsruhe
Shiga Toxin 2 purified	Toxin Technology, Sarasota, USA
D (+) Succrose	Carl Roth, Karlsruhe
TissueTek O.C.T. Compound	Sakura Finetek, Torrance, CA, USA
Triton-X 100	Carl Roth, Karlsruhe
Trypan blue solution	Sigma-Aldrich, München
Veterinary tissue glue (Surgibond)	Sutures, Wrexham, UK
2% Xylazine	Ceva, Libourne, France

4.1.3 Antibodies/Dyes

Table 4.3: Antibodies used for flow cytometry

Antigen	Clone	Fluorophore	Dilution	Company
CD11b	M1/70	APC	1:200	BioLegend, Fell
CD45	30-F11	APC cy7	1:400	BioLegend, Fell
		BV421	1:200	
CD115	AFS98	APC	1:200	BioLegend, Fell
		BV421	1:200	
		PE	1:200	
F4/80	BM8.1	APC	1:200	Tonbo Biosciences,
		PE	1:200	San Diego, USA
Ly6G	1A8	FITC	1:200	BioLegend, Fell
Gr1	RB6-8C5	PerCPcy 5.5	1:1000	BioLegend, Fell

Table 4.4: Antibodies/Dyes for histology/intravital microscopy

Antigen	Clone	Fluorophore	Dilution	Company
DAPI	n/a		1:5000	*life*Technologies, Darmstadt

F4/80	BM8.1	APC	1:100	Tonbo Biosciences, San Diego, USA
Gr1	RB6-8C5	PE	10µl (2µg) i.v	BioLegend, Fell
QTracker655	n/a	Qdot® 655 nanocrystals	10µl (0,2µM) i.v	*life*Technologies, Darmstadt

Table 4.5: Antibodies for *in vivo* experiments

Antigen	Clone	Injected dose (µg/g bodyweight)	Company
CD49d	P/S2	5	BioXCell, Bicester, UK
CD18	M18/2	5	BioXCell, Bicester, UK
CD29	KMI6	5	BioXCell, Bicester, UK
Gr1	RB6-8C5	0,1	BioLegend, Fell
Isotype IgG2a	2A3	5	BioXCell, Bicester, UK
Isotype IgG2b	LTF-2	5	BioXCell, Bicester, UK
VCAM-1	112734	5	R&D Systems, Wiesbaden

4.1.4 Solutions/Buffers/Media

Table 4.6:Solutions/Buffers/Media

Solutions/buffers media	Composition	Storage
Anesthesia	8 ml 1x PBS 1 ml Ketamine (100 mg/ml) 1 ml Xylazine (20 mg/ml)	4 °C
Digestion buffer	RPMI 1640 10% FCS 1% Penicillin/Streptomycin 0,1% NaAzid	4 °C
FACS buffer	1x PBS 2% FCS 0,1% NaAzid	4 °C
IHC Blocking Buffer	50 ml PBT 500 µg BSA	4 °C
20% Paraformaldehyde (PFA)	20 g PFA 80 ml PBS heat to max. 70 °C add NaOH until the solution is clear	-20 °C

	fill up to 100 ml with PBS adjust pH to 7,4	
1x PBS	1 tablet in 500 ml ddH_2O	4 °C
PBT	500 ml 1xPBS 250 µl Triton-X 100	4 °C
L-Lysine solution (0,2 M)	6,59 g L-Lysine 200 ml P-buffer	-20 °C
Na_2HPO_4 (0,2 M)	14,2 g Na_2HPO_4 500 ml ddH_2O	RT
NaH_2PO_4 (0,2 M)	6,24 g NaH_2PO_4 200 ml ddH_2O	RT
P-buffer	243 ml Na_2HPO_4 57 ml NaH_2PO_4 300 ml ddH_2O adjust pH to 7,4	-20 °C
Protease Inhibitor Mix	1 tablet complete protease inhibitor mix (Roche, Mannheim) 10 ml PBS	Was prepared shortly before use, on ice
PLP buffer	6,25 ml 4% PFA 9,4 ml 0,2 M L-Lysine solution 9,4 ml P-Buffer 0,053 g $NaIO_4$ Adjust pH to7,4	Was prepared shortly before use, on ice
RPMI 1640 With HEPES Without L-Glutamine	PAA Laboratories GmbH, Pasching, Austria	4 °C
RCB buffer	145 mM NH_4CL 100 mM EDTA Di-sodium 12 mM $NaHCO_3$ in ddH_2O pH = 7,3	-20 °C
30% Sucrose	60 g D (+) Saccharose 200 ml P-buffer	-20 °C

4.1.5 Kits

Table 4.7: Kits

Kits	Company
NucleoSpin RNA II Kit	Machery-Nagel, Düren
SYBR green PCR Master Mix	Thermo Fisher, Darmstadt
High Capacity cDNA Reverse Transcription Kit	Apllied Biosystems, Darmstadt
LEGENDplex™ Mouse Proinflammatory Chemokine Panel (13-plex)	BioLegend, Fell
LIVE/DEAD® Fixable Near-IR Dead Cell Stain Kit, for 633 or 635 nm excitation	*life*Technologies, Darmstadt
Mouse sVCAM-1/CD106 Quantikine ELISA Kit	R&D Systems, Wiesbaden

4.1.6 Primer

Table 4.8: Primer sequences

Transcript	Forward/reverse	Sequence
KIM-1 (Mm *havcr1)*	Fwd	TCCTGAGGATGTCACAGTGC
	Rev	CACACATGGACTCACAAACCA
HPRT (Mm *hprt*)	Fwd	GTCCCAGCGTCGTGATTAGCGAT
	Rev	GGGCCACAATGTGATGGCCTCC
Mm_Vcam1_1_SG QuantiTect primer assay	Fwd + Rev	*Sequence unknown,* ordered from Qiagen, Hilden

4.1.7 Machines/Equipment

Table 4.9: Machines/Equipment

Machines/Equipment	Type	Company
Autoclave	VX-150	Systec, Linden
Axio Observer.Z1 and Apotome		Zeiss, Oberkochen
Centrifuge	5424R 5819R	Eppendorf, Hamburg Eppendorf, Hamburg

Cryostate	CM1950	Leica, Wetzler
Dispenser/Homogenizer	ULTRA-TURRAX T10	IKA, Staufen
Dissecting microscope	S8AP0	
Electronic Scales	New classic ML	Mettler Toledo, Gießen
Flow cytometer	LSR Fortessa	BD Biosciences, Heidelberg
Fridge/Freezer	+4 °C -20 °C -80 °C	Liebherr, Biberach a. d. Riß
Ice machine	AF 100	Scotman Ice-System, Vernon Hills, USA
Inveon microPET scanners		Siemens Medical Solutions USA, Inc., Knoxville, TN, USA
Isofluorane anestetic device		UNO, Zevenaar, NL
IVC mouse cages	SealSafe PLUS	Tecniplast, Hohenpeißenberg
Laboratrory Counter		BD Biosciences, Heidelberg
Laminar Flow cabinet	Safe2020	Thermo Scientific, Braunschweig
Light cycler	LC480	Roche, Mannheim
Multichannel pipette	Pipet-Lite XLS	Mettler Toledo, Gießen
NanoDrop	ND-1000	PeqLab, Erlangen
Neubauer chamber	Neubauer improved	Hecht-Assistant, Sondheim
Optical microscope	DMIL	Leica, Wetzler
Microplate Reader	FLx-800 LB 90 Mithra	BioTek, Bad Friedrichshall Berthold Technologies, Bad Wildbad
Pipettes		Eppendorf, Hamburg
Shaker	MTS2/4	IKA, Staufen
Storage Phosphor Screen		Molecular Dynamics, Sunnyvale, CA, USA
STORM Phosphor-Imager (Molecular Dynamics)		Molecular Dynamics, Sunnyvale, CA, USA
TCS SP8 MP and FLIM		Leica, Wetzler
Thermocycler		SensoQuest, Göttingen
Thermostat Cabine		Aqualitic, Dortmund
7 T small-animal scanner		Biospec, Bruker Biospin MRI

		GmbH, Ettlingen, Germany
Vortexer	Vortex-Genie 2	Scientific Industries Inc., Bohemia, New York, USA
Waterbath		Julabo, Seelbach

4.1.8 Consumables

Table 4.10: Consumables

Consumables	Company
6-, 12- well plate	TPP, Trasadingen, Switzerland
Centrifuge Tube	Greiner Bio One, Nürtingen
Coverslips 40x 24mm	Oehmen Labortechnik, Essen
Cryomolds	Weckert Labortechnik, Kitzingen
Disposal bag	Oehmen Labortechnik, Essen
Eppendorf tube (0,2; 0,5; 1,5; 2,0 ml)	Sarstedt, Nürnbrecht
Falcon cell strainer 40µm	BD, Heidelberg
Flow cytometer tube	Sarstedt, Nümbrecht
Gloves	B Braun, Melsungen
Heparinized capillary tubes	Brand , Wertheim
Hypodermic needle 0,3 x 13 mm	BD, Heidelberg
Hypodermic needle 0,45 x 23 mm	BD, Heidelberg
Hypodermic needle 0,6 x 25 mm	BD, Heidelberg
Leukosilk	BSN Medical, Hamburg
Light Cycler Multiwell plate 96-well	Roche, Mannheim
Multichannel pipette reservoire	Brand, Wertheim
Nylon net	Oehmen Labortechnik, Essen
PCR 8-er SoftStrips 0,2 µl	Biozym Biotech Trading, Oldendorf
Pipette filter tip 0,2-10 µl	Greiner Bio One, Nürtingen
Pipette filter tip 200 µl	Greiner Bio One, Nürtingen
Pipette filter tip 100-1000 µl	Greiner Bio One, Nürtingen
Pipette tip (10 µl, 200 µl, 1000 µl, 5 ml)	StarLab, Hamburg
Serological pipette (5 ml; 10 ml; 25 ml)	Greiner Bio One, Nürtingen
Syringe 1 ml	BD, Heidelberg
Syringe 10 ml	BD, Heidelberg
Insulin syringe U-100	BD Biosciences, Heidelberg

4.1.9 Software

Table 4.11: Software

Software	Company
Adobe Illustrator CS5	Adobe, San Jose, USA
EndNote X7	Tomson Reuters, New York, USA
FACSDiva 6.0	BD Biosciences, Heidelberg
FCAP Array	Soft Flow, St. Louis Park, MN, USA
FlowJo 8.7	Tree Star Inc., Ashland, USA
GraphPad Prism5	GraphPad, San Diego, USA
Imaris 7.6.5	Bitplane, Zurich, Switzerland
LEGENDplexTM data Analysis Software Version 7.1	BioLegend, Fell
Microsoft Office 2011	Microft, Redmond, USA
Pmod Software	PMOD Technologies Ltd., Zurich, Switzerland
ZEN blue	Zeiss, Oberkochen

4.2 Methods

4.2.1 Mouse model for Stx-induced kidney damage

Due to activity loss of the Shiga toxin 2 (Stx; Toxin Technology, Sarasota, USA) over the time, the appropriate Stx-dose was determined by a lethal challenge experiment before the experiments were conducted. To this end, serial dilutions of Stx in combination with a sublethal dose of LPS (56,25 ng/g mouse; Invivogen, San Diego, USA) diluted in PBS were injected intravenously (i.v.) into mice. The Stx dose that induces 100% mortality between 96 h and 120 h (approximately 2 ng Stx/mouse) was selected for the experiments.

4.2.2 Blocking experiments

To target interactions between VCAM-1 and VLA-4, either a 100 µg VCAM-1 antibody (112734; R&D Systems, Wiesbaden) or 100 µg of antibodies against both VLA-4 subunits (P/S2, KMI6; BioXCell, Bicester, UK) were injected i.v. into the mice 1 h before Stx/LPS administration (d0). The antibody injection was repeated after

24 h and 48 h. To exclude unspecific effects of antibody injection, the control group was injected with appropriate isotype controls. To this end the control group for VLA-4 blocking was injected with 100 µg IgG2a (2A3; BioXCell, Bicester, UK) and 100 µg IgG2b (LTF-2; BioXCell, Bicester, UK).

For blocking the CD18/CD11b axis 100 µg of CD18 antibody (M16/2; BioXCell, Bicester, UK) were injected i.v. 1 h before Stx/LPS injection (d0) and at day 1 and 2 after Stx/LPS administration. The control group was injected with 100 µg IgG2a isotype control (2A3; BioXCell, Bicester, UK) at same time points.

To inhibit the CXCR2-signalling the selective CXCR2 antagonist SB225002 (2 µg/g bodyweight; Sigma-Aldrich, München) or vehicle (1% DMSO in PBS; PanReac, AppliChem, Darmstadt) was injected intraperitoneally (i.p.) 30 min before Stx/LPS administration (d0) and at day 1 and 2 post Stx/LPS injection.

4.2.3 Blood isolation from mice *ex vivo* and *in vivo*

For plasma preparation, mice were sacrificed by CO_2 inhalation and venous blood was taken directly from the heart by cardiac puncture of the right heart chamber with a heparinized syringe equipped with a 26 G cannula containing 2 µl Heparin (Ratiopharm, Ulm) and 28 µl PBS. Alternatively, for flow cytometric analysis peripheral blood was collected from the tail vein of living mice with heparinized micro capillaries.

4.2.4 Pharmacological analysis of plasma

For pharmacological analysis the blood was obtained by cardiac puncture as described above (4.2.3). The heparinized blood was centrifuged for 10 min with 13.000 rpm at 4 °C. Then, the plasma containing supernatant was transferred into a new tube. Levels of blood urea nitrogen (BUN) and lactate dehydrogenase (LDH) were measured using standard laboratory methods in the central laboratories of the University Hospital Bonn, Essen and Hannover. In order to pool data from different experiments, relative BUN values were calculated due to slight inter-experimental differences. The average BUN level of the Stx/LPS-treated wild type group was set as reference level.

4.2.5 Preparation of single cell suspension from peripheral blood

To prepare a single cell suspension from peripheral blood 1 ml ice-cold red cell lysis buffer (RCB) was added to 20 µl blood sample for erythrocyte elimination. After an incubation period of 5 min at room temperature, the red cell lysis was stopped by adding 2 ml FACS buffer. Subsequently, the samples were centrifuged for 5 min at 1200 rpm, 4 °C and the supernatants were discarded. If the red cell lysis was incomplete and the cell pellets were still red, the procedure was repeated with an incubation period of 1 min.

4.2.6 Isolation of murine renal leukocytes

Renal leukocytes were isolated by cutting the kidneys into small pieces and digesting with 1 mg/ml collagenase and 0,1 mg/ml DNAse-I (both from Sigma-Aldrich, München) in RPMI (PAA Laboratories GmbH, Pasching, Austria) containing 10% FCS (Biochrome, Berlin) and 0,1% sodium azide (Carl Roth, Karlsruhe). After an incubation period of 20 min at 37 °C while shaking, kidneys were mashed with a syringe plunger and again incubated for 20 min at 37 °C. Samples were homogenized by vigorously pipetting up and down 10 times using 1000 µl tips and the supernatants were passed through a 100 µm nylon mesh. Then, samples were washed by adding 3 ml ice-cold FACS buffer and subsequent centrifugation for 7 min at 1200 rpm, 4 °C. After the supernatant was discarded the erythrocytes were lysed as described in section 4.2.5.

4.2.7 Flow cytometry

Cell surface molecules can be visualized via fluorochrome-coupled antibodies. Thus, by flow cytometric analysis cells cannot only be characterized by size (FSC) and granularity (SSC), but also by the expression of surface marker. For cell counting and surface marker detection, the single cell suspension prepared from peripheral blood and kidney samples were analyzed by flow cytometry.

To minimize unspecific F_c-receptor binding the fluorochrome-coupled antibodies were diluted in 1,5 mg/ml human immunoglobuline (Privigen, CSL Behring, Marburg) diluted in FACS buffer. Cells were stained in the dark in a staining volume

of 100 µl for 20 min at 4 °C. The antibody clones, provider and dilutions are listed in table 4.4.

For discrimination between viable and non-viable cells, either Hoechst (Invitrogen, Karlsruhe) diluted 1:10.000 or LIVE/DEAD Fixable Dead Cell stain kit (Invitrogen, Karlsruhe) diluted 1:1000 was added to the antibody staining mix. Absolute cell numbers were determined by adding fixed numbers of CaliBRITE® APC-beads (6 µm) (BD Biosciences, Heidelberg) before the flow cytometric measurement. Flow cytometry analysis was performed on a BD LSR Fortessa II and data was analyzed with Flow-Jo® software (Tree Star Inc., Ashland, USA).

4.2.8 RNA extraction

For RNA extraction, kidneys from sacrificed mice were removed and the lower pol of the right kidney (approximately one third) was subsequently frozen in liquid nitrogen and stored at -80 °C to prevent RNA degradation by RNases. Shortly before RNA extraction, the weight of frozen kidney samples was measured and 350 µl of the Lysis-buffer LBP was added. After disrupting the frozen sample with an electric tissue homogenizer ULTRA-TURRAX® (IKA, Heidelberg), total RNA was extracted with the NucleoSpin® RNA II kit (Machery&Nagel, Düren) according to the manufacturer`s protocol. The RNA was eluted with 60 µl RNase-free water and the purity as well as the concentration of RNA were spectrophotometrically determined at a wavelength of 260 nm by a NanoDrop ND-1000 (PeqLab, Erlangen).

4.2.9 cDNA synthesis

Immediately after RNA extraction, 300 ng RNA for VCAM-1 qRT-PCR or 410 ng RNA for KIM-1 qRT-PCR were reversely transcribed into cDNA using the QuantiTect® Reverse Transcription Kit (Qiagen, Hilden). To remove genomic DNA (gDNA), RNA was incubated with 1x gDNA Wipeout Buffer at 42 °C for 2 min. The PCR Master Mix and the thermal cycler conditions for the reverse transcription are listed in table 4.12 to 4.14.

Table 4.12: Genomic DNA elimination reaction components

Component	Volume (µl)
7x gDNA Wipeout Buffer	2
Template RNA	300 ng/410 ng in variable volume
RNase-free water	Ad 14 µl

Table 4.13: Thermal cycler conditions for gDNA elimination reaction

	Step 1
Temperature (°C)	42
Time (min)	2

Table 4.14: PCR master mix for cDNA synthesis

Component	Volume/Reaction (µl)
Quantiscript Reverse Transcriptase	1
5x Quantiscript RT Buffer	4
RT Primer Mix	1
Template RNA (gDNA elimination reaction)	14
Total per Reaction	**20**

Table 4.15: Thermal cycler conditions for cDNA synthesis

	Step 1	Step 2	Step 3
Temperature (°C)	42	95	4
Time (min)	15	3	∞

4.2.10 Quantitative Real-Time PCR (qRT-PCR)

Gene expressions of KIM-1 and VCAM-1 were relatively quantified by qRT-PCR using the SYBR Green PCR Master Mix (Applied Biosystems, Darmstadt) with self-designed KIM-1 primer (table 4.8) or VCAM-1 QuantiTect Primer Mix (Qiagen, Hilden). The qRT PCR was performed in a 96-well plate and each sample was analyzed in duplicates. The gene expression was normalized to values for the reference gene *hprt* (table 4.8). For qRT-PCR the LightCycler 480II from Roche, Mannheim was used. The fold induction of VCAM-1 expression was calculated and pooled for two individual experiments The PCR master mix and the thermal cycler conditions for

qRT-PCR are listed in table 4.16 to 4.18.

Table 4.16: Master mix for KIM-1 qRT-PCR

Component	Volume/Reaction (µl)
2x SYBR Green PEC Mix	10
Forward primer (100µM)	0,08
Reverse primer (100µM)	0,08
Template (cDNA)	2
RNase-free water	7,84
Total per Reaction	**20**

Table 4.17: Master mix for VCAM-1 qRT-PCR

Component	Volume/Reaction (µl)
2x SYBR Green PEC Mix	10
QuantiTect Primer Mix 10x	2
Template (cDNA)	2
RNase-free water	6
Total per Reaction	**20**

Table 4.18: Thermal cycler conditions for qRT-PCR

Cycle name	Temperature (°C)	Time
Denaturation	95	00:05:00
Amplification (40cycles)	95	00:00:15
	60	00:00:10
	72	00:00:20
Melting	95	00:00:05
	65	00:01:00
Cooling	4	∞

4.2.11 Kidney homogenate preparation

The kidney was removed from sacrificed mice and immediately placed into 1 ml pre-cooled 1x PBS supplemented with complete protease inhibitor mix (Roche, Mannheim). The kidney was homogenized twice for 30 s with an ULTRA-TURRAX® (IKA, Heidelberg). The homogenized samples were centrifuged at 13.000 rpm, 4 °C for 10 min and the supernatants were transferred into new tubes.

4.2.12 Cytokine analysis

The protein levels of cytokines in the supernatant of mechanically homogenized murine kidneys (4.2.11) were determined by using the flow-cytometry based beads assay LEGENDplex™ Mouse Proinflammatory Chemokine Panel (13-plex) according to the manufactures protocol (BioLegend, Fell). The fluorescence of protein levels was measured by flow cytometry and the data were analyzed using LEGENDplex™ data Analysis Software Version 7.1 (BioLegend, Fell).

4.2.13 Analysis of human data

Expression levels of serum cytokines and chemokines in patients admitted to Medical Center Hamburg-Eppendorf were detected by flowcytometric bead-array using CBA flex-sets according to the manufacturer´s protocol (BD Biosciences, Heidelberg). The fluorescence of protein levels was measured by flow cytometry and the data were analyzed using FCAP software (Soft Flow, St. Louis Park, MN, USA).

Patients admitted to Hannover Medical School during the EHEC serotype O104:H4 outbreak in 2011 who consented in writing to donating blood for scientific evaluation were included in this study. The protocol was carried out according to the Declaration of Helsinki and approved by the Institutional Review Board at Hannover Medical School. Standard laboratory values were measured at the central clinical laboratory. Flow cytometry was performed on EDTA- anticoagulated whole blood to determine the number of monocytes and neutrophils[107].

4.2.14 VCAM-1 Enzyme-Linked Immunosorbent Assay (ELISA)

Plasma (4.2.3) and supernatants of kidney homogenates (4.2.11) of Stx/LPS-injected and untreated control mice were obtained as previously described. These samples were diluted 1:50 and VCAM-1 protein levels were analyzed by Mouse sVCAM-1/CD106 Quantikine ELISA Kit according to the manufacture's protocol (R&D Systems, Wiesbaden) by using a plate reader (LB 940, Berthold Technologies, Bad Wildbad) at a wavelength of 450 nm. Relative changes in VCAM-1 protein levels were calculated and pooled for two individual experiments.

4.2.15 *In vivo* PET-MR imaging

To quantify the endothelial damage in Stx-treated mice an *in vivo* positron emission tomography-magnetic resonance (PET-MR) imaging was performed in cooperation with Kerstin Fuchs at the Werner-Siemens Imaging center in Tübingen.
The PET-MR imaging combines the features of two approaches, the Positron emission tomography (PET), which is highly sensitive and enables tracking of labeled proteins and cells, with the magnet resonance (MR) imaging, which gives information about the structural features of tissues.

For endothelial damage detection, a [^{64}Cu]NOTA-GPVI-Fc tracer, that specifically binds to free collagen, was used for PET-MR imaging. This tracer is composed out of a radioactive label [^{64}Cu] linked to a NOTA-spacer and the soluble form of the dimeric GPVI fusion protein, which specifically binds to collagen[108, 109]. Collagen is exposed upon endothelial injury, thereby enabling subsequent tracer binding.

High-resolution non-invasive *in vivo* PET images were acquired using two small animal Inveon microPET scanners (Siemens Medical Solutions USA, Inc., Knoxville, TN, USA) with a transaxial field of view (FOV) of 10 cm, and an axial FOV of 12.7 cm and a spatial resolution of 1.5 mm in the reconstructed PET images.

For imaging, mice were anesthetized with 1.5% isoflurane-O_2 (1.5 L/minute, 1.5% isoflurane, Abbott GmbH, Wiesbaden) and injected intravenously with 9.5±0.9 MBq [^{64}Cu]NOTA-GPVI-Fc tracer 24 h after Stx/LPS injection. Static PET acquisitions were performed under isoflurane anesthesia 24 h, 48 h and 72 h after Stx/LPS injection. During PET scans mice were placed on a heating mat (37 °C) to maintain body temperature.

For reconstruction of the PET images, list mode data were processed applying the statistical iterative ordered subset expectation maximization (OSEM) 2D algorithm.
All data were corrected for decay and normalized for each animal to the injected activity. Data were analyzed by drawing regions of interests (ROIs) around the right kidney of each mouse. The left kidney was not analyzed to exclude false positive values caused by spillover effects from the unspecific signal in the liver. Image analysis was performed with the Pmod Software (PMOD Technologies Ltd., Zurich, Switzerland).

MRI was performed using a 7 T small-animal scanner (Biospec, Bruker Biospin MRI GmbH, Ettlingen). All mice were anesthetized with 1.5 vol% isoflurane and placed within the scanner`s FOV. Imaging was performed using a 3D TurboRARE (TE/TR 58/1800 ms) sequence.

4.2.16 Autoradiography

To localize the endothelial damage within the kidney of Stx/LPS-injected mice an autoradiography was performed. To this end, animals were injected with 9.5±0.9 MBq [^{64}Cu]NOTA-GPVI-Fc tracer 24 h after Stx/LPS injection. 72 h after Stx/LPS injection, mice were sacrificed and kidneys were removed and embedded in a cutting compound (TissueTek; Sakura Finetek, Torrance, CA, USA). Autoradiography was performed on 20 µm kidney slices with a Storage Phosphor Screen (Molecular Dynamics, Sunnyvale, CA, USA). After an exposure time of 24 h the phosphor screen was scanned at a resolution of 50 µm/pixel with a STORM Phosphor-Imager (Molecular Dynamics, Sunnyvale, CA, USA). The autoradiography was performed by Kerstin Fuchs at the Werner Siemens Imaging Center in Tübingen.

4.2.17 Excretion of FITC-dextrane

In order to investigate the excretory function of the kidney, mice were injected intravenously with 10 µg/g 70 kDa Fluorescein isothiocyanate (FITC)-dextrane (Sigma-Aldrich, München). Then, mice were maintained for 4 h within metabolic cages, in which the urine was collected. FITC Fluorescence of 70-100 µl urine was measured by fluorometry at a wavelength of 535 nm in a plate reader (LB940 Mithra, Berthold Technologies, Bad Wildbad).

4.2.18 Histology, image preparation and analysis

To visualize Gr1^{high} monocytes and neutrophils 2 µg of the anti-Gr-1 antibody (PE, RB6-8C5, BD Bioscience, Heidelberg) were injected intravenously 10 min before sacrificing the mice. 24h after Stx/LPS injection mice were sacrificed and kidneys were isolated and fixed with 0.05 M phosphate buffer containing 0.1 M L-lysine (pH

7.4; Carl Roth, Karlsruhe), 2 mg/ml NaIO4 (Carl Roth, Karlsruhe) and 10 mg/ml paraformaldehyde (Sigma-Aldrich, München) over night at 4 °C. After washing kidneys twice with P-buffer, organs were equilibrated in 30% sucrose (Carl Roth, Karlsruhe) solution for 24 h. Tissues were then frozen in OCT (Weckert Labortechnik) and stored at -80 °C. Consecutive sections (10 µm) were mounted on Super Frost Plus glass slides, dried for 10 min at 70 °C, rehydrated with PBS containing 0,05% Triton X-100 (Carl Roth, Karlsruhe) and blocked for 1 h with PBS containing 1% bovine serum albumin (PAA Laboratories GmbH, Pasching, Austria) and 0.05% Triton X-100. The staining was performed in the dark with 200 µl blocking buffer per section at room temperature. The F4/80 antibody (APC, BM8.1; Tonbo bioscience, San Diego, USA) was used in a dilution of 1:100 and incubated for 1 h, DAPI (2 mg/ml, Life Technologies, Darmstadt) was diluted 1:5000 and incubated for 5 min. After each staining step, three washing steps of 5 min with 0.05% Triton X-100 in PBS were performed. Sections were imaged by the Zeiss Axio Observer.Z1 and Apotome (Zeiss, Oberkochen) at the Imaging Center Essen and analyzed by the ZEN Software (Zeiss, Oberkochen) and FIJI. The immunofluorescent imaging and analysis was performed with Julia Volke as part of her Master project under my supervision.

4.2.19 Intravital microscopy

For intravital imaging, juvenile *Cx3cr1*$^{gfp/+}$ mice (3-4 weeks) were used, due to elevated numbers of superficial glomeruli in these mice. The CXCR2 antagonist or control solvent (1% DMSO; PanReac, AppliChem, Darmstadt) were injected i.p. 1 h prior to Stx/LPS injection and 24 h later, directly before imaging. 24 h after Stx/LPS administration intravital imaging of the exposed murine kidney was performed for 1.5 h. Anesthesia was induced by 100 mg/kg Ketamine (Medistar) and 20 mg/kg Xylazine i.p. (Ceva). During the entire surgery and imaging procedure the mouse body temperature was maintained by the use of a heating pad. The right kidney was exteriorized through a small dorsal incision and then immobilized in the heated mold of a custom-built imaging stage. Immobilization was achieved by usage of the veterinary tissue glue (Sutures). The exposed kidney was moisturized with PBS and subsequently coverslipped. The imaging chamber was sealed with high vacuum

grease (Sigma-Aldrich, München) to prevent leakage and dehydration of the kidney. Neutrophils were stained by intravenous injection of Gr-1 antibody (RB6-8C5, 2 µg/mouse, ebioscience), intravenous injection of QDots (10 µl, AF 655, 0,2 µM, Life Technologies, Darmstadt) was performed to label the vasculature. During intravital imaging, anesthesia was maintained by adding 0.8 vol% isoflurane to the murine respiratory air. The kidneys were imaged using a Leica TCS SP8 multi-photon microscope equipped with a Chameleon Vision II Laser and HyD detectors. The microscope was equipped with a N2.1HCX IRAPO objective with a magnification of 25x used in PBS immersion. The imaging was performed using an excitation wavelength of 960 nm (Laser output 1.4W). Three different regions were imaged for 30 min in all individual mice. Z-Stacks (at least 100 µm) were recorded every 30 s with a stepsize of 6 µm. The intravital imaging was performed with Julia Volke as part of her Master project.

The analysis was performed using the gallery mode of the Imaris image analysis software (Bitplane, Zurich, Switzerland). Neutrophils were defined as adherent if they were visible in two subsequent images (60 s).

4.2.20 Statistical analysis

Appropriate assumptions of data (normal distribution or similar variation between experimental groups) were examined by D´Agostino and Pearson omnibus normality test before statistical tests were conducted. Comparisons were made using non-parametric Mann-Whitney or two-tailed t-test. For comparison of survival curves a Log-rank (Mantel-Cox) test was performed. Results are expressed as mean ± s.e.m, *$p < 0.05$; **$p < 0.01$; ***$p < 0.001$.

5 Results

5.1 Stx/LPS Administration Leads to Kidney Damage in Mice

C57BL/6 mice were intravenously injected with Stx2 in combination with LPS to induce Stx-mediated kidney damage.

In order to assess the overall health status, the bodyweight of Stx/LPS-injected mice was monitored for three days. Stx/LPS-treated mice showed significant weight loss during the course of the experiment. Three days post Stx/LPS administration, mice had lost 16% of their initial bodyweight (Fig. 5.1 A). Next, tissue damage was assessed by analyzing serum levels of lactate dehydrogenase (LDH), a universal tissue damage marker. The LDH levels were elevated at day one and day three after Stx/LPS injection indicating Stx/LPS-induced tissue injury (Fig. 5.1 B).

It is known, that Stx specifically targets endothelial cells within the kidney and thereby reduces renal functionality. To assess renal injury in Stx/LPS-injected mice, kidney damage markers were measured and the renal excretory function was analyzed. Indeed, blood urea nitrogen (BUN) levels were mildly elevated in the serum of Stx/LPS-injected mice from day two on. At day three BUN levels were strongly increased by more than 4 times in Stx/LPS-injected mice (Fig. 5.1 C). Furthermore, renal expression of the Kidney Injury Molecule-1 (KIM-1), which is associated with renal damage, was analyzed. One day after Stx/LPS injection the expression of KIM-1 was strongly increased by about 30-fold compared to untreated control mice. Moreover, KIM-1 expression remained strongly elevated until day three (Fig. 5.1 D). Taken together, increased levels of kidney damage parameters in Stx/LPS-injected mice indicated renal injury in these mice.

Next, the excretory function of the kidney was analyzed by injecting 70kDa FITC-Dextran intravenously into mice. It is reported that 70 kDa FITC-Dextran is rapidly excreted into the urine within hours after administration[110]. The urine was collected over a time period of 4 h after intravenous FITC-Dextran injection. Then, the amount of excreted FITC-dextran was evaluated by measuring the FITC-florescence within the urine. The FITC fluorescence in urine of untreated mice (Fig. 5.1 E and F, 1st column) indicates the background signal of the urine. Upon FITC-Dextran injection the FITC-

fluorescence signal was increased in the urine of untreated mice (Fig. 5.1 E and F, 2nd column) indicating excretion of this molecule in healthy mice. However, the FITC-Fluorescence in the urine of Stx/LPS-injected mice remained at background levels, indicating defective FITC-dextran excretion two and three days after Stx/LPS injection (Fig. 5.1 E and F, 4th column).

In summary these data reveal severe tissue damage and reduced renal functionality in mice injected with Stx/LPS.

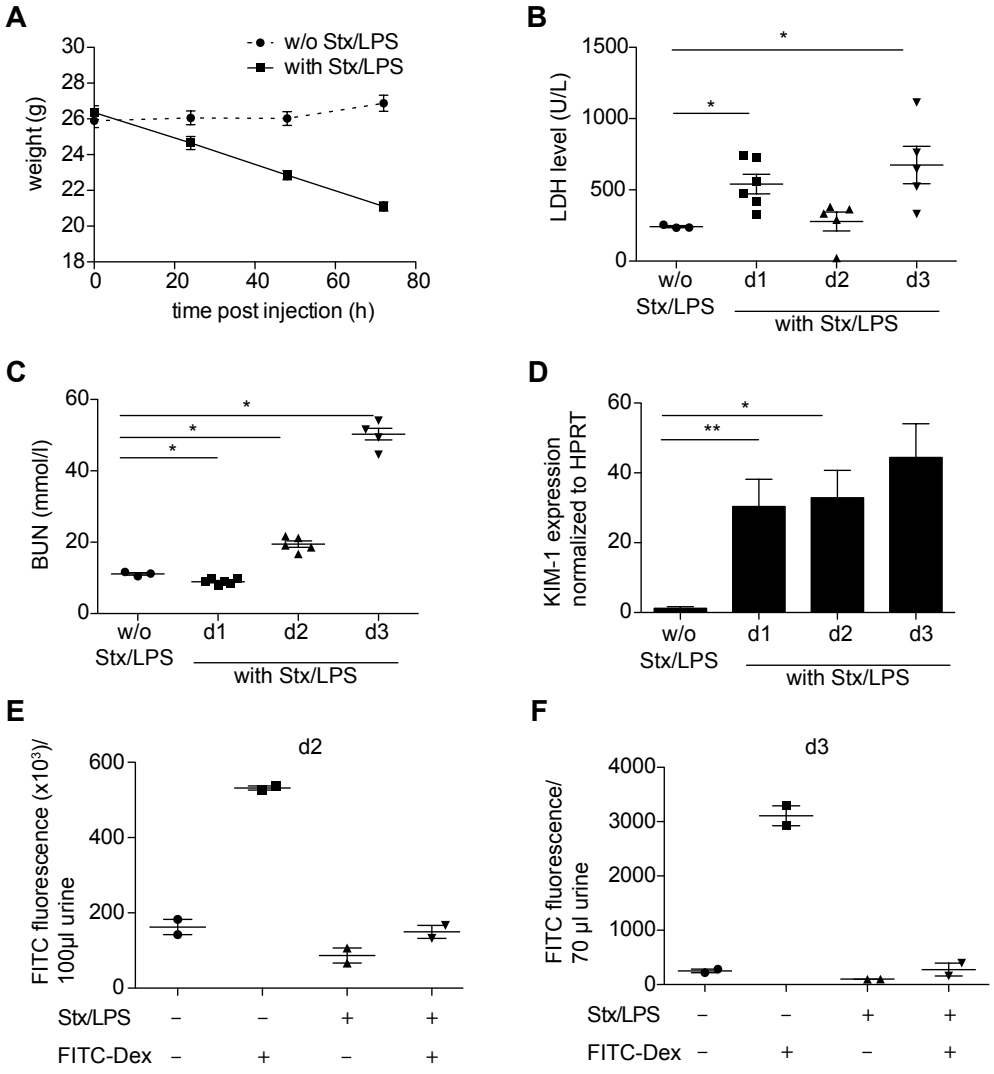

Figure 5.1: Stx/LPS injection leads to kidney damage.
(**A**) Bodyweight of Stx/LPS-injected mice (solid line) and control mice (dashed line). (**B, C**) LDH (**B**) and BUN levels (**C**) in serum of control (w/o Stx/LPS) and Stx/LPS-treated mice (with Stx/LPS) on day one to day three after injection. (**D**) Relative expression of KIM-1 in kidney samples was determined by qRT-PCR on day one to day three after Stx/LPS administration and normalized to HPRT expression. (**E**, **F**) FITC fluorescence was determined within the urine two (**E**) and three days (**F**) after Stx/LPS injection. Results are given as means +/- s.e.m. *p < 0.05; **p < 0.01. d = day; LDH = lactate dehydrogenase; BUN = blood urea nitrogen; KIM = Kidney Injury Molecule.

5.2 Monocytes and Macrophages in Stx-induced Kidney Injury

5.2.1 Monocyte counts in blood correlate with disease severity in STEC HUS-patients

The STEC-outbreak in 2011 in Northern Germany caused hundreds of severe cases of HUS. Collaborators from the Medical Center Hamburg-Eppendorf and the Hannover Medical School collected blood samples from these STEC-HUS patients during the outbreak.

STEC-HUS patients showed a severe monocytosis, characterized by an increased abundance of monocytes within the blood (Fig. 5.2 A). The kidney injury, which was determined by serum creatinine levels, directly correlated with the monocyte number in the blood. The Pearsons`correlation coefficient (0,68) indicated a positive association between creatinine values and monocyte frequency in the blood of STEC-HUS patients (Fig. 5.2 B).

Additionally, expression levels of various inflammatory mediators in the serum of STEC-patients with uncomplicated and severe HUS were determined by a flow-cytometric bead-assay. Inflammatory molecules, which are typically associated with myeloid cells, such as soluble tumor necrosis factor receptor 1 and 2 (TNFRI, TNFRII) as well as the soluble interleukin-1 receptor 1 (IL1-RI), were increased within the serum of patients with severe HUS. However, serum levels of these markers in patients with an uncomplicated course of HUS were unchanged compared to healthy controls (Fig. 5.2 C).

Taken together these data suggested an involvement of monocytes/macrophages in the pathogenesis of STEC-HUS and provided the rationale to investigate the role of monocytes and macrophages in Stx/LPS-induced HUS mouse model.

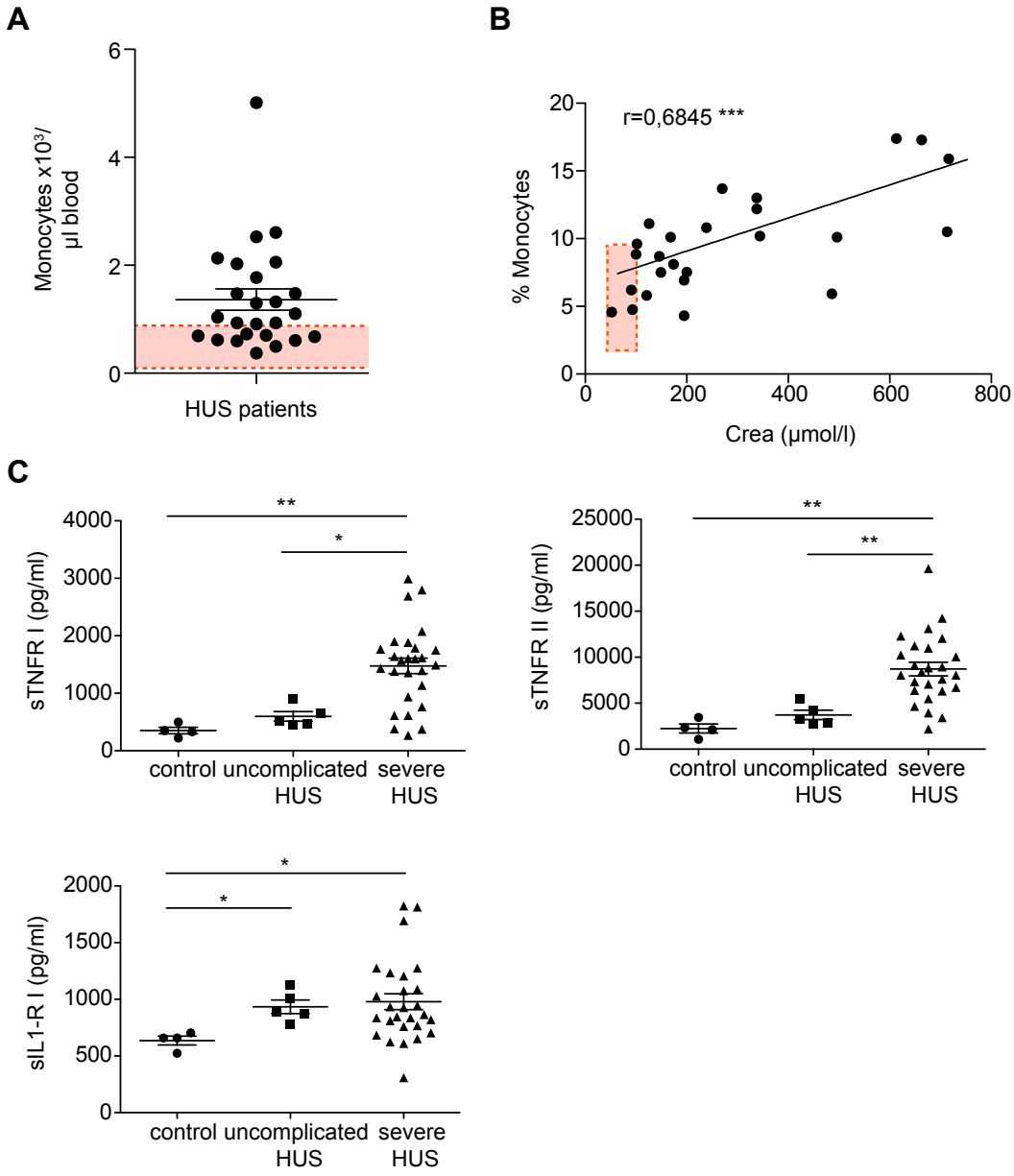

Figure 5.2: Monocyte counts correlate with kidney injury in STEC-HUS patients.
(**A**) Absolute numbers of monocyte counts in blood of STEC-HUS patients. The red area indicates standard values for healthy controls. (**B**) Scatterplot of monocyte frequencies and creatinine levels of STEC-HUS patients. The Pearson`s correlation coefficient r is given. The red area indicates standard values for healthy controls. (**C**) Levels of differentially expressed proteins in patients with uncomplicated or severe STEC-HUS compared to the healthy controls. Results are given as means +/- s.e.m. *p < 0.05; **p < 0.01; *** p < 0.001. Crea = Creatinine. These data were collected by Sibylle von Vietinghoff, Hannover Medical School (A and B) and Hans-Joachim Paust, University Hospital Hamburg-Eppendorf (C).

5.2.2 Blood monocyte abundance and activity in HUS mouse model

Data of our collaborators showed that STEC-HUS patients have increased monocytes counts in the blood. Moreover, chemokines associated with myeloid cells were increased in serum and kidney in STEC-HUS-patients (Fig. 5.2)[111, 112, 113]. These data suggested a potential role of monocytes and macrophages in the pathogenesis of HUS.

To investigate blood monocytes in the mouse model of Stx-mediated kidney injury, C57BL/6 mice were injected with Stx/LPS and blood leukocytes were analyzed by flow cytometry. According to size and granularity single cells were included and cell debris as well as cell clumps were eliminated from the analysis in the FSC/SSC-plot. Furthermore, only Ly6G negative cells were investigated to exclude neutrophils from the analysis. CD115-expressing cells were defined as monocytes. In order to discriminate between patrolling and inflammatory monocytes, blood monocytes ($CD115^+$) were analyzed for Gr1 expression by flow cytometry. The gating strategy for blood monocytes is shown in Figure 5.3.

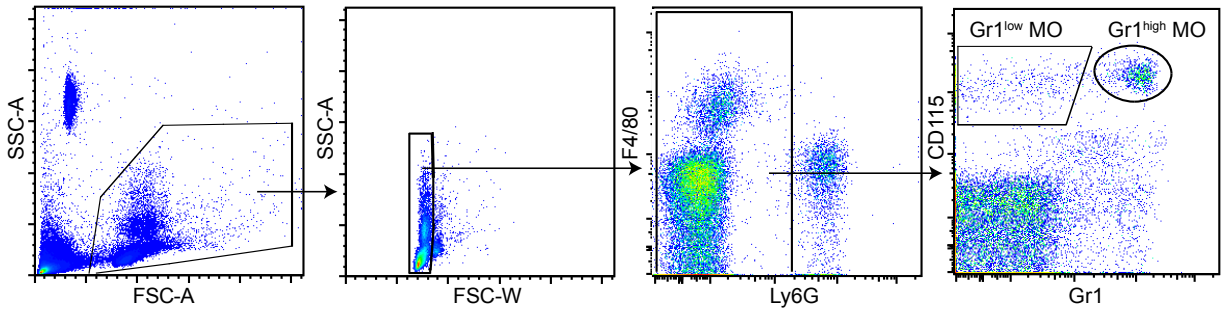

Figure 5.3: Gating strategy for blood monocytes.
The SSC/FSC plot (1st plot) indicates all events detected in blood of an untreated mouse by flow cytometry. Small particles were removed from further analysis by setting a leukocyte gate. In the next step, cell clumps and doublets were excluded from the analysis (2nd plot). Then, neutrophils were excluded by gating on $Ly6G^-$ cells (3rd plot). Finally, $Ly6G^-$ cells were analyzed for CD115 and Gr1 expression (4th plot). $CD115^+$ $Gr1^-$ cells were defined as $Gr1^{low}$ patrolling monocytes and $CD115^+$ $Gr1^+$ cells as $Gr1^{high}$ inflammatory monocytes.

Flow cytometric analysis of blood samples from Stx/LPS-injected mice revealed an increased frequency of $Gr1^{low}$ monocytes on day one and two post Stx/LPS-injection (Fig. 5.4 A left gate, B). In contrast, the abundance of inflammatory monocytes was strongly decreased on day two and three after Stx/LPS injection. On day three only 0,18% $Gr1^{high}$ monocytes were detected in the blood of Stx/LPS-treated mice (Fig. 5.4 A right gate, C).

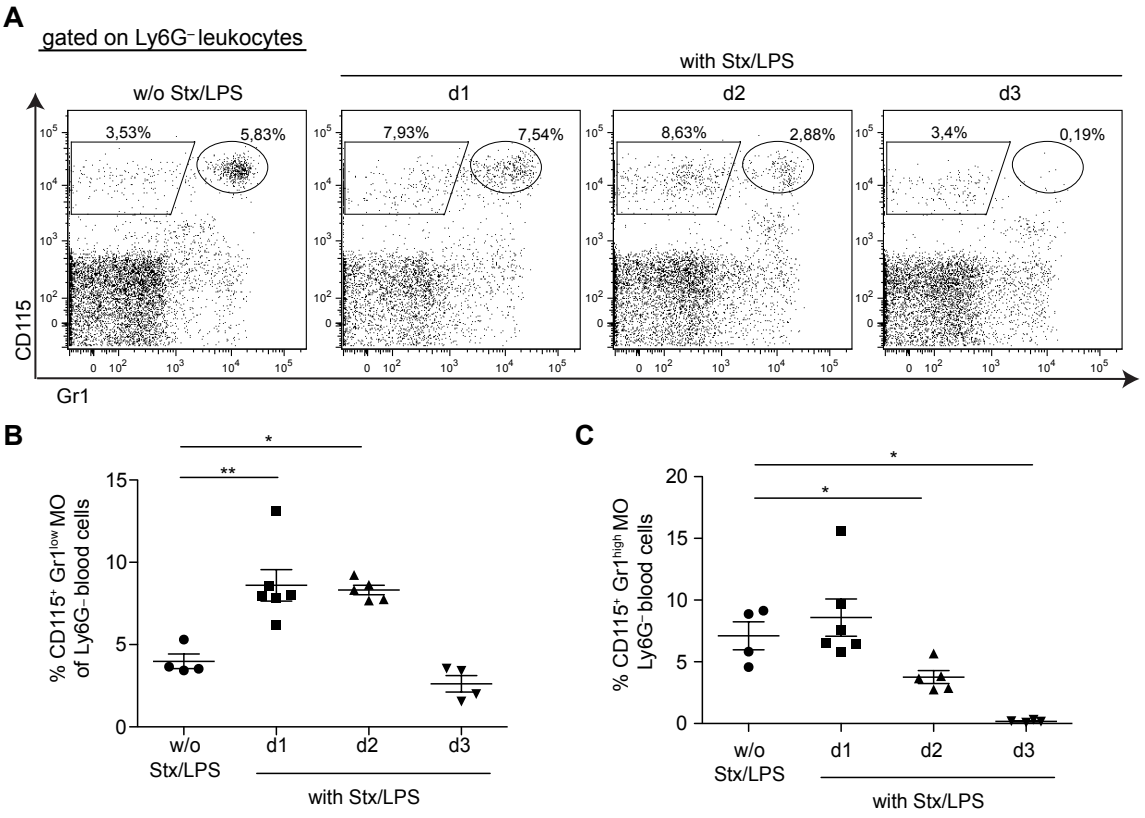

Figure 5.4: Application of Stx/LPS changes abundance of blood monocytes.
(A) Ly6G^{-} blood leukocytes were analyzed by flow cytometry for their CD115 and Gr1 expression in steady state (w/o Stx/LPS) and on day one to day three after Stx/LPS injection (with Stx/LPS). (**B**, **C**) Frequencies of Gr1^{low} (CD115^{+} Gr1^{low})(**B**) and Gr1^{high} monocytes (CD115^{+} Gr1^{high})(**C**) analyzed on day one to day three after Stx/LPS administration. Data in (A) are representative for *n* = 4-6 mice. Results are given as means +/- s.e.m. *p < 0.05; **p < 0.01. d = day; MO = monocytes.

Next, the activation status of blood monocytes was analyzed by determining the mean fluorescence intensity (MFI) of CD11b, an integrin associated with activation and adhesion. CD11b levels were elevated on both monocyte subtypes one day after Stx/LPS injection indicating cellular activation. On the following days CD11b expression decreased to base line levels (Fig. 5.5 A, B).

In summary, these data showed changes in cell abundances and increased activation of monocytes after Stx/LPS treatment suggesting a potential role of these cells in Stx-mediated kidney injury.

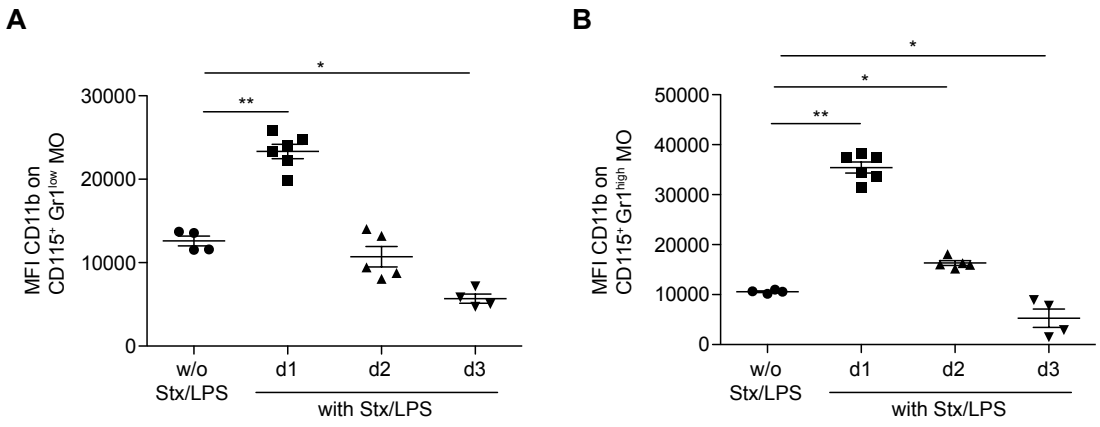

Figure 5.5: Increased monocyte activation upon Stx/LPS treatment.
(**A**, **B**) Mean fluorescence intensity (MFI) of CD11b on $Gr1^{low}$ (**A**) and $Gr1^{high}$ (**B**) blood monocytes of untreated control mice (w/o Stx/LPS) and on day one to day three (d1 – d3) after Stx/LPS-injection (with Stx/LPS). Results are given as means +/- s.e.m. *$p < 0.05$; **$p < 0.01$. d = day; MO = monocytes; MFI = mean fluorescence intensity.

5.2.3 Elevated levels of monocyte-recruiting chemokines in Stx-treated mice

In order to determine whether renal injury in Stx/LPS-injected mice (Fig. 5.1) is associated with myeloid infiltrates into the kidney the amounts of monocyte-attracting chemokines within the kidney were determined. To this end, a flow cytometry-based bead assay, which analyzes levels of multiple chemokines in parallel, was performed. A strong induction of CCL2, CCL3, CCL4 and CCL5 was detected in kidney homogenates one day upon Stx/LPS injection. Notably, CCL3 and CCL4 levels, which showed the strongest induction after Stx/LPS treatment, remained slightly increased on day two. However, three days after disease induction the chemokine levels returned to baseline levels (Fig. 5.6).

The strong increase of the aforementioned chemokines within kidney homogenates one day after Stx/LPS administration identifies a potential stimulus for the recruitment of monocytes to the kidney.

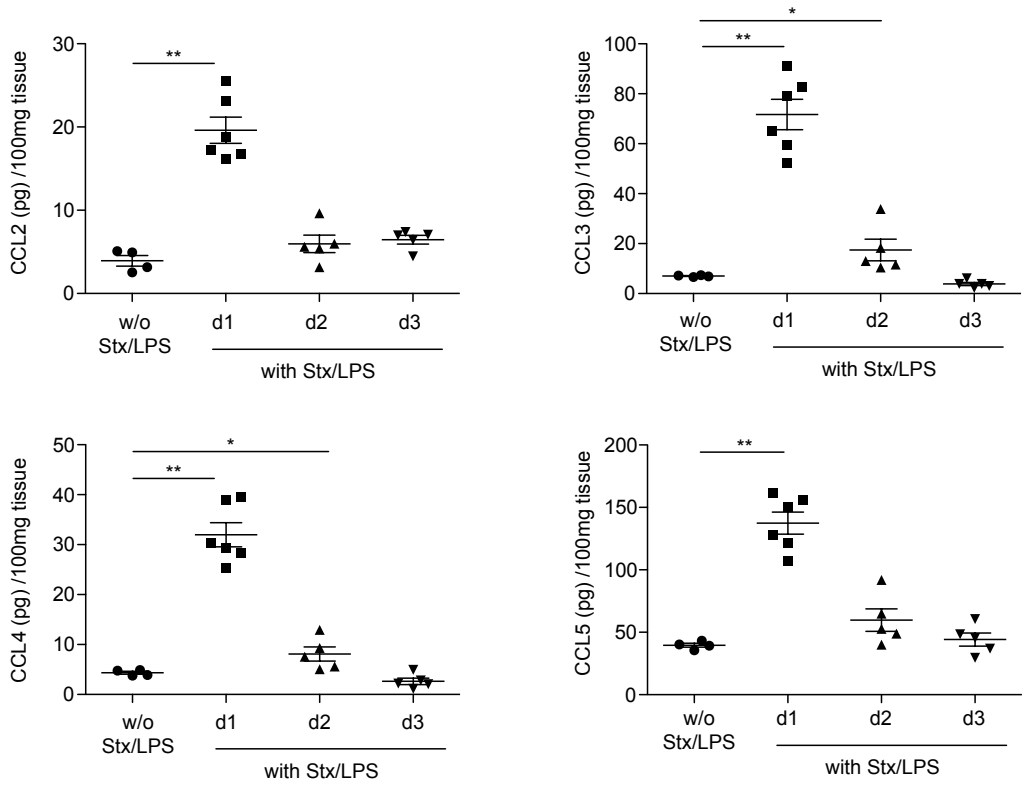

Figure 5.6: Elevated chemokine expression in Stx/LPS-treated mice.
The amounts of CCL2, CCL3, CCL4 and CCL5 were determined in the supernatant of mechanically homogenized kidneys of untreated (w/o Stx/LPS) and Stx-injected mice (with Stx/LPS). Results are given as means +/- s.e.m. *p < 0.05; **p < 0.01. d = day.

5.2.4 Gr1^{high} monocytes are increased in the kidney of Stx-injected mice

Elevated renal levels of monocyte-attracting chemokines (Fig. 5.6) suggested recruitment of monocytes to the kidney. To test this hypothesis the monocyte- and macrophage-compartment was analyzed in renal single cell suspensions by flow cytometry. In the FSC/SSC-plot single cells were included for further analysis. To exclusively investigate renal immune cells, cells were analyzed for expression of CD45, a common leukocyte antigen. In the next gating step, renal monocytes and macrophages (F4/80^{+}) were analyzed for Gr1 expression to discriminate between resident Gr1^{low} macrophages and inflammatory Gr1^{high} monocytes. The gating strategy for renal Gr1^{low} macrophages and Gr1^{high} monocytes is depicted in Figure 5.7.

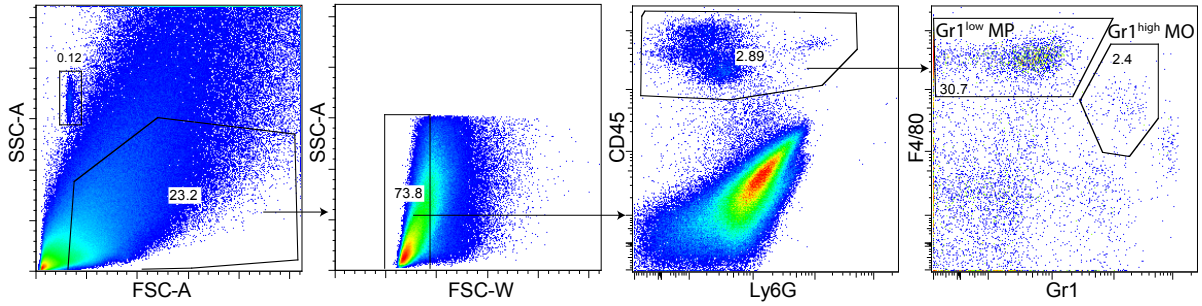

Figure 5.7: Gating strategy for renal monocytes and macrophages.
In the SSC/FSC plot (1st plot) small particles were removed from further analysis and cells were gated according to size and granularity. Then, cell clumps were excluded from analysis (2nd plot). In the next step, renal leukocytes were selected for further analysis by gating on $CD45^+$ events (3rd plot). These renal immune cells were analyzed for F4/80 and Gr1 expression (4th plot). $F4/80^+$ $Gr1^-$ cells were defined as $Gr1^{low}$ macrophages and $F4/80^+$ $Gr1^+$ cells were defined as $Gr1^{high}$ monocytes.

Flow cytometry analysis revealed that kidneys of untreated mice mainly harbored resident $Gr1^{low}$ macrophages (28,5%), and only a minor portion of $Gr1^{high}$ monocytes (2,2%) (Fig. 5.8 A to C).

One day after Stx/LPS treatment the abundance of $Gr1^{high}$ monocytes increased to approx. 170.000 $Gr1^{high}$ monocytes per kidney, suggesting cellular infiltration. At later time points (d2, d3) cell numbers of $Gr1^{high}$ monocytes were decreasing to levels of untreated mice (Fig. 5.8 A, C). Notably, the amount of $Gr1^{low}$ macrophages was not elevated demonstrating a selective recruitment mechanism for $Gr1^{high}$ monocytes during HUS. In contrast, the abundance of $Gr1^{low}$ macrophages was even slightly decreased at day two (19,3%), but at baseline levels at day one and day three (Fig. 5.8 A, B).

In summary these data showed, that elevated chemokine concentrations after Stx/LPS administration coincided with increased abundance of $Gr1^{high}$ monocytes, whereas the $Gr1^{low}$ macrophage fraction in the kidney was unchanged (Fig. 5.6 and 5.8).

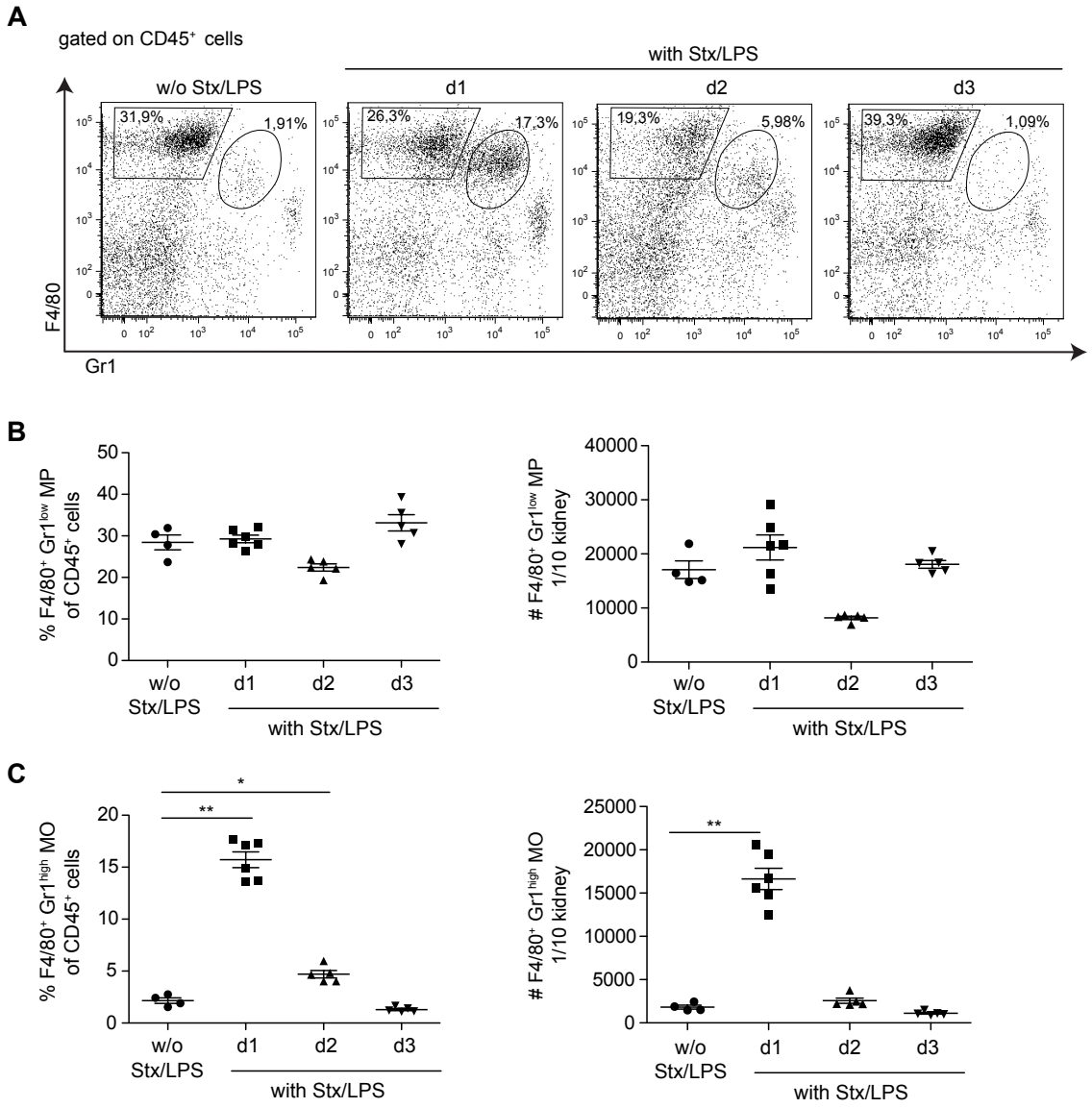

Figure 5.8: Increased abundance of Gr1^{high} monocytes in the kidney after Stx/LPS treatment.
(**A**) Flow cytometric analysis of renal leukocytes (gated on CD45$^+$ cells) for F4/80 and Gr1 expression on day one to day three after Stx/LPS injection. (**B**, **C**) Frequencies (left scatter plots) and absolute cell counts (right scatter plots) of (**B**) Gr1^{low} macrophages (F4/80$^+$ Gr1^{low}) and (**C**) Gr1^{high} monocytes (F4/80$^+$ Gr1^{high}) were analyzed on day one to day three after Stx/LPS injection by flow cytometry. Data in (**A**) are representative for *n* = 4-6 mice. Results are given as means +/- s.e.m. *p < 0.05; **p < 0.01. d = day; MO = monocytes; MP = macrophages.

5.2.5 Stx/LPS leads to increased cellular activation of renal Gr1^{low} macrophages and Gr1^{high} monocytes

In order to investigate the cellular activation of monocytes and macrophages within the kidney, the CD11b-expression on these cells was analyzed by flow cytometry. Although the numbers of renal Gr1^{low} macrophages were unchanged upon Stx/LPS treatment

(Fig. 5.8 B), these cells showed increased CD11b expression from day one to day three (Fig. 5.9 A). Comparable to cell numbers, the CD11b expression of Gr1^{high} monocytes was elevated at day one, but returned to baseline levels on the following days (Fig. 5.9 B).

Increased expression of the integrin CD11b on Gr1^{low} macrophages and Gr1^{high} monocytes in the kidney demonstrates cellular activation of both, Gr1^{low} macrophages and Gr1^{high} monocytes.

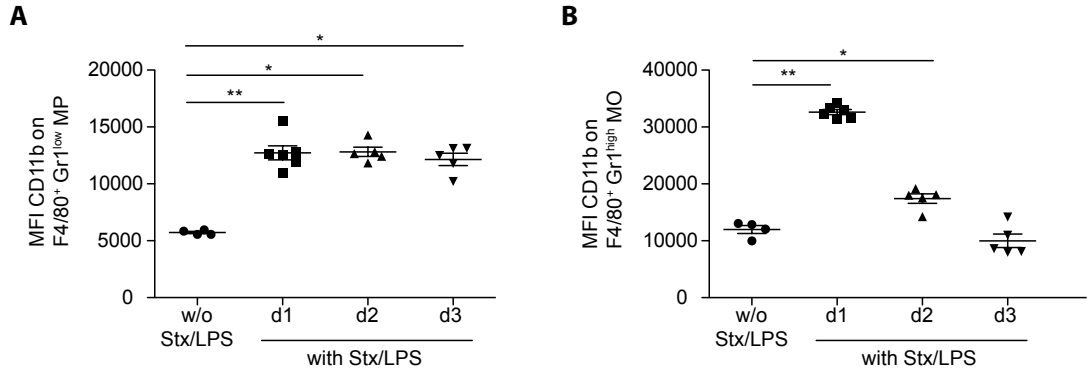

Figure 5.9: Increased cellular activation of Gr1^{low} macrophages and Gr1^{high} monocytes in the kidney.
(**A**, **B**) Mean fluorescence intensity (MFI) of CD11b on Gr1^{low} macrophages (**A**) and Gr1^{high} monocytes (**B**) of untreated control mice (w/o Stx/LPS) and one day to three days (d1-d3) after Stx/LPS-injection (with Stx/LPS). Results are given as means +/- s.e.m. *p < 0.05; **p < 0.01. d = day; MO = monocytes; MP = macrophages; MFI = mean fluorescence intensity.

5.2.6 Gr1^{high} monocytes are located within the renal cortex

Next, the localization of monocytes and macrophages within the kidney of C57BL/6 mice was analyzed one day after Stx/LPS treatment, because flow cytometry data revealed increased Gr1^{high} monocyte numbers at this time point. The kidney slices were stained with the monocyte/macrophage marker F4/80 as well as Gr1 to discriminate between Gr1^{high} monocytes and Gr1^{low} macrophages. F4/80^{+} Gr1^{-} (green) cells were defined as Gr1^{low} macrophages and F4/80^{+} Gr1^{+} cells (green, red) were defined as Gr1^{high} monocytes.

Immunofluorescent images revealed morphological differences among the investigated monocyte and macrophage subtypes. Gr1^{low} macrophages had an elongated shape with high numbers of dendrites. In contrast, Gr1^{high} monocytes were much smaller and had a

round shape (Fig. 5.10 A). Moreover, histological images indicated that the abundance of resident Gr1^{low} macrophages is much higher than the number of Gr1^{high} monocytes in the kidney of untreated mice. In line with the flow cytometry results, the number of Gr1^{low} macrophages remained unchanged, whereas abundance of Gr1^{high} monocytes increased on day one after Stx/LPS injection (Fig. 5.10 A).

In order to determine spatial distribution of Gr1^{high} monocytes and Gr1^{low} macrophages within the kidney, these cells were quantified within the different renal compartments. In line with flow cytometry data (Fig. 5.8) immunofluorescent microscopy revealed numerous resident Gr1^{low} macrophages within kidney of healthy control mice. The majority of these cells was located within the medulla. Upon Stx/LPS treatment the abundance of Gr1^{low} macrophages remained unaltered in the renal cortex as well as in the medulla (Fig. 5.10 B, C).

Quantification of Gr1^{high} monocytes revealed that under steady state conditions only few inflammatory Gr1^{high} monocytes were located within the kidney. In contrast to Gr1^{low} macrophages, most of these cells were located within the renal cortex. Upon Stx/LPS treatment Gr1^{high} monocytes predominantly increase within the renal cortex, whereas the number of these cells in the medulla remained unchanged (Fig. 5.10 D, E).

In summary, the histological analysis revealed a selective increase of Gr1^{high} monocytes in particular within the renal cortex upon Stx/LPS injection.

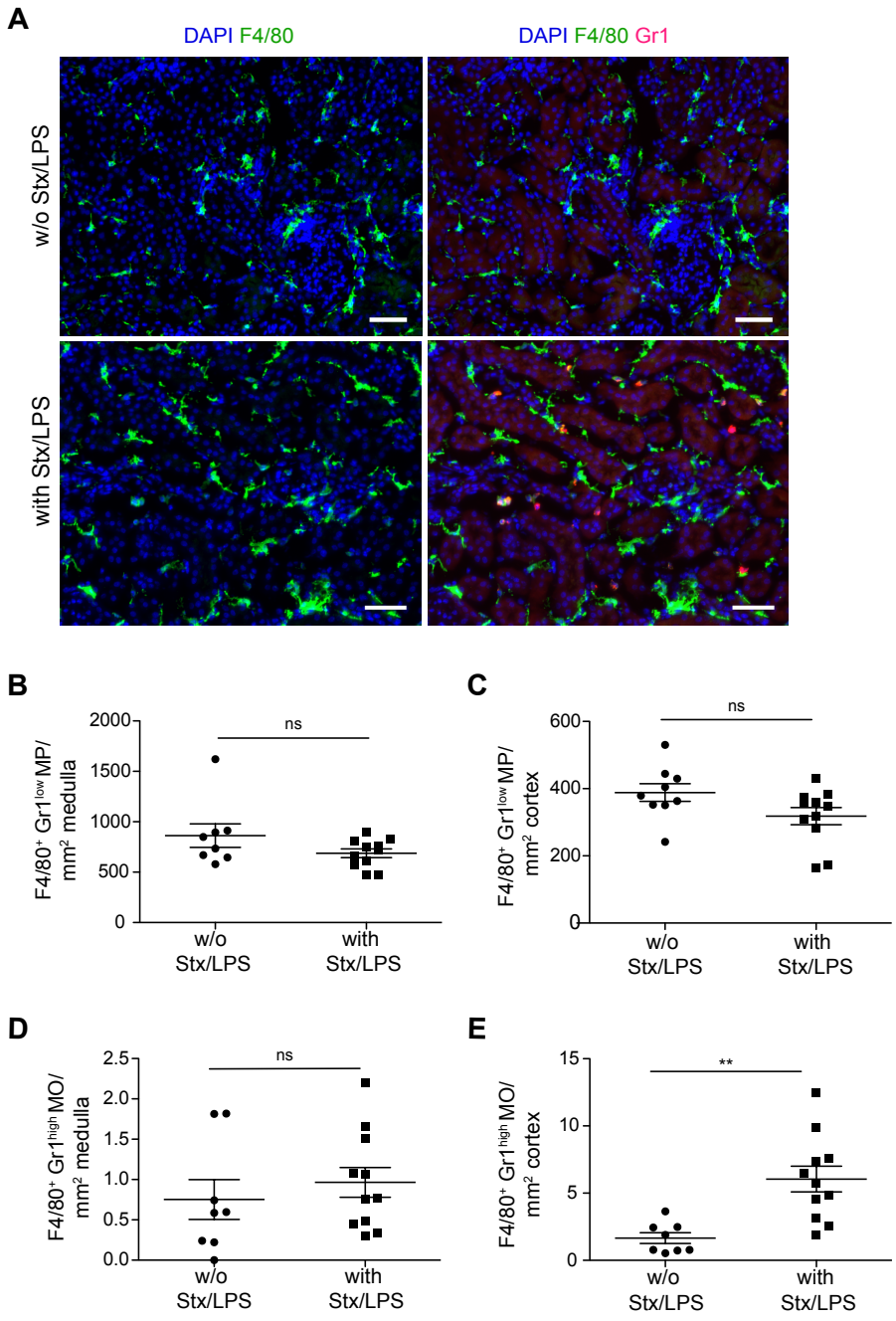

Figure 5.10: Elevated abundance of Gr1^{high} monocytes in the renal cortex.
(A) Immunofluorescent images from the renal cortex of untreated mice (upper row) and one day post Stx/LPS injection (lower row). Kidney slices were stained for Gr1 (red), F4/80 (green) and for cellular nuclei (DAPI, dark-blue). The white bar indicates 50 µm. (**B-E**) Numbers of Gr1^{low} macrophages (F4/80^{+} Gr1^{low}) (B and C) and Gr1^{high} monocytes (F4/80^{+} Gr1^{high}) (D and E) in the medulla (B and D) and in the renal cortex (C and E) 1 day after Stx/LPS injection. Representative data of $n = 9$ (w/o Stx/LPS), $n = 12$ (with Stx/LPS). Results are given as means +/- s.e.m. *$p < 0.05$; **$p < 0.01$. d = day, MO = monocytes, MP = macrophages. The kidney slices were stained and imaged by Julia Volke as part of her master project under my supervision.

5.2.7 Elevated endothelial injury within the renal cortex

To analyze whether this cortical monocytic infiltrates were associated with kidney damage, endothelial damage was localized in the kidney by a novel imaging technique. For this purpose, positron emission tomography (PET) combined with co-registered magnet resonance (MR) imaging were performed in the Werner Siemens Imaging Center in Tübingen. For PET imaging a [^{64}Cu]NOTA- glycoprotein VI (GPVI)-Fc tracer was injected into mice 24 h after Stx/LPS treatment. This tracer is composed of a radioactive label [^{64}Cu] linked to a NOTA-spacer and the soluble form of the dimeric GPVI fusion protein, which specifically binds to collagen[108, 109]. Subendothelial collagen is exposed after endothelial damage leading to [^{64}Cu]NOTA-GPVI-Fc tracer binding.

As shown in Figure 5.11 uptake of the [^{64}Cu]NOTA-GPVI-Fc tracer was enhanced within the kidneys of Stx/LPS-injected mice, indicated by the red color (Fig. 5.11 A). These findings demonstrate endothelial damage primarily in kidneys of Stx/LPS-treated mice. Notably, accumulation of the tracer was also observed in the liver of healthy and Stx/LPS-injected mice (Fig. 5.11 A). This is a common phenomenon for ^{64}Cu-labelled tracers due to the trans-chelation process of copper by liver enzymes[114] rather than direct endothelial damage in the liver. Quantification of *in vivo* PET-MR analysis revealed a significant increase of tracer uptake within the kidney at day two. However, tracer uptake of mice injected with Stx/LPS was increased compared to untreated control mice over the complete course of the experiment (Fig. 5.11 B).

The elevated tracer uptake in Stx/LPS-injected mice measured by PET-MR imaging revealed endothelial damage and identified a novel-non-invasive imaging technique to evaluate endothelial damage in HUS.

Next, e*x vivo* autoradiography, which has a higher resolution than the *in vivo* imaging, was performed to discriminate between endothelial damage in the renal cortex and the medulla. This method revealed that tracer-uptake was considerably elevated within the cortex (Fig. 5.11 A, lower right image) indicating cortical injury. Hence, monocytic infiltrates shown by histology in Figure 5.10 are associated with cortical inflammation suggesting that the local appearance of Gr1^{high} monocytes in the renal cortex may cause kidney injury.

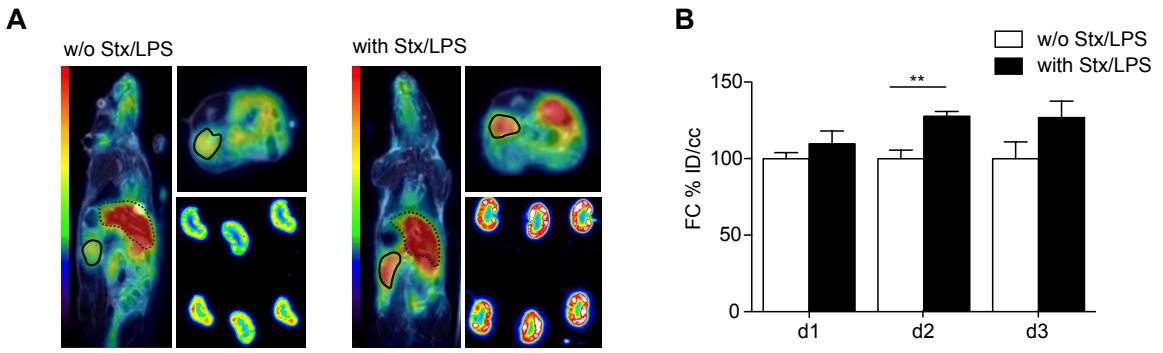

Figure 5.11: Endothelial injury in the renal cortex after Stx/LPS injection.
(A) Representative *in vivo* PET images in healthy control mice (w/o Stx/LPS; left and upper right image) and two days after Stx/LPS-injection (with Stx/LPS; left and upper right image). The right kidney (solid line) and the liver (dashed line) are encircled for visualization. E*x vivo* autoradiography (images with 6 kidney slices (lower right image)) were analyzed in healthy controls and 3 days after Stx/LPS injection. (**B**) *In vivo* quantification of [^{64}Cu]NOTA-GPVI-Fc uptake in kidneys of untreated (white bar) and Stx/LPS-treated mice (black bar) on day one to day three (raw images in A, upper right image). The values are indicated as the mean of % injected dose (ID)/cc. (Representative data of (A and B) *n* = 3 (w/o Stx/LPS), *n* = 5 (with Stx/LPS). Results are given as means +/- s.e.m. *p < 0.05; **p < 0.01; *** p < 0.001. FC = Fold change; %ID/cc = percentage injected dose per cubic centimeter; d = day. These data were generated by Kerstin Fuchs in the Werner Siemens Imaging Center in Tübingen.

5.2.8 Targeting monocytes and macrophages ameliorates Stx-mediated kidney injury

To test whether monocytic cell recruitment to the renal cortex facilitates Stx-mediated kidney damage, renal injury was assessed in the absence of monocytes. To analyze the contribution of Gr1^{high} monocytes to renal damage, *Ccr2*-deficient mice were employed. The number of Gr1^{high} monocytes was strongly reduced in the blood and kidney of *Ccr2*-deficient animals (*Ccr2*$^{-/-}$ *Cx$_3$cr1*$^{+/gfp}$) (Fig. 5.12 A, B). Of note, also the frequency of Gr1^{low} monocytes in the blood of *Ccr2*$^{-/-}$ mice was slightly diminished. However, the numbers of Gr1^{low} macrophages in the kidney were not affected by *Ccr2*-deficiency (Fig. 5.12 C, D).

Ccr2-deficient mice were injected with Stx/LPS and serum BUN levels on day three were measured. *Ccr2*-deficient mice showed reduced BUN levels in the serum, which suggest that Gr1^{high} monocytes partially induce kidney damage. However, BUN levels were not reduced to levels of healthy controls indicating residual kidney damage in *Ccr2*-deficient animals (Fig. 5.12 E). This finding demonstrates that Gr1^{high} monocytes are partially involved in HUS induction.

Next, the survival rate of *Ccr2*-deficient mice was determined. The survival was prolonged in the absence of Gr1^{high} monocytes after Stx/LPS treatment. Approximately 35% of *Ccr2*-deficient mice survived Stx/LPS injection, whereas the survival rate of C57BL/6 mice was only 5% (Fig. 5.12 F). In summary, these data suggested ameliorated kidney damage in absence of Gr1^{high} monocytes.

The partial reduction of kidney damage suggested that other *Ccr2*-independent cells might be involved in the pathology of HUS. Given that CX_3CR1 has been considered, crucial for the survival of Gr1^{low} monocytes and macrophages[115, 116] and for the pathology of HUS in humans[117], kidney damage was investigated in the absence of CX_3CR1 and CCR2. To investigate if the residual kidney damage in *Ccr2*-deficient mice was mediated by CX_3CR1-expressing Gr1^{low} cells, *Ccr2*-deficient animals were crossed to *Cx$_3$cr1*-deficient mice. The abundance of Gr1^{low} monocytes in the blood and Gr1^{low} macrophages in the kidney was significantly reduced in *Ccr2$^{-/-}$ Cx$_3$cr1$^{gfp/gfp}$* animals compared to *Ccr2$^{-/-}$* and wildtype control mice (Fig. 5.12 C, D). Due to the *Ccr2*-deficiency also Gr1^{high} monocytes were absent in blood and kidney of these mice (Fig. 5.12 A, B).

In comparison to C57BL/6 and *Ccr2$^{-/-}$* mice, *Ccr2$^{-/-}$ Cx$_3$cr1$^{gfp/gfp}$* mice showed significantly and strongly reduced BUN levels in the serum upon Stx/LPS treatment. Notably, the BUN levels of *Ccr2$^{-/-}$ Cx$_3$cr1$^{gfp/gfp}$* reached baseline levels indicating complete protection of these mice from Stx-mediated kidney injury (Fig. 5.12 E).

Ccr2$^{-/-}$ Cx$_3$cr1$^{gfp/gfp}$ mice also showed prolonged survival after Stx/LPS injection compared to C57BL/6 and CCR2-deficient mice. About 67% of *Ccr2$^{-/-}$ Cx$_3$cr1$^{gfp/gfp}$* animals survived a Stx/LPS-dose that was lethal for 95% of the control mice (Fig. 5.12 F). However, although *Ccr2$^{-/-}$ Cx$_3$cr1$^{gfp/gfp}$* mice were completely protected from kidney injury, 33% of these mice died after Stx/LPS treatment, suggesting Stx/LPS-mediated damage in other organs than the kidney.

Taken together these results suggest an involvement of both cell subtypes, Gr1^{high} monocytes and Gr1^{low} macrophages, in kidney damage and lethality in HUS.

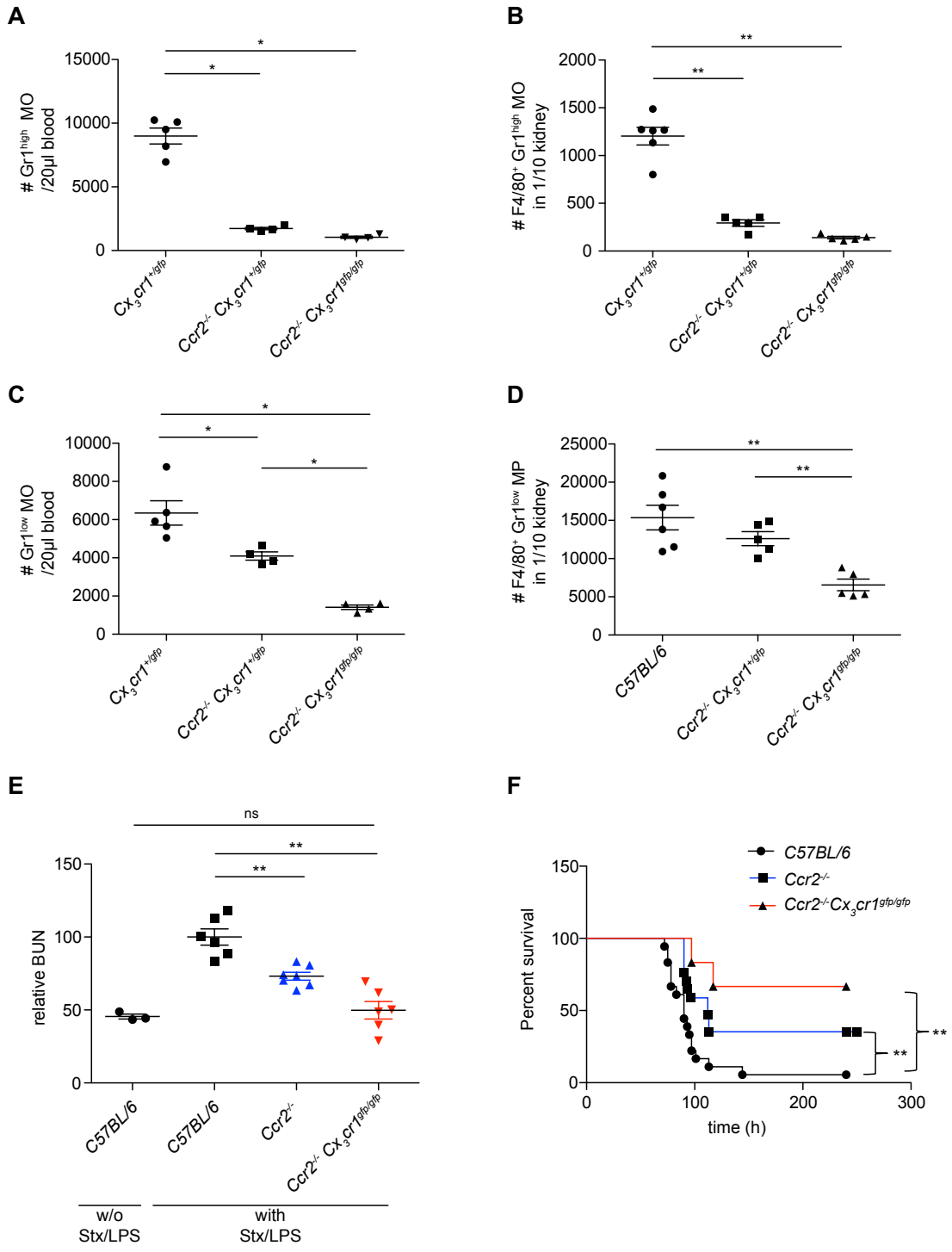

Figure 5.12: Lack of monocytes and macrophages protects from Stx-mediated renal damage.
(**A, B**) Absolute cell counts of Gr1^{high} blood MOs (**A**) and renal Gr1^{high} MOs (**B**) in *Cx$_3$cr1$^{+/gfp}$ or* C57BL/6, *Ccr2$^{-/-}$ Cx$_3$cr1$^{+/gfp}$* and *Ccr2$^{-/-}$ Cx$_3$cr1$^{gfp/gfp}$* mice. (**C, D**) Numbers of Gr1^{low} blood MOs (**C**) and Gr1^{low} kidney MPs (**D**) in *Cx$_3$cr1$^{+/gfp}$ or* C57BL/6, *Ccr2$^{-/-}$ Cx$_3$cr1$^{+/gfp}$* and *Ccr2$^{-/-}$ Cx$_3$cr1$^{gfp/gfp}$* mice. (**E**) Fold change of plasmatic BUN levels three days after Stx/LPS injection in C57BL/6 (black), *Ccr2$^{-/-}$* (blue) and *Ccr2$^{-/-}$ Cx$_3$cr1$^{gfp/gfp}$* (red) mice (with Stx/LPS) compared to untreated C57BL/6 mice (w/o Stx/LPS). (**F**) Survival of C57BL/6 (black), *Ccr2$^{-/-}$* (blue) and *Ccr2$^{-/-}$ Cx$_3$cr1$^{gfp/gfp}$* (red) mice, which were injected with Stx/LPS. Representative data of (F) C57BL/6 *n* = 18 mice, *Ccr2$^{-/-}$ n* = 15 mice. Results are given as means +/- s.e.m. *p < 0.05; **p < 0.01. MO = monocytes; MP = macrophages; BUN = blood urea nitrogen.

5.3 Neutrophil Migration and Adhesion in Stx-induced Kidney Injury

In the second part of this thesis the involvement of neutrophil adherence and recruitment in the pathogenesis of HUS was investigated.

5.3.1 Stx/LPS increases neutrophil abundance in the blood

It is well known that STEC-HUS patients have increased neutrophil counts within the blood[100]. Also, clinical data from our collaborators indicated increased neutrophil counts in STEC-HUS patients from the E.Coli O4:H104 outbreak in 2011 (data not shown). To investigate neutrophil abundance in the HUS-mouse model, blood from Stx/LPS-injected mice was investigated by flow cytometry. For this purpose, cells were analyzed for Ly6G expression, which is specific for neutrophils. The gating strategy for blood neutrophils is shown in figure 5.13.

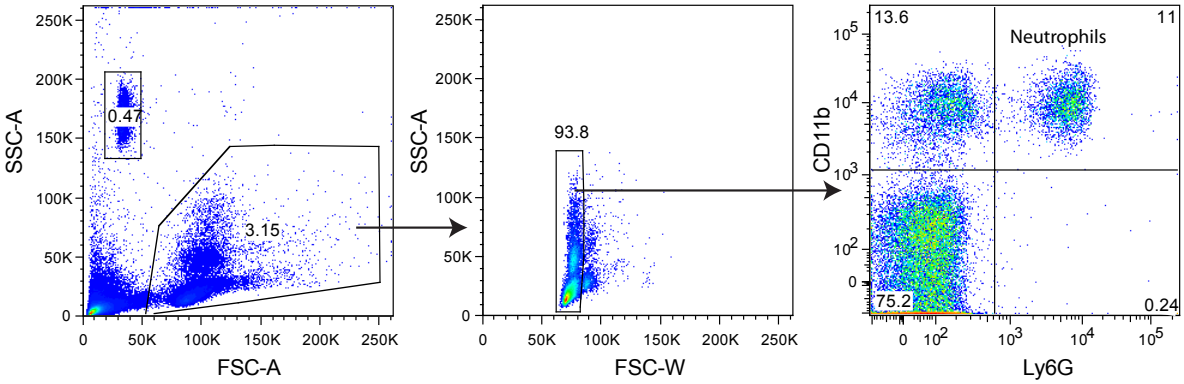

Figure 5.13: Gating strategy for neutrophils in blood.
The SSC/FSC plot (1st plot) indicates all events detected by flow cytometry in blood of an untreated mouse. First, small particles were removed from further analysis by setting a leukocyte gate (2nd plot). In the next step cell clumps and doublets were excluded from analysis (3rd plot). Then, Ly6G and CD11b positive events were gated (upper right quadrant) and defined as neutrophils.

Flow cytometric analysis revealed 11,81% neutrophils in the blood of untreated control mice. Upon Stx/LPS treatment the neutrophil fraction was strongly increased in the blood with a peak frequency of 50,6% neutrophils at day one. At day two the abundance of neutrophils was decreasing. However, neutrophil frequencies at days two (26,2%) and three (20,0%) remained slightly elevated compared to untreated control mice (Fig. 5.14 A, B).

Next, the activation of these blood neutrophils was analyzed by measuring the MFI of CD11b. A profound induction of CD11b expression was detected one day after Stx/LPS treatment indicating cellular activation. Comparable to neutrophil abundances the CD11b expression was decreased on the following days, but did not reach basal levels of untreated mice (Fig. 5.14 C).

In summary, these data showed that Stx/LPS treatment led to increased proportion and elevated activation of neutrophils in the blood suggesting an involvement of neutrophils in HUS.

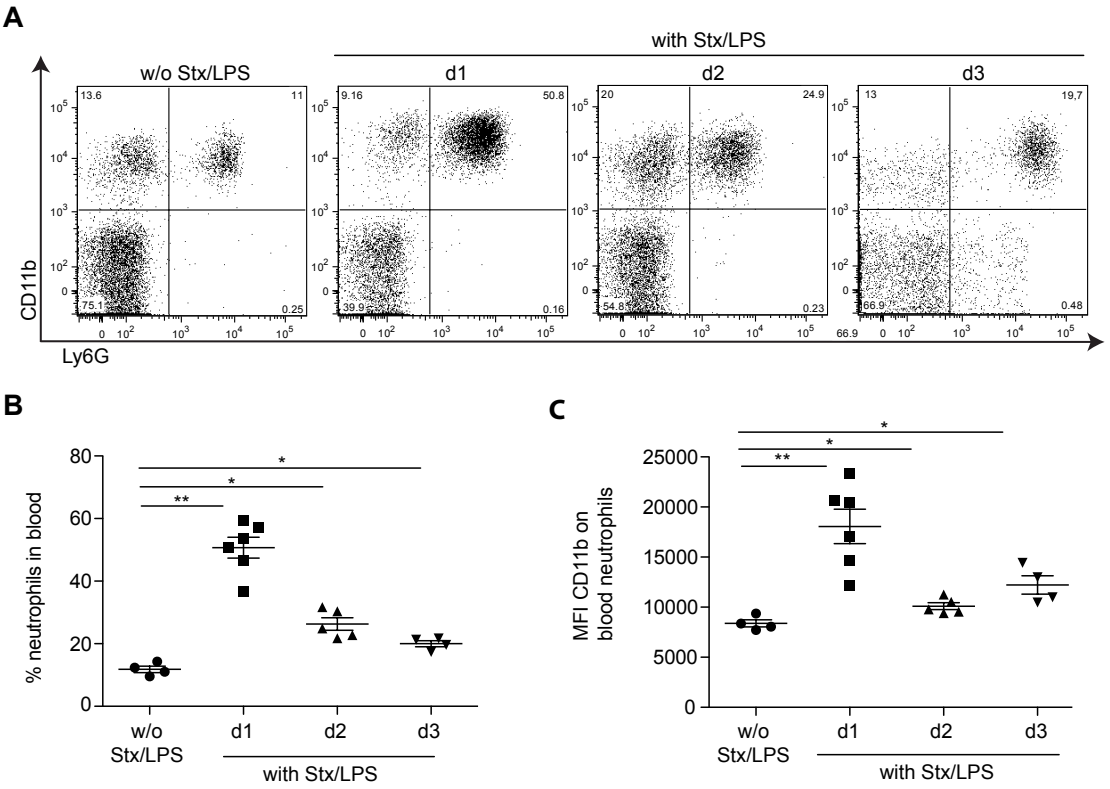

Figure 5.14: Increased abundance and activation of blood neutrophils.
(**A**) Flow cytometry analysis of blood cells in untreated mice (w/o Stx/LPS) and on day one to day three after Stx/LPS treatment (with Stx/LPS, d1-d3). Blood cells were analyzed for CD11b and Ly6G expression. (**B**) Frequency of neutrophils within the blood of untreated mice (w/o Stx/LPS) and on day one to day three (d1-d3) in Stx/LPS-injected mice (with Stx/LPS). (**C**) Mean fluorescence intensity (MFI) of CD11b on neutrophils in the blood of Stx/LPS-treated (with Stx/LPS) and control mice (w/o Stx/LPS). Results are given as means +/- s.e.m. *$p < 0.05$; **$p < 0.01$. d = day; MFI = mean fluorescence intensity.

5.3.2 Stx/LPS leads to neutrophil recruitment into the kidney

Previous experiments demonstrated increased abundance and elevated activation of neutrophils in blood of Stx/LPS-treated mice suggesting a potential role of these cells in the pathogenesis of HUS. In the following experiments, the role of neutrophil infiltration into the kidney during HUS was investigated.

To this end renal levels of the neutrophil-attracting chemokine CXCL1 were measured and flow cytometric analysis of single cell suspensions from the kidney were performed. $CD45^+$ immune cells were analyzed for Ly6G expression to identify neutrophils. The gating strategy for neutrophils within the kidney is shown in Figure 5.15.

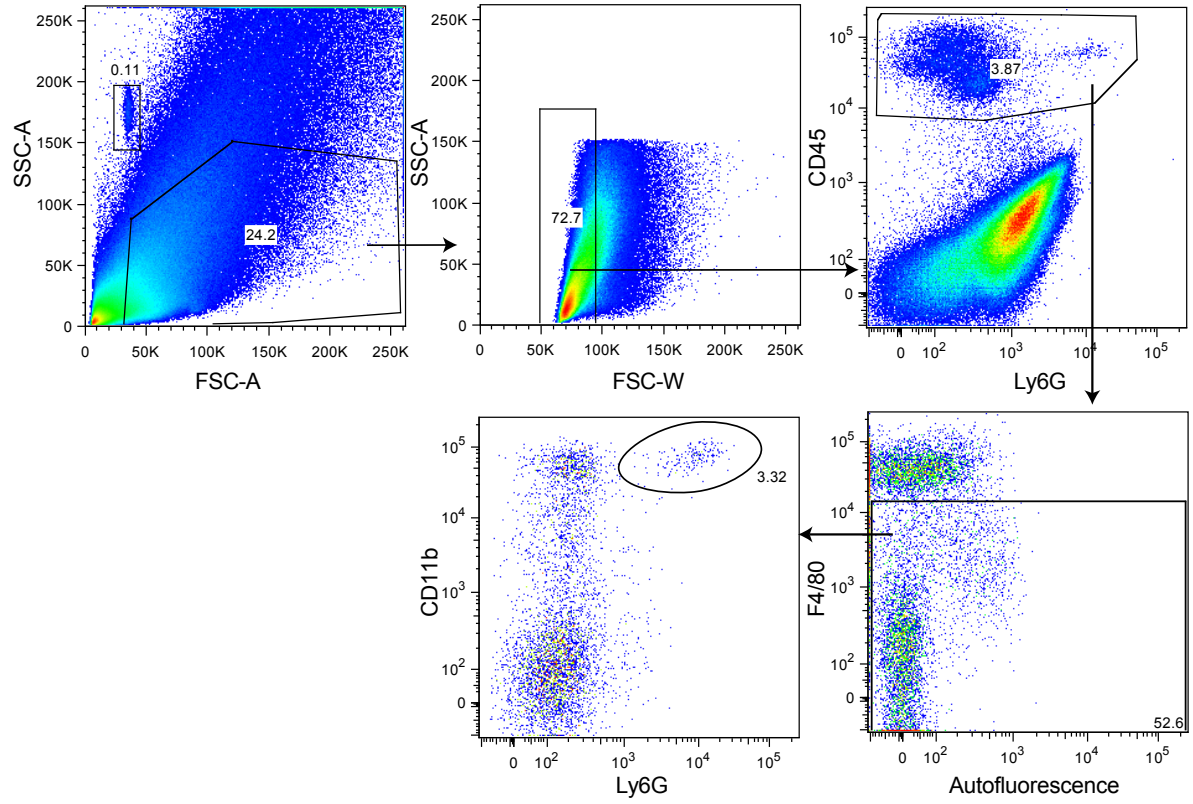

Figure 5.15: Gating strategy for neutrophils in kidney.
The SSC/FSC plot (upper left) shows all events detected in the kidney of an untreated mouse by the flow cytometry. First, small particles were removed from further analysis by setting a leukocyte gate (1st row, left plot). In the next step, cell clumps and doublets were excluded from analysis (1st row, middle plot). Then, renal immune cells were selected by gating for $CD45^+$ cells (1st row, right plot). Next, macrophages were excluded from further analysis by gating $F4/80^-$ cells (2nd row, right plot). Finally, Ly6G and CD11b positive events were gated (2nd row, left plot) and defined as neutrophils.

First, protein levels of CXCL1, a potent chemoattractant for neutrophils, was analyzed in supernatants of homogenized kidneys in control and Stx/LPS-treated mice. Renal CXCL1 levels were increased on day one and three upon Stx/LPS administration, representing a potential stimulus for neutrophil recruitment (Fig. 5.16 A).

Consistent with this finding, renal neutrophil abundance was increased upon Stx/LPS-treatment. Neutrophil frequencies peaked with 10,5% on day one. Then, neutrophil fraction was decreasing on the following days. However, the frequencies did not return to baseline levels (3,7%), but remained slightly increased (6,6% on day two, 5,6% on day three) compared to untreated mice (Fig 5.16 B and C).
Moreover, the CD11b expression by neutrophils located in the kidney was analyzed. In accordance with CXCL1 levels, the CD11b expression was increased at day one and three after Stx/LPS injection, indicating cellular activation of renal neutrophils (Fig. 5.16 D).

Taken together these data demonstrate that increased renal CXCL1 level correlated with recruitment and activation of neutrophils in the kidneys of Stx/LPS-injected mice.

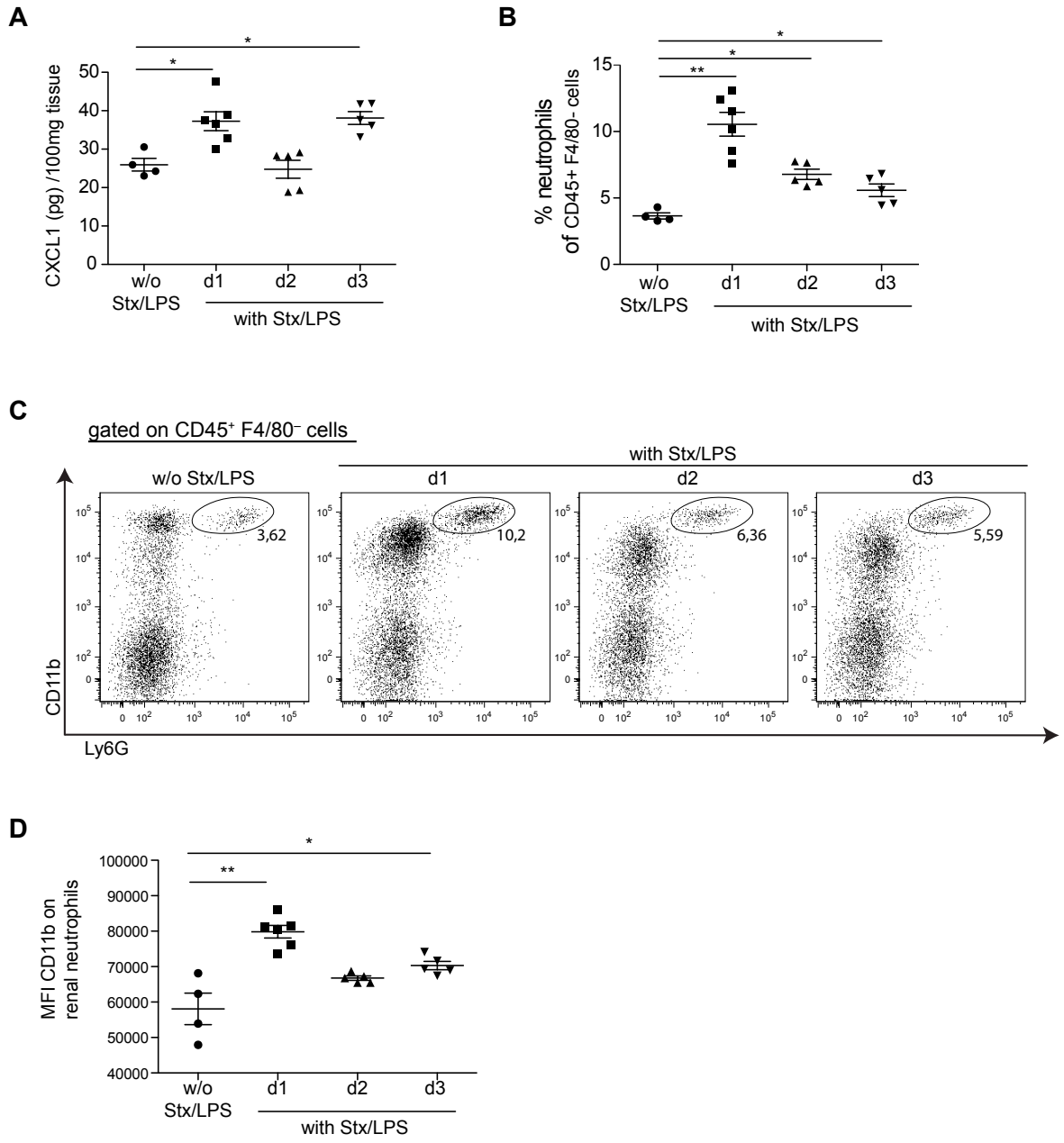

Figure 5.16: Increased neutrophil recruitment and activation in kidneys of Stx/LPS-injected mice. (**A**) CXCL1 levels in kidney homogenates of untreated (w/o Stx/LPS) and Stx/LPS-injected mice (with Stx/LPS) on day one to day three (d1-d3). (**B**) Frequencies of neutrophils analyzed on day one to day three after Stx/LPS administration. (**C**) Renal leukocytes ($CD45^+$) were analyzed for their CD11b and Ly6G expression on day 1 to day 3 (d1-d3) by flow cytometry in untreated (w/o Stx/LPS) and Stx-treated mice (with Stx/LPS). (**D**) Mean fluorescence intensity (MFI) of CD11b on neutrophils in the kidney of Stx/LPS-treated (with Stx/LPS) and control mice (w/o Stx/LPS). Data in (C) are representative for n = 4-6. Results are given as means +/- s.e.m. *$p < 0.05$; **$p < 0.01$. d = day; MFI = mean fluorescence intensity.

5.3.3 Accumulation of neutrophils within the renal cortex

The flow cytometry analysis indicated infiltration of neutrophils into the kidney of Stx/LPS-treated mice. Next, the localization of neutrophils in the kidney was investigated by histology.

Histological sections were stained with antibodies against Gr1, which bind to Ly6G and Ly6C. In order to distinguish $Ly6G^+$ neutrophils from $Gr1^{high}/Ly6C^+$ inflammatory monocytes the sections were also stained with the macrophage marker F4/80. Cells, which were not expressing F4/80 (green), but showed Gr1 expression (red), were defined as neutrophils.

Consistent with flow cytometry data (Fig. 5.16 B), immunofluorescent images revealed low numbers of neutrophils in kidneys of untreated mice. However, Stx/LPS treatment led to an increase of neutrophils in the kidney (Fig. 5.17 A). Quantification of these cells in the different renal compartments showed, that neutrophils were predominantly increased within the renal cortex, whereas the neutrophil number in the medulla remained unchanged (Fig. 5.17 A to C). This finding indicates that neutrophils are specifically recruited into the renal cortex, which is in line with the increased presence of cortical $Gr1^{high}$ monocytes (Fig. 5.10). Moreover, thorough analysis of cortical neutrophil infiltrates indicated, that upon Stx/LPS treatment neutrophils were more numerous in particular within the glomerulus, which represents the filter unit of the kidney (Fig. 5.18).

These data demonstrate local appearance of neutrophils in cortex and the glomerulus upon Stx/LPS treatment, which might result in cortical endothelial damage (Fig. 5.11) and impaired functionality of the kidney (Fig. 5.1).

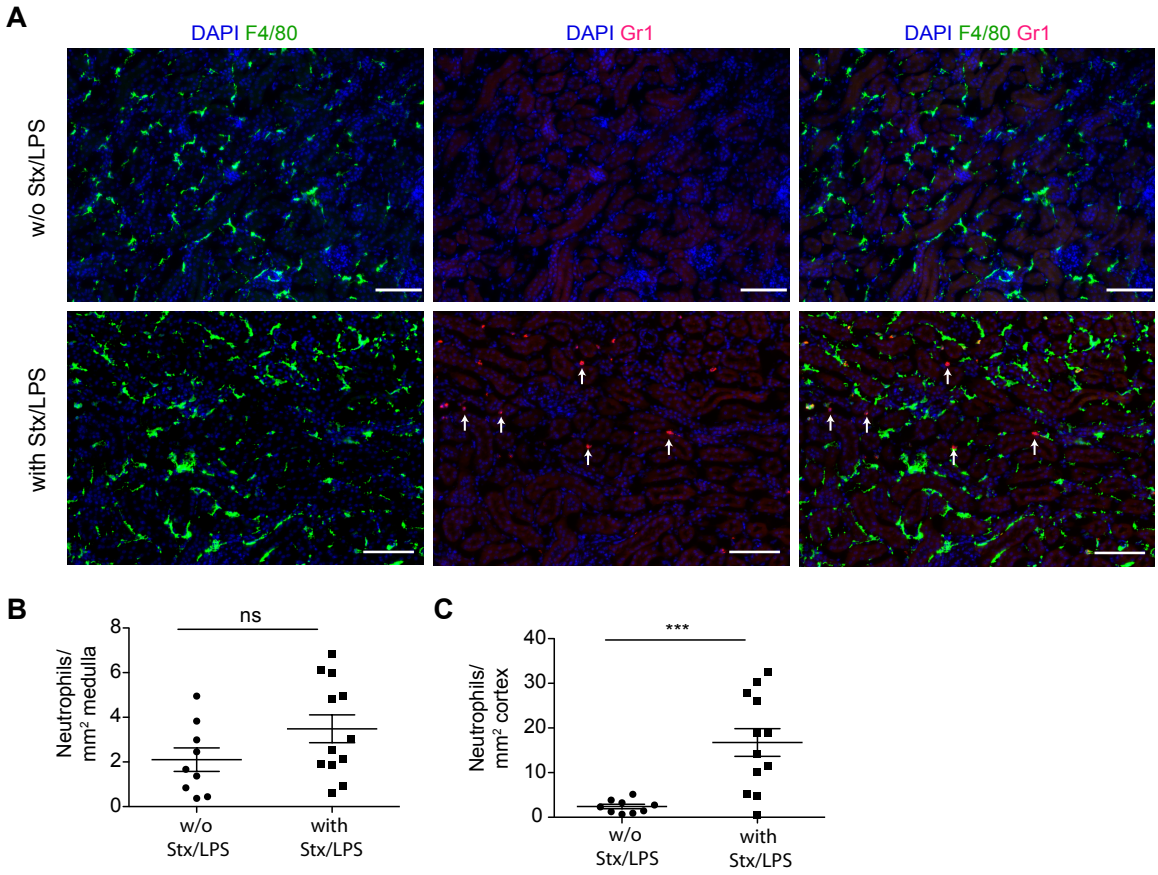

Figure 5.17: Stx/LPS induces neutrophil recruitment to the renal cortex.
(**A**) Immunofluorescent images from the renal cortex of untreated (upper row) and Stx/LPS-injected (lower row) mice, which were stained for Gr1 (red), F4/80 (green) and for cellular nuclei (DAPI, dark-blue). The white arrow points on neutrophils. The white bar indicates 50 µm. (**B**, **C**) Number of neutrophils in the medulla (**B**) and in the renal cortex (**C**) one day after Stx/LPS injection. Representative data of (A) $n = 3$ w/o Stx/LPS $n = 9$, with Stx/LPS $n = 12$. Results are given as means +/- s.e.m. *** $p < 0.001$. Imaging and quantification was performed by Julia Volke as part of her Master project under my supervision.

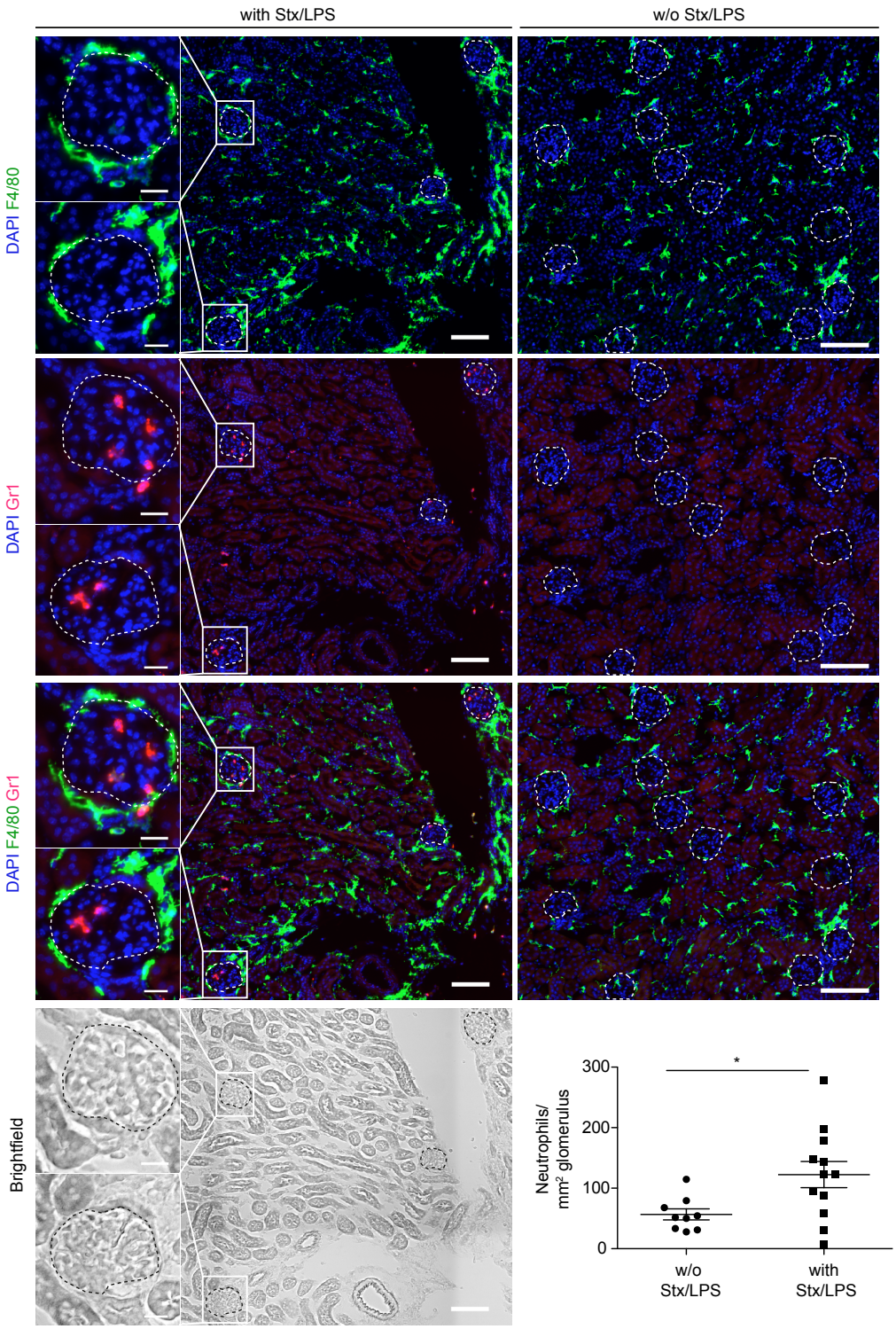

Figure 5.18: Intraglomerular neutrophils in Stx/LPS-treated mice.
Cryosections from kidneys of untreated (w/o Stx/LPS, right panel) and Stx/LPS-injected (with Stx/LPS, left panel) mice one day after Stx/LPS injection. Sections were stained for Gr1 (red), F4/80 (green) and for cellular nuclei (DAPI, dark-blue). The white dashed line highlights the glomerulus and the white bar indicates 100 µm. The detailed images (left side) show representative images of glomeruli with $Gr1^+$ neutrophils. The white bar indicates 10 µm. The scatter plot shows the quantification of neutrophils within the glomeruli one day after Stx/LPS injection. Representative data *of* w/o Stx/LPS $n = 9$, with Stx/LPS, $n = 12$. Results are given as means +/- s.e.m. *$p < 0.05$. Imaging and quantification was performed by Julia Volke as part of her Master project under my supervision.

5.3.4 Role of integrin-dependent adhesion for kidney damage in HUS

Increased numbers of neutrophils within the renal cortex and in particular within the glomerulus imply potential involvement of neutrophil recruitment and adhesion for cortical endothelial damage during HUS. Harding *et al*. showed in a mouse model of *Staphylococcus aureus* infection, that neutrophil recruitment and capillary crawling is mainly mediated by α4- and β2-integrins[118]. Thus, the following experiments focused on the role of these two integrin types in the pathogenesis of HUS.

5.3.4.1 Increased VCAM-1 expression in HUS

At first the role of the α4ß1-integrin, also know as Very Late Antigen-4 (VLA-4), was investigated during HUS. VLA-4 is expressed on leukocytes and binds to the Vascular Cell Adhesion Molecule-1 (VCAM-1), which is expressed by endothelial cells. Clinical data from our collaborator revealed a strong increase of soluble VCAM-1 the in the serum of STEC-HUS patients. Moreover, the expression level of VCAM-1 directly correlated with disease severity. Thus, patients with uncomplicated HUS had only slightly increased VCAM-1 levels, whereas patients with severe HUS had significantly elevated levels of VCAM-1 in the serum (5.19 A). These findings suggested potential involvement of VLA-4-VCAM-1 interactions in HUS.

In order to validate the patient data in our mouse model, VCAM-1 expression levels were investigated in the serum and kidney of Stx/LPS-injected mice by ELISA and qRT-PCR. Notably, Stx/LPS-injected mice showed elevated VCAM-1 protein levels in the serum and in kidney homogenates of Stx/LPS-injected mice demonstrating systemic and local induction of this protein (Fig. 5.19 B, C). This finding was corroborated by a 2-fold induction of VCAM-1 mRNA within the kidney (Fig. 5.19 D). Hence, the HUS mouse model confirms the Stx-mediated VCAM-1 induction, observed in STEC-HUS patients.

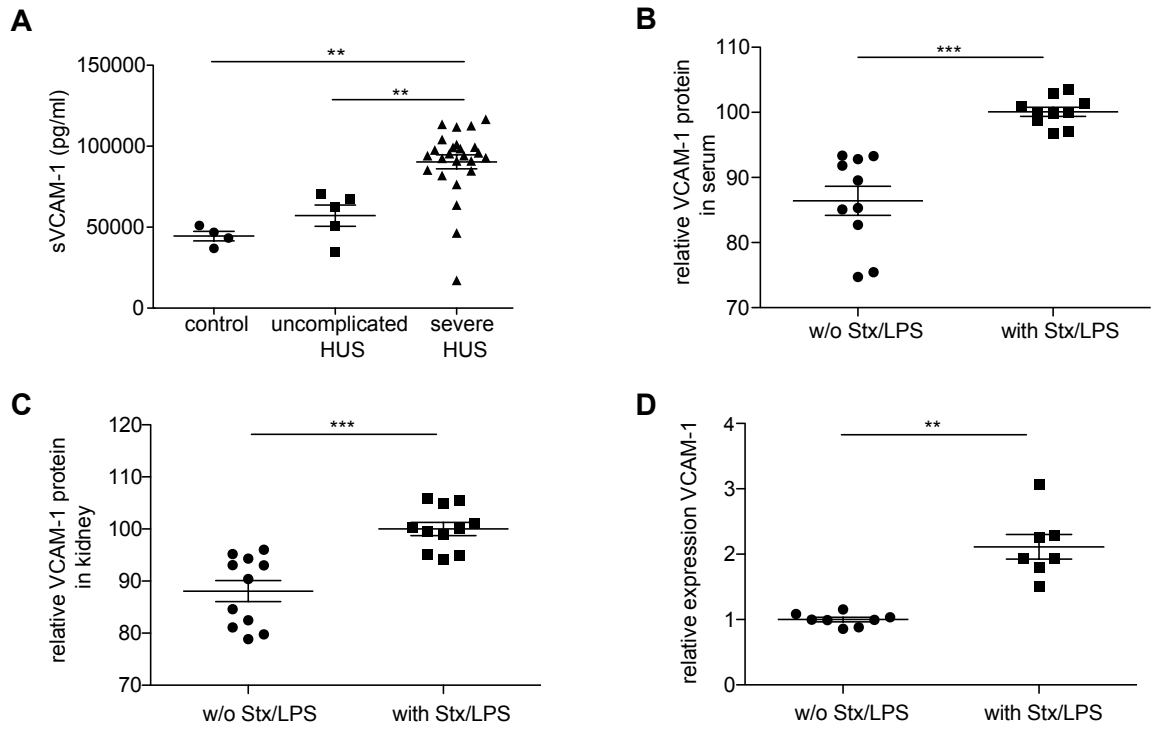

Figure 5.19: Elevated VCAM-1 expression in kidney and serum during HUS.
(**A**) Protein levels of VCAM-1 in patients with uncomplicated or severe STEC-HUS compared to the healthy controls. (**B**, **C**) Relative VCAM-1 protein level in serum (**B**) and kidney (**C**) of Stx/LPS-injected (with Stx/LPS) and untreated mice (w/o Stx/LPS). (**D**) Relative expression of VCAM-1 in kidney samples was determined by qRT-PCR in untreated control mice (w/o Stx/LPS) and on day 1 to day 3 after Stx/LPS administration and normalized to HPRT expression. Results are given as means +/- s.e.m. *$p < 0.05$; **$p < 0.01$. Data in (A) were collected by Hans-Joachim Paust, University Hospital Hamburg-Eppendorf.

5.3.4.2 Targeting VCAM-1-VLA-4 interaction does not ameliorate kidney damage

The induction of the VLA-4-ligand VCAM-1 in STEC-HUS patients and Stx/LPS-injected mice suggested a potential involvement of VCAM-1-VLA-4 mediated neutrophil adhesion in the pathogenesis of HUS. To examine the contribution of these interactions to kidney damage, VCAM-1 or VLA-4-mediated binding was prevented by injecting antibodies against these molecules.

Stx/LPS-injected mice, which were treated with an anti-VCAM-1-antibody (α-VCAM-1), had comparable BUN levels to mice injected with the corresponding isotype control. This data indicated that α-VCAM-1 treatment could not prevent Stx-mediated renal injury (Fig. 5.20 A).

Next, VLA-4 was targeted in Stx/LPS-injected mice and kidney injury was examined. In order to completely block the VLA-4 complex, antibodies against both subunits (CD49d and CD29) were injected. Of note, BUN values of Stx/LPS-injected mice in general were only slightly increased compared to untreated control mice, demonstrating reduced Stx-toxicity in this experiment. However, comparable BUN levels in the isotope- and α-VLA-4-treated groups indicated, that targeting VLA-4 did not reduce kidney damage (Fig. 5.20 B).

Collectively these findings could not demonstrate a potential contribution of VCAM-1-VLA-4-mediated neutrophil adhesion to kidney damage in the mouse model of HUS.

5.3.4.3 Blocking ß-2 Integrin does not improve renal injury in Stx/LPS-injected mice

In addition to the α4–integrin, neutrophil recruitment also depends on ß2–integrin, known as CD18[118]. CD18 forms dimers with four different α-chains, which are CD11a, CD11b, CD11c and CD11d. Previous experiments indicated strong induction of CD11b expression on neutrophils in blood and kidney upon Stx/LPS injection (Fig. 5.14, 5.16) suggesting involvement of this integrin during HUS.

To determine whether CD18-mediated adhesion leads to renal injury in HUS mouse model, mice were treated with anti-CD18-antibody (α-CD18). The BUN levels of mice treated with α-CD18 were mildly decreased compared to mice injected with the isotype control. On average BUN levels were decreased by approx. 20% after injecting α-CD18 in Stx/LPS-treated mice. However, this analysis did not reach statistical significance (Fig. 5.20 C). Taken together these results showed, that blocking CD18 might slightly ameliorate, but could not prevent kidney damage in Stx/LPS-treated mice.

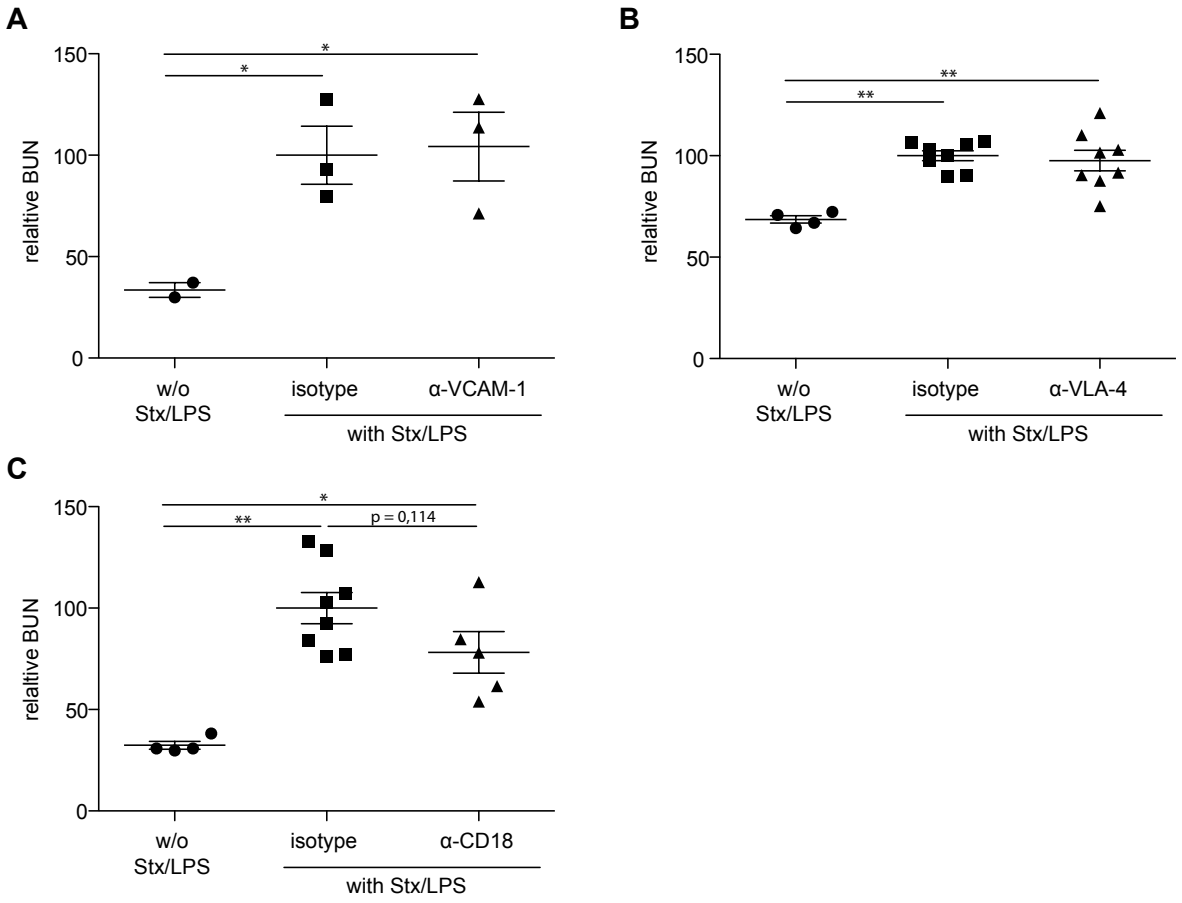

Figure 5.20: Targeting α4- and β2-integrins does not ameliorate Stx-mediated kidney injury.
(**A**, **B**, **C**) Fold change of plasmatic BUN levels three days after Stx/LPS administration (with Stx/LPS) in animals injected daily with either (**A**) VCAM-1 antibody (α-VCAM-1), (**B**) a combination of CD49d and CD29d antibodies (α-VLA-4) or (**C**) CD18 antibody (α-CD18). As control BUN levels of untreated mice (w/o Stx/LPS) and Stx/LPS-injected mice treated with the corresponding isotype were analyzed.

5.3.5 Targeting CXCR2-dependent neutrophil recruitment improves clinical outcome in Stx/LPS-treated mice

Elevated CXCL1 expression and increased neutrophil numbers in the kidney suggested neutrophil recruitment in a CXCR2-dependent manner. To test whether infiltration of neutrophils to the kidney facilitates the disease development, kidney injury was assessed in the absence of the chemokine-dependent neutrophil recruitment. To this end, mice were treated with a selective CXCR2 inhibitor (SB 225002). Moreover, *Cxcr2*-deficient mice (*Cxcr2*$^{d/d}$) were employed.

Mice treated with the CXCR2 antagonist showed significantly reduced BUN levels compared to the control solvent (1% DMSO). The pharmacological CXCR2-blockage

reduced BUN levels by 20% upon Stx/LPS treatment (Fig. 5.21 A). However, serum BUN levels in CXCR2 antagonist-injected mice were increased compared to untreated control mice, demonstrating residual renal injury also after CXCR2 blocking. Thus, pharmacological inhibition of CXCR2-signalling by SB 225002 could not completely prevent Stx-mediated renal injury.

To ensure complete blockage of CXCR2-signaling, *Cxcr2*-deficient mice were employed. Stx/LPS-injected heterozygous littermates (*Cxcr2*$^{d/+}$), in which CXCR2-signalling is still functional, showed increased BUN level compared to untreated control mice. In contrast, BUN levels of *Cxcr2*-deficient mice (*Cxcr2*$^{d/d}$) were not elevated after Stx/LPS injection indicating normal kidney functionality (Fig. 5.21 B). Thus, *Cxcr2*-deficiency results in complete protection from Stx-induced kidney damage.

Next, survival experiments with *Cxcr2*-deficient mice and heterozygous littermates were performed. These experiments demonstrated significantly reduced mortality in absence of CXCR2-signalling. However, Stx/LPS treatment was still lethal in a small portion of *Cxcr2*-deficient mice suggesting Stx-mediated tissue damage in other organs than the kidney (Fig. 5.21 C).

In summary, these data revealed an improved clinical outcome in Stx/LPS-injected mice if CXCR2-signalling was inhibited, suggesting a crucial role of CXCR2-dependent neutrophil recruitment during HUS.

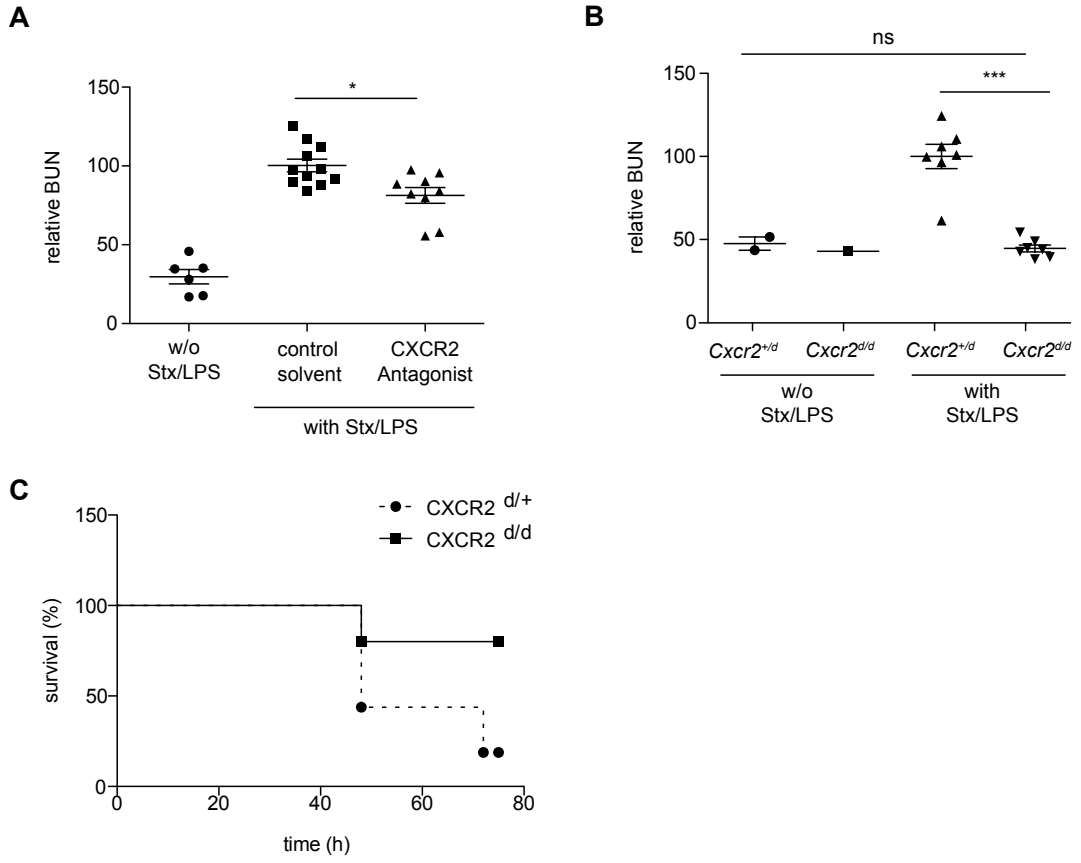

Figure 5.21: Targeting CXCR2 leads to improved clinical outcome in HUS.
(**A**) Fold change of plasmatic BUN 3 days after Stx/LPS administration (with Stx/LPS) in animals injected daily with either CXCR2 antagonist or the control solvent (1%DMSO) compared to untreated control mice (w/o Stx/LPS). (**B**) Plasmatic BUN levels in Stx-treated (with Stx/LPS) and untreated (w/o Stx/LPS) *Cxcr2*$^{+/d}$ and *Cxcr2*$^{d/d}$ mice. (**C**) Survival of *Cxcr2*$^{+/d}$ and *Cxcr2*$^{d/d}$ injected with Stx/LPS. Data in (C) are representative for *Cxcr2*$^{+/d}$ $n = 16$, *Cxcr2*$^{d/d}$ $n = 5$. Results are given as means +/- s.e.m. *p < 0.05; **p < 0.01. d = day.

5.3.6 Reduced numbers of adherent neutrophils within the glomerulus after CXCR2 blocking

Improved kidney functionality upon CXCR2 blockade suggested, that this chemokine receptor might facilitate renal injury by mediating recruitment and adhesion of neutrophils to the glomerulus. Intravital microscopy was performed to investigate adhering neutrophils in the glomeruli. To this end *Cx$_3$cr1$^{+/gfp}$* reporter mice were used to identify macrophages by CX$_3$CR1-expression. Additionally, mice were intravenously injected with anti-Gr1 antibody to enable discrimination of resident macrophages (CX$_3$CR1$^+$ Gr1$^-$), inflammatory monocytes (CX$_3$CR1$^+$ Gr1$^+$) and neutrophils (CX$_3$CR1$^-$ Gr1$^+$). Further, the vasculature was visualized by intravenous injection of Qdots.

Intravital microscopy revealed significantly increased numbers of neutrophils adhering to the glomerulus after injecting Stx/LPS (Fig. 5.22 A). In total, about eight adherent neutrophils per hour were located in one glomerulus after Stx/LPS administration. Notably, pharmacological inhibition of CXCR2 reduced the number of neutrophils within the glomerulus to the level of healthy controls (Fig. 5.22 A, B) suggesting that the CXCR2-dependent recruitment of neutrophils to the glomerular endothelium might cause kidney injury.

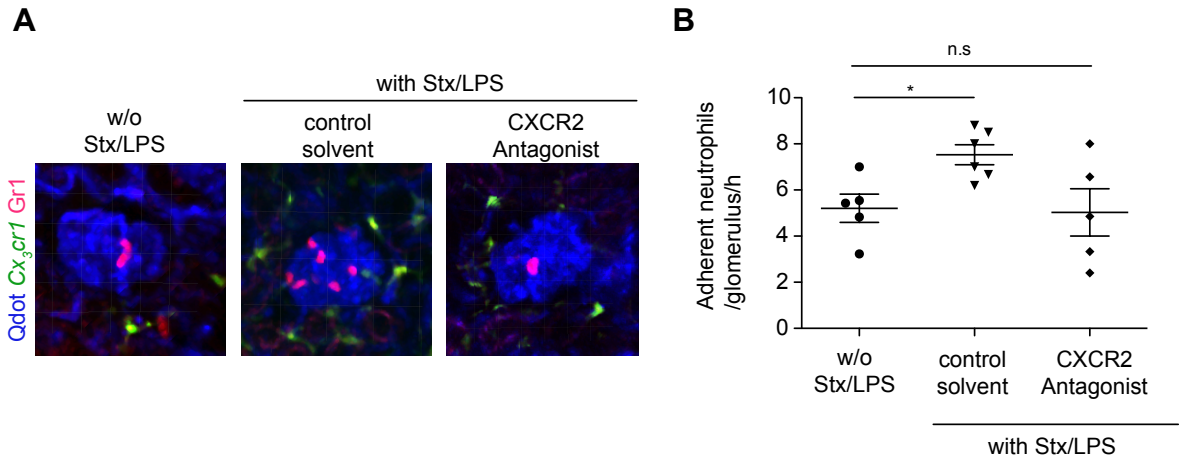

Figure 5.22: Blocking CXCR2 reduced adherent neutrophil in the glomerulus.
(**A**) Adherent neutrophils (red) in glomeruli of Stx/LPS-injected $Cx_3cr1^{gfp/+}$ mice (with Stx/LPS) treated with control solvent (1% DMSO) or CXCR2 antagonist compared to untreated $Cx_3cr1^{gfp/+}$ mice (w/o Stx/LPS) analyzed by intravital microscopy. Glomeruli are stained in blue by intravenous injection of Qdots655. (**B**) Quantification of adherent neutrophils per glomerulus in kidneys of $Cx_3cr1^{gfp/+}$ mice treated with control solvent (1% DMSO) or CXCR2 antagonist and Stx/LPS (with Stx/LPS) compared to untreated $Cx_3cr1^{gfp/+}$ mice (w/o Stx/LPS). Results are given as means +/- s.e.m. *$p < 0.05$. Intravital imaging was performed with Julia Volke as part of her Master project.

6 Discussion

6.1 Monocytes and Macrophages in the Pathogenesis of HUS

Monocytes and macrophages are critical inducers of various kidney diseases and targeting the recruitment and activation of these cells has been proven successful to prevent inflammation and disease induction[116, 119, 120, 121]. However, the role of monocytes and macrophages in HUS is incompletely understood.

Several descriptive studies refer to the importance of monocytes and macrophages in HUS. It was shown that Stx stimulates endothelial cells to secrete chemokines, which recruit and activate monocytes and macrophages[83]. Moreover, the analysis of blood from STEC-HUS patients indicated a correlation between monocyte frequencies and kidney damage, identifying monocyte counts as a potential predictive marker in HUS.

However, interventional studies are missing and the specific role of monocyte and macrophage subsets remains elusive. Thus, this study focused on analyzing the role of $Gr1^{high}$ inflammatory monocytes and $Gr1^{low}$ resident macrophages with regard to kidney damage in HUS.

6.1.1 Role of $Gr1^{high}$ monocytes in HUS

Endothelial cells have been shown to produce CCL2 upon Stx-treatment *in vitro*[83]. Also in HUS patients serum levels of CCL2 were elevated, which was associated with increased monocyte counts in renal biopsies[94]. Moreover, Keepers *et al.* showed that targeting monocyte-recruiting chemokines (CCL2, CCL3, CCL4 and CCL5) reduces the infiltration of monocytes into the kidney, which consequently leads to decreased fibrin deposits in a mouse model of HUS[95].

Consistent with these previous findings, our study demonstrated elevated levels of CCL2, CCL3, CCL4 and CCL5 in the kidney of Stx/LPS-treated mice. These chemokines mediate cell recruitment in a CCR2-dependent manner, which raised the hypothesis whether CCR2-dependent $Gr1^{high}$ monocytes are accountable for kidney damage during HUS.

Indeed, decreased abundance of Gr1^{high} monocytes in the blood and increased cell numbers within the kidney were detected by flow cytometry, which suggest infiltration of these monocyte populations into the kidney. The presence of Gr1^{high} monocytes has previously been associated with inflammation and tissue injury, resulting in reduced function of the kidney[119, 121]. These findings suggest that kidney damage in HUS might be partially caused by the local appearance of Gr1^{high} monocytes.

Beneficial effects of targeting monocyte recruitment into the kidney has been observed in various kidney diseases[119]. To investigate the specific role of Gr1^{high} monocytes to renal damage in HUS, *Ccr2*-deficient mice were injected with Stx/LPS. In line with previous studies[28, 29], the number of Gr1^{high} monocytes was strongly decreased in the blood and kidney of these mice. Of note, also the abundance of Gr1^{low} monocytes was slightly diminished in the blood of these mice, which might be explained by the lack of Gr1^{high} monocytes as progenitor cell[9]. However, the numbers of Gr1^{low} resident macrophages in the kidney were unchanged implying a normal ontogeny of these cells in the kidney. Additionally, these data suggest that the major part of Gr1^{low} macrophages in the kidney does not originate from CCR2-dependent blood monocytes. Stx/LPS injection into *Ccr2*-deficient mice, indeed, partially reduced Stx-induced kidney injury and lethality indicating a contribution of Gr1^{high} monocytes to the pathogenesis in HUS.

However, Stx/LPS treatment still induced residual kidney damage and mortality in *Ccr2*-deficient mice, strongly arguing for the involvement of other CCR2-independent cells in the pathogenesis of HUS.

6.1.2 CX_3CR1-deficiency in Stx/LPS-mediated kidney damage

Given that the chemokine receptor CX_3CR1 has been shown to be essential for the adherence of Gr1^{low} monocytes to the renal vasculature[25] and an involvement of CX_3CR1^+ leukocytes has been suggested in the pathology of HUS[122, 123], *Ccr2*-deficient animals were crossed to *Cx$_3$cr1*-deficient mice in order to investigate whether the residual kidney damage is caused by this receptor. The importance of these chemokine receptors for monocyte/macrophage trafficking to the kidney was shown previously in a model of ischemia-reperfusion injury[124]. We found significantly reduced abundance of Gr1^{low} monocytes in the blood and Gr1^{low} macrophages in the kidney. The reduction of

Gr1^{low} monocytes and macrophages in *Ccr2 x Cx$_3$cr1*-deficient animals is most likely due to a combinatory effect of the lack of the CCR2$^+$ Gr1^{high} progenitor cells[28], and the important role of CX$_3$CR1 for the survival of Gr1^{low} macrophages[115, 116]. As expected also Gr1^{high} monocytes were absent in these mice, due to CCR2-deficiency.

Indeed, Stx/LPS-injected *Ccr2$^{-/-}$ Cx$_3$cr1$^{gfp/gfp}$* mice were completely protected against kidney damage. However, although mortality was strongly reduced in *Ccr2$^{-/-}$ Cx$_3$cr1$^{gfp/gfp}$* mice, Stx/LPS treatment was still lethal for about 33% of these mice. This suggests lethal Stx/LPS-induced damage in other organs than the kidney. Aside the kidney, the CNS is the prime target for Stx-mediated toxicity[74, 75]. Thus, mortality in *Ccr2$^{-/-}$ Cx$_3$cr1$^{gfp/gfp}$* mice might be explained by Stx-induced neurological disorders. Moreover, this finding indicates that tissue damage in the brain or other organs during HUS might not be mediated by monocytes and macrophages.

Taken together, these data provide direct evidence that both Gr1^{high} monocytes and Gr1^{low} monocytes/macrophages are crucially involved in kidney damage in HUS. Given that *Ccr2$^{-/-}$ Cx$_3$cr1$^{gfp/gfp}$* mice lack Gr1^{low} monocytes and showed reduced number of resident Gr1^{low} macrophages, the individual role of these cell types cannot be determined with the models available. Further studies are required to clarify the specific role of Gr1^{low} blood monocytes in the renal vasculature and resident Gr1^{low} macrophages in the kidney. However, Gr1^{low} macrophages are directly located at the target organ and strongly outnumber Gr1^{low} monocytes, suggesting a contribution of Gr1^{low} macrophages rather than Gr1^{low} monocytes to kidney damage during HUS.

Moreover, these data demonstrate an essential role of chemokine receptors in the pathogenesis of HUS. These findings further corroborate a previous study, showing the importance of CCR1 for renal damage in HUS[125]. Notably, the expression of CCR2 and CX$_3$CR1 was also increased on monocytes from HUS patients[122, 126] underlining the importance of chemokine-receptor mediated processes in this disease. Thus, interfering with these processes, for example with novel small molecule compounds that block the CCR2 or CX$_3$CR1 receptor[127, 128, 129, 130], might represent a promising intervention strategy to ameliorate kidney damage during HUS.

6.2 Neutrophils in the Pathogenesis of HUS

Our data demonstrate an increased abundance of neutrophils in the blood upon Stx/LPS treatment indicating an involvement of these cells in HUS. This finding coincides with a previous study, showing a direct correlation of increased neutrophil counts with poor disease prognosis[117]. Moreover, flow cytometric analysis revealed elevated neutrophil counts in the kidney of Stx/LPS-treated mice suggesting neutrophil recruitment to the kidney in this model.

The increased neutrophil infiltration into the kidney during HUS may have been induced by elevated expression of the chemokine CXCL1, which has been shown to induce the adhesion and activation of neutrophils in previous studies[131, 132, 133]. IL-8, the functional homologue for CXCL1 in humans has also been shown to be increased in the serum and urine of STEC-HUS patients identifying a potent stimulus for neutrophil recruitment[94, 134]. Moreover, histological analysis revealed an increase of neutrophils within the renal cortex predominantly within the glomerulus, which coincides with previously reported elevated expression of CXCL1 within the glomerulus in a murine HUS model[135]. Notably, intraglomerular neutrophils have been associated with focal necrosis of endothelial cells by secreting ROS under inflammatory conditions[136, 137]. These data imply an important role of neutrophil recruitment and adhesion for kidney damage in HUS.

6.2.1 Involvement of integrin-dependent adhesion to Stx/LPS-mediated renal damage

In a mouse model of *Staphylococcus aureus* it was demonstrated that neutrophil crawling and recruitment is mainly mediated by α4 (VLA-4)- and β2 (CD18)-integrins and blocking these integrins reduced skin lesions[118, 138]. Moreover, integrins are able to initiate intracellular signaling cascades in neutrophils promoting extravasation, ROS production and degranulation[139]. Antibodies against these integrins are potent therapeutic agents to ameliorate various diseases, including renal disorders[137, 140, 141, 142]. Taken together, these data suggest an essential role for integrin-dependent neutrophil recruitment and function in diseases. Indeed, the present study demonstrated increased expression of the adhesion molecule VCAM-1, the corresponding ligand for α4-integrins, in the serum and kidneys of Stx/LPS-treated

mice. Moreover, clinical data from collaborators showed elevated VCAM-1 levels in the serum of STEC-HUS patients. These observations were corroborated with *in vitro* data showing increased VCAM-1 expression in an endothelial cell line upon Stx stimulation[143].

Taken together these findings raised the hypothesis of a potential involvement of VCAM-1-VLA-4-mediated neutrophil adhesion in inducing endothelial damage during HUS. However, targeting VCAM-1-VLA-4 interactions was not sufficient to protect Stx/LPS-injected mice from kidney injury dissenting a role of the VCAM-1–VLA-4 axis in this context. Nevertheless, other adhesion molecules than VCAM-1 and VLA-4 might mediate neutrophil adhesion and subsequent renal damage during HUS.

In vitro experiments showed, increased expression of ICAM-1, which represents an adhesion molecule for the β2-intgerin (CD18), on endothelial cells upon stimulation with Stx[143]. Moreover, neutrophils, that were isolated from STEC-HUS patients showed increased adherence to endothelial cells in a CD18-dependent manner[144]. Interestingly, here it was demonstrated, that the integrin CD11b, which forms a dimer with CD18 and mediates binding to the adhesion molecule ICAM-1[118], was strongly increased on the surface of neutrophils. Additionally, CXCL1 which has been shown to stimulate CD11b/CD18-mediated binding by neutrophils[145], was elevated in renal homogenates. Indeed, blocking CD18 slightly ameliorated renal damage, however these results did not reach statistical significance.

Conclusively, there is no direct proof for an essential role of integrin-dependent neutrophil adhesion in HUS. Elevated levels of CD11b on neutrophils during HUS and slight, although not significant, amelioration of the disease by blocking CD18 might hint to a minor involvement of CD11b/CD18–mediated binding of neutrophils during disease progression. CD18 targeting by antibodies might be incomplete and loss of function may have been compensated by other adhesion molecules as integrin redundancy is a well-established phenomena[146, 147]. Thus, further studies with transgenic mice, which specifically lack particular groups of integrins on neutrophils, are required to investigate the role of integrin-dependent neutrophil adhesion in endothelial damage during HUS.

6.2.2 CXCR2-mediated neutrophil recruitment in HUS

We found strong expression of CXCL1, the major ligand of CXCR2, in the kidney during HUS and periglomerular expression of this chemokine has already been demonstrated previously[102]. Microscopy revealed that cortical neutrophils were indeed more numerous within the glomerulus indicating that periglomerular CXCL1 expression may mediate an increased recruitment and adhesion of neutrophils to the glomerular endothelium. Furthermore, CXCR2-signalling induces conformational changes of integrins for the arrest and firm adhesion of neutrophils to the endothelium[148] thereby playing a superordinate role in the neutrophil recruitment process. Together, these findings suggest an essential role of CXCR2 in HUS.

We found that inhibiting the CXCR2-axis by pharmacological blockage indeed ameliorated the disease, whereas complete absence of CXCR2-signallling in *Cxcr2*-deficient mice completely prevented kidney injury during HUS. Intravital microscopy indicated that targeting CXCR2 significantly reduces the number of neutrophils adhering to the glomerular endothelium, suggesting that CXCR2-dependent neutrophil recruitment and adhesion in the glomerulus mediates endothelial damage in HUS. Notably, neutrophils adhering to the glomerular endothelium were also found in healthy mice consistent with a recent finding[137]. This constitutive adhesive behavior might be an explanation for the susceptibility of the glomerulus for immune-mediated diseases and identifies the glomerulus as a unique microenvironment.

However, Stx/LPS-induced mortality was not completely prevented in CXCR2-deficient mice. This finding again points on Stx-induced tissue damage in other organs than the kidney, which is independent of CXCR2-mediated neutrophil recruitment.

Conclusively, these findings suggest an essential role for glomerular neutrophil adhesion to endothelial damage and identify the CXCR2-dependent recruitment of neutrophils as a potential target against kidney damage in HUS. Extensive studies on CXCR2 antagonizing compounds as therapeutics for various other disease are ongoing[149, 150]. Hence targeting CXCR2 is a promising candidate to inhibit renal neutrophil invasion and thereby ameliorating kidney damage during HUS.

6.3 Non-Invasive *In Vivo* Imaging Reveals Endothelial Damage in HUS

The main function of the kidney is to filter blood and to remove unwanted substances from the body. This functionality is mainly facilitated by the glomerulus, which is located in the kidney cortex. An increased accumulation of the tracer [^{64}Cu]NOTA-GPVI-Fc within the kidney cortex, visualized by PET-MR imaging, indicated exposed subendothelial collagen and hence endothelial injury in this compartment. Moreover, microscopy revealed the presence of Gr1^{high} monocytes and neutrophils in the renal cortex and intravital imaging indicated increased abundance of adherent neutrophil in the glomerulus suggesting a causal connection between these cellular infiltrates and endothelial damage in the cortex.

Notably, elevated tracer uptake was also observed in the liver of healthy and Stx/LPS-treated mice (Fig. 5.11 A). As this is a common phenomenon for ^{64}Cu-labelled tracers due to the trans-chelation process of copper by liver enzymes[114], it cannot be associated to endothelial damage within the liver. However, Stx-mediated endothelial damage in the liver cannot be completely excluded.

Conclusively, the PET-MR imaging technique in combination with the [^{64}Cu]NOTA-GPVI-Fc tracer identify an important non-invasive diagnostic approach to evaluate the level of kidney injury during HUS. Furthermore, this technique might also be applicable to patients with other renal diseases involving endothelial injury.

6.4 Cellular Cross Talk in HUS

For many years Stx-mediated inhibition of the protein synthesis has been considered as the only cause for endothelial damage in HUS. This concept has changed due to emerging evidence for leukocyte involvement in the pathogenesis of HUS and it needs to be investigated whether myeloid cells are only indirectly involved in endothelial damage by amplifying the Stx-mediated toxic effects or if these cells also directly contribute to the endothelial damage during HUS.

It has been shown that Stx-stimulated endothelial cells produce chemokines, such as CCL2 and IL-8, which represent strong chemoattractants for monocytes and neutrophils[83]. Monocytes produce IL-1β and TNF-α, which in turn increase the expression of Gb3 on the endothelial surface thereby sensitizing the endothelial cells

towards the toxin[91, 92]. These data indicate a cellular crosstalk between monocytes/macrophages and endothelial cells in the context of HUS.

Moreover, the experiments demonstrated that targeting one of both myeloid cell types, either monocytes/macrophage or neutrophils, is sufficient to reduced kidney damage. This finding suggests that these myeloid cells are dependent on one another and argues in favor of a cellular crosstalk between monocytes, macrophages and neutrophils. Increased adhesion and recruitment of neutrophils in HUS may have been induced by elevated expression of the chemokine CXCL1, that has been shown to induce the adhesion and activation of these cells[131, 132, 133]. As afore mentioned, a study revealed periglomerular expression of CXCL1 in a murine HUS model[135]. Interestingly, we observed localization of $Gr1^{low}$ macrophages around the glomerulus and CXCL1 production by macrophages after stimulation with bacterial components has been shown previously[151] suggesting an interaction between $Gr1^{low}$ macrophages and neutrophils. In order to investigate whether $Gr1^{low}$ macrophages are the source of periglomerular CXCL1, histology experiments need to be conducted that aim at co-localizing CXCL1 and $Gr1^{low}$ macrophages around the glomeruli. The importance of a cellular crosstalk between monocytes, macrophages and neutrophils has already been demonstrated in other disease models[14, 152]. Nevertheless, the sequential steps of the cellular crosstalk, including cytokine production, chemokine-receptor-dependent monocyte and neutrophil recruitment in HUS needs to be unraveled to fully understand the involvement of these leukocytes in this disease.

Next to the above-described indirect role in kidney injury, myeloid cells may directly contribute to endothelial damage. In accordance with a previous publication[100], this study demonstrate elevated level of endothelial adhesion molecules and elevated CD11b on neutrophils, a molecule associated to cell-adhesion. Additionally, intravital microscopy revealed an elevated number of adherent neutrophils in Stx/LPS-treated mice. These finding suggest an increased neutrophil adhesion to endothelial cells during HUS and a potential involvement of CXCR2, CD11b and CD18. Moreover, there is evidence for increased plasmas levels of neutrophils elastase[153] and elevated ability for NET formation[154] and ROS production[117] indicating an increased functional state of adherent neutrophils. Adhesive and activated neutrophils might directly harm endothelial cells as it has been demonstrated in a model for glomerulonephritis[155].

In summary, these findings raise the hypothesis that myeloid cells might also directly contribute to endothelial damage. Hence, blocking myeloid cell recruitment and function can be important for future therapies not only to limit the inflammatory response but also by preventing cell-mediated endothelial damage during HUS.

7 Conclusions

In this thesis the role of distinct monocyte/macrophage subsets and the involvement of chemokine receptor-mediated recruitment of neutrophils to the kidney was investigated in a mouse model of HUS.

Elevated levels of CCR2-binding chemokines in the kidney were associated with increased abundance of $Gr1^{high}$ monocytes in the kidney of Stx/LPS-injected mice. Targeting CCR2-dependent $Gr1^{high}$ monocytes partially ameliorated kidney damage and prolonged the survival of *Ccr2*-deficient mice, indicating an important involvement of this cell type. Moreover, histological analysis revealed increased abundance of $Gr1^{high}$ monocytes in the renal cortex and non-invasive PET-MR imaging indicated endothelial damage in this area. Thus, $Gr1^{high}$ monocytes might be directly associated with endothelial damage during HUS. Additionally, these experiments identified PET-MR as a promising non-invasive method to evaluate kidney damage in HUS patients, which might be also applicable for other diseases in which the endothelium is injured. The residual kidney damage in *Ccr2*-deficient mice was caused by CX_3CR1-dependent $Gr1^{low}$ macrophages, as transgenic mice deficient in both chemokine receptors (*Ccr2*$^{-/-}$ *x* *Cx*$_3$*cr1*$^{gfp/gfp}$) were completely protected from kidney damage. Conclusively, these data demonstrated an involvement of both monocyte/macrophage subtypes and underlines the importance of chemokine-receptor-mediated recruitment of these cells to the kidney during HUS.

In the second part of this thesis the role of neutrophil recruitment and adhesion in the pathogenesis of HUS was investigated. Although an induced expression of endothelial adhesion molecules was shown in Stx/LPS-treated mice, a contribution of α4- and β2-mediated neutrophil adhesion to kidney damage could not be demonstrated. A possible explanation for this finding might be an incomplete blocking by antibody treatment or compensation of loss-of-function by redundant integrins. Thereby, an involvement of adhesion proteins in HUS cannot be fully excluded. To further investigate the role of integrins during HUS, experiments with mice lacking distinct integrins in a cell-type specific manner are suggested.

However, it was successfully demonstrated in this thesis, that renal CXCL1 levels lead to neutrophil infiltration to the kidney upon Stx/LPS treatment. Targeting CXCR2-signalling ameliorated renal damage and reduced mortality upon Stx/LPS treatment. Intravital imaging indicated, that CXCR2 targeting leads to reduced neutrophil adherence in the glomerulus, implying an essential role of CXCR2-dependent neutrophil adhesion for kidney injury during HUS.

Taken together these findings demonstrate the essential role for chemokine-dependent recruitment and activation of monocytes, macrophages and neutrophils in HUS. Blocking CCR2, CX_3CR1 and CXCR2 might serve as future therapies by restraining inflammatory responses in HUS. However, future experiments are required to delineate the cellular crosstalk between these cells in the pathogenesis of HUS to develop potent intervention strategies against this devastating disease.

8 References

1. Alberts, B. *et al.* Molecular biology of the cell. new york: Garland science; 2002. *Classic textbook now in its 5th Edition* (2002).

2. Murphy, K. & Weaver, C. *Janeway's immunobiology*. Garland Science, 2016.

3. Delves, P. & Roitt, I. The Immune System (second of two parts). *N Engl J Med* **343**, 108-117 (2000).

4. Delves, P. & Roitt, I. The Immune System (first of two parts). *N Engl J Med* **343**, 37-49 (2000).

5. Dranoff, G. Cytokines in cancer pathogenesis and cancer therapy. *Nature Reviews Cancer* **4**, 11-22 (2004).

6. Kawai, T. & Akira, S. The role of pattern-recognition receptors in innate immunity: update on Toll-like receptors. *Nature immunology* **11**, 373-384 (2010).

7. Gordon, S. Pattern recognition receptors: doubling up for the innate immune response. *Cell* **111**, 927-930 (2002).

8. Geissmann, F. *et al.* Development of monocytes, macrophages, and dendritic cells. *Science* **327**, 656-661 (2010).

9. Ginhoux, F. & Jung, S. Monocytes and macrophages: developmental pathways and tissue homeostasis. *Nature Reviews Immunology* **14**, 392-404 (2014).

10. Schulz, C. *et al.* A lineage of myeloid cells independent of Myb and hematopoietic stem cells. *Science* **336**, 86-90 (2012).

11. Auffray, C., Sieweke, M.H. & Geissmann, F. Blood monocytes: development, heterogeneity, and relationship with dendritic cells. *Annual review of immunology* **27**, 669-692 (2009).

12. Franc, N.C., Dimarcq, J.-L., Lagueux, M., Hoffmann, J. & Ezekowitz, R.A.B. Croquemort, a novel Drosophila hemocyte/macrophage receptor that recognizes apoptotic cells. *Immunity* **4**, 431-443 (1996).

13. Final presentation and evaluation of epidemiological finding in the EHEC O104:H4 Outbreak Germany 2011. ww.rki.de/EN/Content/infections/epidemiology/outbreaks/EHEC_O104/EHEC_final_report.pdf?__blob=publicationFile (Robert Koch Institiute 2011).

14. Soehnlein, O. & Lindbom, L. Phagocyte partnership during the onset and resolution of inflammation. *Nature Reviews Immunology* **10**, 427-439 (2010).

15. Geissmann, F., Jung, S. & Littman, D.R. Blood monocytes consist of two principal subsets with distinct migratory properties. *Immunity* **19**, 71-82 (2003).

16. van Furth, R. & Cohn, Z.A. The origin and kinetics of mononuclear phagocytes. *The Journal of experimental medicine* **128**, 415 (1968).

17. Serbina, N.V., Jia, T., Hohl, T.M. & Pamer, E.G. Monocyte-mediated defense against microbial pathogens. *Annu. Rev. Immunol.* **26**, 421-452 (2008).

18. Serbina, N.V., Salazar-Mather, T.P., Biron, C.A., Kuziel, W.A. & Pamer, E.G. TNF/iNOS-producing dendritic cells mediate innate immune defense against bacterial infection. *Immunity* **19**, 59-70 (2003).

19. Randolph, G.J., Inaba, K., Robbiani, D.F., Steinman, R.M. & Muller, W.A. Differentiation of phagocytic monocytes into lymph node dendritic cells in vivo. *Immunity* **11**, 753-761 (1999).

20. Landsman, L. & Jung, S. Lung macrophages serve as obligatory intermediate between blood monocytes and alveolar macrophages. *The Journal of Immunology* **179**, 3488-3494 (2007).

21. Neal, L.M. & Knoll, L.J. Toxoplasma gondii profilin promotes recruitment of Ly6C hi CCR2+ inflammatory monocytes that can confer resistance to bacterial infection. *PLoS Pathog* **10**, e1004203 (2014).

22. León, B., López-Bravo, M. & Ardavín, C. Monocyte-derived dendritic cells formed at the infection site control the induction of protective T helper 1 responses against Leishmania. *Immunity* **26**, 519-531 (2007).

23. Narni-Mancinelli, E. *et al.* Memory CD8+ T cells mediate antibacterial immunity via CCL3 activation of TNF/ROI+ phagocytes. *Journal of Experimental Medicine* **204**, 2075-2087 (2007).

24. Auffray, C. *et al.* Monitoring of blood vessels and tissues by a population of monocytes with patrolling behavior. *Science* **317**, 666-670 (2007).

25. Carlin, L.M. *et al.* Nr4a1-dependent Ly6C low monocytes monitor endothelial cells and orchestrate their disposal. *Cell* **153**, 362-375 (2013).

26. Nahrendorf, M. *et al.* The healing myocardium sequentially mobilizes two monocyte subsets with divergent and complementary functions. *Journal of Experimental Medicine* **204**, 3037-3047 (2007).

27. Helmy, K.Y. *et al.* CRIg: a macrophage complement receptor required for phagocytosis of circulating pathogens. *Cell* **124**, 915-927 (2006).

28. Serbina, N.V. & Pamer, E.G. Monocyte emigration from bone marrow during bacterial infection requires signals mediated by chemokine receptor CCR2. *Nature immunology* **7**, 311-317 (2006).

29. Engel, D.R. *et al.* CCR2 mediates homeostatic and inflammatory release of Gr1high monocytes from the bone marrow, but is dispensable for bladder infiltration in bacterial urinary tract infection. *The Journal of Immunology* **181**, 5579-5586 (2008).

30. Tsou, C.-L. *et al.* Critical roles for CCR2 and MCP-3 in monocyte mobilization from bone marrow and recruitment to inflammatory sites. *The Journal of clinical investigation* **117**, 902-909 (2007).

31. Shi, C. & Pamer, E.G. Monocyte recruitment during infection and inflammation. *Nature Reviews Immunology* **11**, 762-774 (2011).

32. Auffray, C. *et al.* CX3CR1+ CD115+ CD135+ common macrophage/DC precursors and the role of CX3CR1 in their response to inflammation. *Journal of Experimental Medicine* **206**, 595-606 (2009).

33. Landsman, L. *et al.* CX3CR1 is required for monocyte homeostasis and atherogenesis by promoting cell survival. *Blood* **113**, 963-972 (2009).

34. Karlmark, K.R. *et al.* The fractalkine receptor CX3CR1 protects against liver fibrosis by controlling differentiation and survival of infiltrating hepatic monocytes. *Hepatology* **52**, 1769-1782 (2010).

35. Engel, D.R. *et al.* CX3CR1 reduces kidney fibrosis by inhibiting local proliferation of profibrotic macrophages. *The Journal of Immunology* **194**, 1628-1638 (2015).

36. Sheshachalam, A., Srivastava, N., Mitchell, T., Lacy, P. & Eitzen, G. Granule protein processing and regulated secretion in neutrophils. *Secretion of Cytokines and Chemokines by Innate Immune Cells*, 27 (2015).

37. Kolaczkowska, E. & Kubes, P. Neutrophil recruitment and function in health and inflammation. *Nature Reviews Immunology* **13**, 159-175 (2013).

38. Colotta, F., Re, F., Polentarutti, N., Sozzani, S. & Mantovani, A. Modulation of granulocyte survival and programmed cell death by cytokines and bacterial products. *Blood* **80**, 2012-2020 (1992).

39. Borregaard, N. Neutrophils, from marrow to microbes. *Immunity* **33**, 657-670 (2010).

40. Lieschke, G. *et al.* Mice lacking granulocyte colony-stimulating factor have chronic neutropenia, granulocyte and macrophage progenitor cell deficiency, and impaired neutrophil mobilization. *Blood* **84**, 1737-1746 (1994).

41. Summers, C. *et al.* Neutrophil kinetics in health and disease. *Trends in immunology* **31**, 318-324 (2010).

42. Häger, M., Cowland, J. & Borregaard, N. Neutrophil granules in health and disease. *Journal of internal medicine* **268**, 25-34 (2010).

43. Brinkmann, V. *et al.* Neutrophil extracellular traps kill bacteria. *science* **303**, 1532-1535 (2004).

44. Hasenberg, A. *et al.* Catchup: a mouse model for imaging-based tracking and modulation of neutrophil granulocytes. *Nature methods* **12**, 445-452 (2015).

45. Becher, B. *et al.* High-dimensional analysis of the murine myeloid cell system. *Nature immunology* **15**, 1181-1189 (2014).

46. Himmelfarb, J., Hakim, R.M., Holbrook, D.G., Leeber, D.A. & Ault, K.A. Detection of granulocyte reactive oxygen species formation in whole blood using flow cytometry. *Cytometry* **13**, 83-89 (1992).

47. Luttmann, W., Bratke, K., Küpper, M. & Myrtek, D. *Der Experimentator: Immunologie*. Springer-Verlag, 2014.

48. Benninghoff, A., Drenckhahn, D. & Waschke, J. *Taschenbuch Anatomie*. Elsevier, Urban & Fischer, 2008.

49. Speckmann, E.-J., Hescheler, J., Köhling, R. & Rintelen, H. *Physiologie*. Elsevier, Urban&FischerVerlag, 2008.

50. Kurts, C., Panzer, U., Anders, H.-J. & Rees, A.J. The immune system and kidney disease: basic concepts and clinical implications. *Nature Reviews Immunology* **13**, 738-753 (2013).

51. Lüllmann-Rauch, R. Taschenlehrbuch Histologie, 2., komplett überarbeitete Auflage. Georg Thieme Verlag KG, Stuttgart New York, S; 2006.

52. Haraldsson, B. & Sörensson, J. Why do we not all have proteinuria? An update of our current understanding of the glomerular barrier. *Physiology* **19**, 7-10 (2004).

53. Rippe, C., Rippe, A., Torffvit, O. & Rippe, B. Size and charge selectivity of the glomerular filter in early experimental diabetes in rats. *American Journal of Physiology-Renal Physiology* **293**, F1533-F1538 (2007).

54. Klingberg, A. *et al.* Fully automated evaluation of total glomerular number and capillary tuft size in nephritic kidneys using lightsheet microscopy. *Journal of the American Society of Nephrology*, ASN. 2016020232 (2016).

55. Hochheiser, K. & Kurts, C. Selective Dependence of Kidney Dendritic Cells on CX3CR1—Implications for Glomerulonephritis Therapy. *Crossroads Between Innate and Adaptive Immunity V*. Springer, 2015, pp 55-71.

56. Stevens, L.A., Coresh, J., Greene, T. & Levey, A.S. Assessing kidney function—measured and estimated glomerular filtration rate. *New England Journal of Medicine* **354**, 2473-2483 (2006).

57. Clark, V.L. & Kruse, J.A. Clinical methods: the history, physical, and laboratory examinations. *JAMA* **264**, 2808-2809 (1990).

58. Mayer, C.L., Leibowitz, C.S., Kurosawa, S. & Stearns-Kurosawa, D.J. Shiga toxins and the pathophysiology of hemolytic uremic syndrome in humans and animals. *Toxins* **4**, 1261-1287 (2012).

59. Trachtman, H., Austin, C., Lewinski, M. & Stahl, R.A. Renal and neurological involvement in typical Shiga toxin-associated HUS. *Nature reviews Nephrology* **8**, 658-669 (2012).

60. Scheiring, J., Andreoli, S.P. & Zimmerhackl, L.B. Treatment and outcome of Shiga-toxin-associated hemolytic uremic syndrome (HUS). *Pediatric nephrology* **23**, 1749 (2008).

61. Keir, L.S., Marks, S.D. & Kim, J.J. Shigatoxin-associated hemolytic uremic syndrome: current molecular mechanisms and future therapies. *Drug Des Devel Ther* **6**, 195-208 (2012).

62. O'Brien, A. *et al.* Profile of Escherichia coli O157: H7 pathogen responsible for hamburger-borne outbreak of hemorrhagic colitis and hemolytic uremic syndrome in Washington. *Journal of clinical microbiology* **31**, 2799-2801 (1993).

63. Besser, R.E. *et al.* An outbreak of diarrhea and hemolytic uremic syndrome from Escherichia coli O157: H7 in fresh-pressed apple cider. *Jama* **269**, 2217-2220 (1993).

64. Paton, J.C. & Paton, A.W. Pathogenesis and diagnosis of Shiga toxin-producing Escherichia coli infections. *Clinical microbiology reviews* **11**, 450-479 (1998).

65. Garg, A.X. *et al.* Long-term renal prognosis of diarrhea-associated hemolytic uremic syndrome: a systematic review, meta-analysis, and meta-regression. *Jama* **290**, 1360-1370 (2003).

66. Frank, C. *et al.* Epidemic profile of Shiga-toxin–producing Escherichia coli O104: H4 outbreak in Germany. *New England Journal of Medicine* **365**, 1771-1780 (2011).

67. Jackson, M.P., Neill, R.J., O'Brien, A.D., Holmes, R.K. & Newland, J.W. Nucleotide sequence analysis and comparison of the structural genes for Shiga-like toxin I and Shiga-like toxin II encoded by bacteriophages from Escherichia coli 933. *FEMS Microbiology Letters* **44**, 109-114 (1987).

68. Brigotti, M. *et al.* Clinical relevance of shiga toxin concentrations in the blood of patients with hemolytic uremic syndrome. *The Pediatric infectious disease journal* **30**, 486-490 (2011).

69. Griener, T.P., Mulvey, G.L., Marcato, P. & Armstrong, G.D. Differential binding of Shiga toxin 2 to human and murine neutrophils. *Journal of medical microbiology* **56**, 1423-1430 (2007).

70. Ghosh, S., Polanowska‐Grabowska, R., Fujii, J., Obrig, T. & Gear, A. Shiga toxin binds to activated platelets. *Journal of Thrombosis and Haemostasis* **2**, 499-506 (2004).

71. Bitzan, M. *et al.* Evidence that verotoxins (Shiga-like toxins) from Escherichia coli bind to P blood group antigens of human erythrocytes in vitro. *Infection and immunity* **62**, 3337-3347 (1994).

72. Brigotti, M. *et al.* Identification of TLR4 as the receptor that recognizes Shiga toxins in human neutrophils. *The Journal of Immunology* **191**, 4748-4758 (2013).

73. Karmali, M.A. Prospects for preventing serious systemic toxemic complications of Shiga toxin–producing Escherichia coli infections using Shiga toxin receptor analogues. *Journal of Infectious Diseases* **189**, 355-359 (2004).

74. Ergonul, Z., Hughes, A.K. & Kohan, D.E. Induction of apoptosis of human brain microvascular endothelial cells by Shiga toxin 1. *Journal of Infectious Diseases* **187**, 154-158 (2003).

75. Johannes, L. & Römer, W. Shiga toxins—from cell biology to biomedical applications. *Nature Reviews Microbiology* **8**, 105-116 (2010).

76. Fraser, M.E., Chernaia, M.M., Kozlov, Y.V. & James, M.N. Crystal structure of the holotoxino from shigella dysenteriae at 2.5 Å resolution. *Nature Structural & Molecular Biology* **1**, 59-64 (1994).

77. Bonifacino, J.S. & Rojas, R. Retrograde transport from endosomes to the trans-Golgi network. *Nature reviews Molecular cell biology* **7**, 568-579 (2006).

78. Spooner, R.A. & Lord, J.M. How ricin and Shiga toxin reach the cytosol of target cells: retrotranslocation from the endoplasmic reticulum. *Ricin and Shiga Toxins*. Springer, 2011, pp 19-40.

79. Endo, Y. *et al.* Site of action of a Vero toxin (VT2) from Escherichia coli O157: H7 and of Shiga toxin on eukaryotic ribosomes. *European Journal of Biochemistry* **171**, 45-50 (1988).

80. Ruggenenti, P., Noris, M. & Remuzzi, G. Thrombotic microangiopathy, hemolytic uremic syndrome, and thrombotic thrombocytopenic purpura. *Kidney international* **60**, 831-846 (2001).

81. Morigi, M. *et al.* Alternative pathway activation of complement by Shiga toxin promotes exuberant C3a formation that triggers microvascular thrombosis. *The Journal of Immunology* **187**, 172-180 (2011).

82. van Setten, P.A., Monnens, L., Verstraten, R., Van den Heuvel, L. & Van Hinsbergh, V. Effects of verocytotoxin-1 on nonadherent human monocytes: binding characteristics, protein synthesis, and induction of cytokine release. *Blood* **88**, 174-183 (1996).

83. Zoja, C. *et al.* Shiga toxin-2 triggers endothelial leukocyte adhesion and transmigration via NF-&kgr; B dependent up-regulation of IL-8 and MCP-1. *Kidney international* **62**, 846-856 (2002).

84. Ramegowda, B. & Tesh, V.L. Differentiation-associated toxin receptor modulation, cytokine production, and sensitivity to Shiga-like toxins in human monocytes and monocytic cell lines. *Infection and immunity* **64**, 1173-1180 (1996).

85. Harrison, L.M., van Haaften, W.C. & Tesh, V.L. Regulation of proinflammatory cytokine expression by Shiga toxin 1 and/or lipopolysaccharides in the human monocytic cell line THP-1. *Infection and immunity* **72**, 2618-2627 (2004).

86. Guessous, F. *et al.* Shiga toxin 2 and lipopolysaccharide induce human microvascular endothelial cells to release chemokines and factors that stimulate platelet function. *Infection and immunity* **73**, 8306-8316 (2005).

87. Foster, G.H., Armstrong, C.S., Sakiri, R. & Tesh, V.L. Shiga toxin-induced tumor necrosis factor alpha expression: requirement for toxin enzymatic activity and monocyte protein kinase C and protein tyrosine kinases. *Infection and immunity* **68**, 5183-5189 (2000).

88. Cameron, P., Smith, S.J., Giembycz, M.A., Rotondo, D. & Plevin, R. Verotoxin activates mitogen‐activated protein kinase in human peripheral blood monocytes: role in apoptosis and proinflammatory cytokine release. *British journal of pharmacology* **140**, 1320-1330 (2003).

89. Inward, C., Varagunam, M., Adu, D., Milford, D. & Taylor, C. Cytokines in haemolytic uraemic syndrome associated with verocytotoxin-producing Escherichia coli infection. *Archives of disease in childhood* **77**, 145-147 (1997).

90. Karpman, D., Andreasson, A., Thysell, H., Kaplan, B.S. & Svanborg, C. Cytokines in childhood hemolytic uremic syndrome and thrombotic thrombocytopenic purpura. *Pediatric Nephrology* **9**, 694-699 (1995).

91. Eisenhauer, P.B. *et al.* Tumor necrosis factor alpha increases human cerebral endothelial cell Gb3 and sensitivity to Shiga toxin. *Infection and immunity* **69**, 1889-1894 (2001).

92. Louise, C. & Obrig, T. Shiga toxin-associated hemolytic-uremic syndrome: combined cytotoxic effects of Shiga toxin, interleukin-1 beta, and tumor necrosis factor alpha on human vascular endothelial cells in vitro. *Infection and immunity* **59**, 4173-4179 (1991).

93. Van de Kar, N., Monnens, L., Karmali, M. & Van Hinsbergh, V. Tumor necrosis factor and interleukin-1 induce expression of the verocytotoxin receptor globotriaosylceramide on human endothelial cells: implications for the pathogenesis of the hemolytic uremic syndrome. *Blood* **80**, 2755-2764 (1992).

94. van Setten, P.A. *et al.* Monocyte chemoattractant protein-1 and interleukin-8 levels in urine and serum of patents with hemolytic uremic syndrome. *Pediatr Res* **43**, 759-767 (1998).

95. Keepers, T.R., Gross, L.K. & Obrig, T.G. Monocyte chemoattractant protein 1, macrophage inflammatory protein 1α, and RANTES recruit macrophages to the kidney in a mouse model of hemolytic-uremic syndrome. *Infection and immunity* **75**, 1229-1236 (2007).

96. Ramos, M.V. *et al.* Induction of Neutrophil Extracellular Traps in Shiga Toxin-Associated Hemolytic Uremic Syndrome. *J Innate Immun* **8**, 400-411 (2016).

97. Gomez, S.A. *et al.* The oxidative stress induced in vivo by Shiga toxin-2 contributes to the pathogenicity of haemolytic uraemic syndrome. *Clin Exp Immunol* **173**, 463-472 (2013).

98. Milford, D., Taylor, C.M., Rafaat, F., Halloran, E. & Dawes, J. Neutrophil elastases and haemolytic uraemic syndrome. *Lancet* **2**, 1153 (1989).

99. Fernández, G.C. *et al.* Impaired neutrophils in children with the typical form of hemolytic uremic syndrome. *Pediatric Nephrology* **20**, 1306-1314 (2005).

100. Fernandez, G.C. *et al.* Shiga toxin-2 induces neutrophilia and neutrophil activation in a murine model of hemolytic uremic syndrome. *Clinical immunology* **95**, 227-234 (2000).

101. Fernandez, G. *et al.* Relevance of neutrophils in the murine model of haemolytic uraemic syndrome: mechanisms involved in Shiga toxin type 2 ‐ induced neutrophilia. *Clinical & Experimental Immunology* **146**, 76-84 (2006).

102. Roche, J.K., Keepers, T.R., Gross, L.K., Seaner, R.M. & Obrig, T.G. CXCL1/KC and CXCL2/MIP-2 are critical effectors and potential targets for therapy of Escherichia coli O157:H7-associated renal inflammation. *Am J Pathol* **170**, 526-537 (2007).

103. Keepers, T.R., Psotka, M.A., Gross, L.K. & Obrig, T.G. A murine model of HUS: Shiga toxin with lipopolysaccharide mimics the renal damage and physiologic response of human disease. *Journal of the American Society of Nephrology* **17**, 3404-3414 (2006).

104. Kuziel, W.A. *et al.* Severe reduction in leukocyte adhesion and monocyte extravasation in mice deficient in CC chemokine receptor 2. *Proceedings of the National Academy of Sciences* **94**, 12053-12058 (1997).

105. Jung, S. *et al.* Analysis of fractalkine receptor CX3CR1 function by targeted deletion and green fluorescent protein reporter gene insertion. *Molecular and cellular biology* **20**, 4106-4114 (2000).

106. Cacalano, G. *et al.* Neutrophil and B cell expansion in mice that lack the murine IL-8 receptor homolog. *SCIENCE-NEW YORK THEN WASHINGTON-*, 682-682 (1994).

107. Ge, S. *et al.* Microparticle generation and leucocyte death in Shiga toxin-mediated HUS. *Nephrol Dial Transplant* **27**, 2768-2775 (2012).

108. Bigalke, B. *et al.* Imaging of injured and atherosclerotic arteries in mice using fluorescence-labeled glycoprotein VI-Fc. *European journal of radiology* **79**, e63-e69 (2011).

109. Gawaz, M. *et al.* Implications of glycoprotein VI for theranostics. *Thromb Haemost* **112**, 1-6 (2014).

110. Lencer, W.I., Weyer, P., Verkman, A.S., Ausiello, D.A. & Brown, D. FITC-dextran as a probe for endosome function and localization in kidney. *American Journal of Physiology-Cell Physiology* **258**, C309-C317 (1990).

111. Fernández, G.C. *et al.* Differential expression of function-related antigens on blood monocytes in children with hemolytic uremic syndrome. *Journal of leukocyte biology* **78**, 853-861 (2005).

112. Litalien, C. *et al.* Circulating inflammatory cytokine levels in hemolytic uremic syndrome. *Pediatric Nephrology* **13**, 840-845 (1999).

113. Proulx, F. *et al.* Inflammatory mediators in Escherichia coli O157: H7 hemorrhagic colitis and hemolytic-uremic syndrome. *The Pediatric infectious disease journal* **17**, 899-904 (1998).

114. Rogers, B.E. *et al.* Comparison of four bifunctional chelates for radiolabeling monoclonal antibodies with copper radioisotopes: biodistribution and metabolism. *Bioconjugate chemistry* **7**, 511-522 (1996).

115. Karlmark, K.R. *et al.* The fractalkine receptor CX(3)CR1 protects against liver fibrosis by controlling differentiation and survival of infiltrating hepatic monocytes. *Hepatology* **52**, 1769-1782 (2010).

116. Engel, D.R. *et al.* CX3CR1 Reduces Kidney Fibrosis by Inhibiting Local Proliferation of Profibrotic Macrophages. *J Immunol* **194**, 1628-1638 (2015).

117. Fernandez, G.C. *et al.* The functional state of neutrophils correlates with the severity of renal dysfunction in children with hemolytic uremic syndrome. *Pediatric research* **61**, 123-128 (2007).

118. Harding, M.G., Zhang, K., Conly, J. & Kubes, P. Neutrophil crawling in capillaries; a novel immune response to Staphylococcus aureus. *PLoS Pathog* **10**, e1004379 (2014).

119. Kurts, C., Panzer, U., Anders, H.J. & Rees, A.J. The immune system and kidney disease: basic concepts and clinical implications. *Nat Rev Immunol* **13**, 738-753 (2013).

120. Lim, J.K. *et al.* Chemokine receptor Ccr2 is critical for monocyte accumulation and survival in West Nile virus encephalitis. *J Immunol* **186**, 471-478 (2011).

121. Shi, C. & Pamer, E.G. Monocyte recruitment during infection and inflammation. *Nat Rev Immunol* **11**, 762-774 (2011).

122. Ramos, M.V. *et al.* Involvement of the fractalkine pathway in the pathogenesis of childhood hemolytic uremic syndrome. *Blood* **109**, 2438-2445 (2007).

123. Zanchi, C. *et al.* Fractalkine and CX3CR1 mediate leukocyte capture by endothelium in response to Shiga toxin. *The Journal of Immunology* **181**, 1460-1469 (2008).

124. Li, L. *et al.* The chemokine receptors CCR2 and CX3CR1 mediate monocyte/macrophage trafficking in kidney ischemia–reperfusion injury. *Kidney international* **74**, 1526-1537 (2008).

125. Ramos, M.V. *et al.* Chemokine receptor CCR1 disruption limits renal damage in a murine model of hemolytic uremic syndrome. *The American journal of pathology* **180**, 1040-1048 (2012).

126. Ramos, M.V. *et al.* Association of haemolytic uraemic syndrome with dysregulation of chemokine receptor expression in circulating monocytes. *Clinical Science* **129**, 235-244 (2015).

127. Zhao, Q. *et al.* A CCR2/CCR5-dual antagonist, BMS-A, offers a potential novel oral therapy for the treatment of autoimmune disease (92.6). *J Immunol* **182**, 92.96-92.96 (2009).

128. Anders, H.-J. *et al.* A chemokine receptor CCR-1 antagonist reduces renal fibrosis after unilateral ureter ligation. *The Journal of clinical investigation* **109**, 251-259 (2002).

129. Gladue, R.P. *et al.* CP-481,715, a potent and selective CCR1 antagonist with potential therapeutic implications for inflammatory diseases. *Journal of Biological Chemistry* **278**, 40473-40480 (2003).

130. Shen, F. *et al.* Novel small-molecule CX3CR1 antagonist impairs metastatic seeding and colonization of breast cancer cells. *Molecular Cancer Research* **14**, 518-527 (2016).

131. Amulic, B., Cazalet, C., Hayes, G.L., Metzler, K.D. & Zychlinsky, A. Neutrophil function: from mechanisms to disease. *Annu Rev Immunol* **30**, 459-489 (2012).

132. Soehnlein, O. & Lindbom, L. Phagocyte partnership during the onset and resolution of inflammation. *Nature rev immunol* **10**, 427-439 (2010).

133. Disteldorf, E.M. *et al.* CXCL5 drives neutrophil recruitment in TH17-mediated GN. *J Am Soc Nephrol* **26**, 55-66 (2015).

134. Fitzpatrick, M.M., Shah, V., Trompeter, R.S., Dillon, M.J. & Barratt, T.M. Interleukin-8 and polymorphoneutrophil leucocyte activation in hemolytic uremic syndrome of childhood. *Kidney international* **42**, 951-956 (1992).

135. Roche, J.K., Keepers, T.R., Gross, L.K., Seaner, R.M. & Obrig, T.G. CXCL1/KC and CXCL2/MIP-2 are critical effectors and potential targets for therapy of Escherichia coli O157: H7-associated renal inflammation. *The American journal of pathology* **170**, 526-537 (2007).

136. Carlin, L.M. *et al.* Nr4a1-dependent Ly6C(low) monocytes monitor endothelial cells and orchestrate their disposal. *Cell* **153**, 362-375 (2013).

137. Devi, S. *et al.* Multiphoton imaging reveals a new leukocyte recruitment paradigm in the glomerulus. *Nat Med* **19**, 107-112 (2013).

138. Neumann, J. *et al.* Very-late-antigen-4 (VLA-4)-mediated brain invasion by neutrophils leads to interactions with microglia, increased ischemic injury and impaired behavior in experimental stroke. *Acta neuropathologica* **129**, 259-277 (2015).

139. Zarbock, A. & Ley, K. Mechanisms and consequences of neutrophil interaction with the endothelium. *Am J Pathol* **172**, 1-7 (2008).

140. Goodman, S.L. & Picard, M. Integrins as therapeutic targets. *Trends in pharmacological sciences* **33**, 405-412 (2012).

141. Tang, T. *et al.* A role for Mac-1 (CDIIb/CD18) in immune complex-stimulated neutrophil function in vivo: Mac-1 deficiency abrogates sustained Fcgamma receptor-dependent neutrophil adhesion and complement-dependent proteinuria in acute glomerulonephritis. *J Exp Med* **186**, 1853-1863 (1997).

142. Millard, M., Odde, S. & Neamati, N. Integrin targeted therapeutics. *Theranostics* **1**, 154-188 (2011).

143. Morigi, M. *et al.* Verotoxin-1–induced up-regulation of adhesive molecules renders microvascular endothelial cells thrombogenic at high shear stress. *Blood* **98**, 1828-1835 (2001).

144. Forsyth, K., Fitzpatrick, M., Simpson, A., Barratt, T.M. & Levinsky, R. Neutrophil-mediated endothelial injury in haemolytic uraemic syndrome. *The Lancet* **334**, 411-414 (1989).

145. Detmers, P.A. *et al.* Neutrophil-activating protein 1/interleukin 8 stimulates the binding activity of the leukocyte adhesion receptor CD11b/CD18 on human neutrophils. *J Exp Med* **171**, 1155-1162 (1990).

146. Mercurio, A.M. Lessons from the α2 integrin knockout mouse. *The American journal of pathology* **161**, 3-6 (2002).

147. Li, S. *et al.* Integrin and dystroglycan compensate each other to mediate laminin-dependent basement membrane assembly and epiblast polarization. *Matrix Biology* (2016).

148. Kolaczkowska, E. & Kubes, P. Neutrophil recruitment and function in health and inflammation. *Nat Rev Immunol* **13**, 159-175 (2013).

149. Stadtmann, A. & Zarbock, A. CXCR2: from bench to bedside. *Arrest chemokines*, 91 (2015).

150. Rennard, S.I. *et al.* CXCR2 antagonist MK-7123. A phase 2 proof-of-concept trial for chronic obstructive pulmonary disease. *American journal of respiratory and critical care medicine* **191**, 1001-1011 (2015).

151. De Filippo, K. *et al.* Mast cell and macrophage chemokines CXCL1/CXCL2 control the early stage of neutrophil recruitment during tissue inflammation. *Blood* **121**, 4930-4937 (2013).

152. Schiwon, M. *et al.* Crosstalk between sentinel and helper macrophages permits neutrophil migration into infected uroepithelium. *Cell* **156**, 456-468 (2014).

153. Fitzpatrick, M.M., Shah, V., Filler, G., Dillon, M.J. & Barratt, T.M. Neutrophil activation in the haemolytic uraemic syndrome: free and complexed elastase in plasma. *Pediatric Nephrology* **6**, 50-53 (1992).

154. Ramos, M.V. *et al.* Induction of neutrophil extracellular traps in Shiga toxin-associated hemolytic uremic syndrome. *Journal of innate immunity* **8**, 400-411 (2016).

155. Davies, M., Barrett, A., Travis, J., Sanders, E. & Coles, G. The degradation of human glomerular basement membrane with purified lysosomal proteinases: evidence for the pathogenic role of the polymorphonuclear leucocyte in glomerulonephritis. *Clin Sci Mol Med* **54**, 233-240 (1978).

9 List of Figures

10 List of Tables

11 Abbreviations

Abbreviation	Meaning
°C	Degree Celsius
A	Adenosine
AF	Alexa Fluor
APC	Allophycocyanin
BM	Bone marrow
BSA	Bovine serum albumin
BUN	Blood Urea Nitrogen
C	Cytosine
cc	Cubic centimeter
CCL	C-C motif chemokine ligand
CCR	C-C motif chemokine receptor
CD	Cluster of differentiation
cDNA	complementary Deoxyribonucleic acid
CNS	Central nervous system
CO2	Carbon dioxide
Cu	Cupper
d	Day
DNA	Deoxyribonucleic acid
DAPI	4',6-diamidino-2-phenylindole
DC	Dentritic cell
ddH2O	Double-distilled water
dNTP	Desoxyribonucleotide
EDTA	Ethylenediaminetetraacetic acid
EGFP	Enhanced green fluorescent protein
ELISA	Enzyme-linked immunosorbent assay
FACS	Fluorescence activated cell sorting
FC	Fold change
FCS	Fetal calf serum
Fig.	Figure
FITC	Fluorescein isothiocyanate
FOV	Field of View
FSC	Forward scatter
FWD	Forward
G	Gauge
G	Guanine
gDNA	Genomic desoxyribonucleic acid
GFP	Green Fluorescent protein
Gp	Glycoprotein
h	Hour
H2O	Water

hIgG	Human immunglobuline G
HPRT	Hypoxanthine-guanine phosphoribosyltransferase
HSC	Hematopoetic stemm cell
HUS	Hemolytic uremic syndrome
i.p.	Intraperotoneal
i.v.	Intravenous
ICAM-1	Intracellular Adhesion Molecule-1
IHC	Immunohistochemistry
IL	Interleukin
iNOS	Inducible Nitric oxidase synthase
kDa	Kilodalton
kg	Kilogram
KIM-1	Kideny injury molecule-1
LDH	Lactate dehydrogenase
LPS	Lipopolysaccharide
M	Molar
MBq	Megabecquerel
MDP	Monocyte, macrophage and DC precursor
MFI	Mean fluorescence intensity
min	Minutes
ml	Milliter
MO	Monocytes
MP	Macrophages
mRNA	Messenger riboneucleic acid
NET	Neutrophil extracellular trap
nm	Nanometer
OSEM	Ordered subset expectation maximization
PBS	Phosphate buffered saline
PCR	Polymerase-chain-reaction
PE	Phycoerythrin
Pen/Step	Penicillin/Streptomycin
PerCP	Peridinin chlorophyll
PET	Positron emission tomography
PET-MR	Positronenemission tomography-magnetic resonance
PFA	Paraformaldehyde
qRT-PCR	Quantitative teal-time polymerase chain reaction
RCB	Red cell lysis buffer
Rev	Reverse
RNA	Ribonucleic acid
ROI	Region of interest
ROS	Reactive oxygen species
rpm	Rounds per minute
RPMI	Roswell Park Memorial Institute medium
RT	Reverse Transcriptase
RT	Room Temperature
s	Second

SEM	Standard error of the mean
SSC	Side scatter
STEC	Shiga toxin-producing Escherichia Coli
Stx	Shiga toxin
T	Thimidine
TipDC	TNF- and iNOS producing DC
TNF-α	Tumor Necrosis factor alpha
VCAM-1	Vascular cell adhesion molecule-1
VLA-4	Very Late Antigen-4
vol%	Volume fraction
w/o	Without
µg	Microgram
µl	Microliter
µm	Micrometer
µM	Micromolar

Der Lebenslauf ist aus Gründen des Datenschutzes nicht enthalten.

Eidesstattliche Erklärungen

Hiermit erkläre ich, gem. § 7 Abs. 2, d und f der Promotionsordnung der Fakultät für Biologie zur Erlangung des Dr. rer. nat., dass ich die vorliegende Dissertation selbständig verfasst und mich keiner anderen als der angegebenen Hilfsmittel bedient habe und alle wörtlich oder inhaltlich übernommenen Stellen als solche gekennzeichnet habe.

Essen, den 27.09.2017 Judith-Mira Pohl

Unterschrift des/r Doktoranden/in

Hiermit erkläre ich, gem. § 7 Abs. 2, e und g der Promotionsordnung der Fakultät für Biologie zur Erlangung des Dr. rer. nat., dass ich keine anderen Promotionen bzw. Promotionsversuche in der Vergangenheit durchgeführt habe, dass diese Arbeit von keiner anderen Fakultät abgelehnt worden ist, und dass ich die Dissertation nur in diesem Verfahren einreiche.

Essen, den 27.09.2017 Judith-Mira Pohl

Unterschrift des/r Doktoranden/in

Hiermit erkläre ich, gem. § 6 Abs. 2, g der Promotionsordnung der Fakultät für Biologie zur Erlangung des Dr. rer. nat., dass ich das Arbeitsgebiet, dem das Thema „***Analysis and Manipulation of Cell-mediated Immune Responses in Shiga Toxin-Induced Kidney Injury***" zuzuordnen ist, in Forschung und Lehre vertrete und den Antrag von Judith-Mira Pohl befürworte.

Essen, den Prof. Dr. Daniel Engel

Name d. wissenschaftl. Betreuers/Mitglieds der Universität Duisburg-Essen	Unterschrift d. wissenschaftl. Betreuers/Mitglieds der Universität Duisburg-Essen